Experimental and numerical study of the characteristics of side weir flows

Kiran Mangarulkar

A Thesis

In

The Department

Of

Building, Civil and Environmental engineering

Presented in Partial fulfillment of the requirements
For the Degree of Master of Applied Science (Civil Engineering)
Concordia University
Montreal, Quebec, Canada
November 2010

CONCORDIA UNIVERSITY

School of Graduate Studies

This is to certify that the thesis prepared

By: **Mangarulkar Kiran**

Entitled: **Experimental and Numerical Study of the Characteristics of Side Weir Flows**

and submitted in partial fulfillment of the requirements for the degree of

Master of Applied Science

complies with the regulations of the University and meets the accepted standards with respect to originality and quality.

Signed by the final examining committee:

Dr. S. Li _____ Chair

Dr. W. P. Zhu _____Examiner

Dr. M. Nokken _____ Examiner

Dr. A.S. Ramamurthy _____ Co- Supervisor

Dr. J. Qu _____ Co- Supervisor

Approved by

_____ Dr. K. Ha,

Chair of Department or Graduate Program Director

_____Dr. Robin Drew

Dean of Faculty

Abstract

Experimental and Numerical study of the characteristics of side weir flows

Side weirs are extensively used in hydraulic engineering, irrigation, and environmental engineering applications which involve flow measurement and regulation. Flows through side weirs are typical examples of spatially varied flow (SVF) with decreasing discharge.

The flow emerging out from the side weir is three-dimensional (3D) due to variations in the water surface profile. These flow characteristics can be obtained by experimental methods, numerical modeling or by theoretical analysis. The present study is confined to the rectangular side weir located in a horizontal rectangular channel having zero sill height. Experiments were performed on the rectangular side weir to locate the stagnation zone, the region of separation and the water surface profile. A Laser Doppler Anemometry (LDA) unit was used to measure the mean and turbulent velocity components of the flow. Experimental results are analyzed to find the detailed flow characteristics using data related to the velocity distribution, velocity vectors, separation streamlines, stagnation point and water surface profiles for different weir flow configurations.

The predictions of the 3D numerical turbulence model were validated using the experimental results. The 3D equations, Reynolds's averaged Navier-Stokes (RANS) equations and the two-equation renormalized relations (RNG k-ε) were verified using experimental results. The volume of fluid (VOF) scheme was incorporated in the model to find free surface profiles of the open channel flow configuration denoting the side weir flow. The simulation result provided

detailed analysis of flow patterns, velocity distributions, water surface profiles, flow separation zone, stagnation zone, and separation streamlines. In general, the experimental data validated the predictions of the numerical model. The location of the stagnation point on the near wall was also determined based on the existing ideal flow analysis of Michell for flow past a rectangular outlet in a 2D conduit and was shown to be close to both test results and model predictions.

KEYWORDS:

Side weir ; flow separation ; separation streamline ; RANS equation ; 3D simulation ; RNG k-epsilon model ; velocity distribution ; water surface profile ; LDA.

Acknowledgements

I would like to thank my supervisors Dr. A.S. Ramamurthy and Dr. J. Qu for suggesting the research topic.

I also wish to thank Dr. Sang Soo Han for assistance offered with regards to LDA system operation, development of the experimental setup and for assistance in the development of the CFD model. I would also like to thank Dr. Rahim Tadayon for useful suggestions related to the experimental work. Also, I would like to thank the technician of hydraulic lab (Mr. N Lang Vo) for the help offered during the installation of experimental setup.

I would like to dedicate this work to my loving parents, to whom I will be forever grateful for their untold sacrifice, support, encouragement and patience which has played an important role in finishing this research work.

TABLE OF CONTENTS

LIST OF FIGURES

LIST OF TABLES

EXPERIMENTAL FLOW CONDITIONS

NOTATION AND ABBREVATIONS

---

1. Common Notations

B = Width of channel (m)

C_R= Recirculation zone.

F_r = Froude number

g = Acceleration due to gravity (m/sec^2)

L = Length of the side weir (m)

L_S = Length of separation zone.

p = Pressure (N/m^2)

Q = Discharge (m^3/sec)

Q_1 = Total discharge (Inflow) (cum/sec)

Q_2 = Downstream / through discharge (cum/sec)

Q_3 = Side weir discharge (cum/sec)

Q_R = Discharge ratio = Q_3 / Q_1

R = Reattachment point.

R_h= Hydraulic radius (m)

R_N =Reynolds number

S = Separation point

S' = Stagnation point

SDR= Separation zone

S_f = Frictional slope

S_L = Dividing / Separation / branching streamline

So = Longitudinal slope

S_{TE} =Stagnation point by experimental method.

S_{TS} =Stagnation point by numerical simulation.

S_{TT} =Stagnation point by theoretical method.

S_{TV} =Stagnation point by flow visualization.

t = time (sec)

T_1 =Upstream end of the side weir (weir entry)

T_2 = Downstream corner of the side weir (weir exit), origin=0,0,0.

u = Axial /stream wise velocity (parallel to channel walls) (m/sec)

$\bar{u}$ = Mean axial velocity (m/sec)

v = upward (vertical) velocity (m/sec)

w= Transverse velocity (parallel to width of channel) (m/sec)

W_S= Width of separation zone.

X, Y, Z = Coordinates at three dimensions (m)

Y= Flow depth (m)

y_1 =Flow depth at upstream end of side weir (m)

y_2 =Flow depth at downstream end of side weir (m)

y_c = Critical depth (m)

y_e = End depth (m)

ϕ = Width of the jet

2. Notations for numerical simulation of the side weir model:

2D = two-dimensional;

3D = three-dimensional;

PISO = Pressure-Implicit with Splitting of Operators;

VOF = Volume of fluid;

FVM = Finite Volume Method;

RANS = Reynolds averaged Navier Stokes;

RNG = Renormalized group;

3. Symbols:

ρ = Density of water (kg/m^3)

γ = Specific weight of water

α = Energy coefficient correction factor

β = Momentum coefficient correction factor

ε = Dissipation of kinetic energy

η = Normal distance from wall at the cell center

μ= Viscosity (kg/ms)

τ = Shear stress (Pa)

4. Abbreviations:

u/s upstream

d/s downstream

CHAPTER 1

INTRODUCTION

1.1 Spatially-varied flow

Spatially varying flow occurs when the free surface flow depth in an open channel changes gradually due to the change in the discharge along the length of the channel. This change can be a result of the flow added to or subtrated from the channel boundaries. The resulting varied flow is known as a spatially varied flow (SVF). This type of flow is observed in side-weirs, side channel spillways, wash water troughs, road side gutters and irrigation systems (drainage channel and feeding channel).

Flow over a side weir is a typical example of spatially varied flow with decreasing discharge. In the past, side weirs were studied extensively because of their wide range of applications in hydraulic engineering and sanitary engineering. Many experimental studies were conducted to calculate discharge coefficient (C_d) of side weir. The objective of study is to obtain the detailed flow characteristics such as flow profile, flow separation, and stagnation streamline for flow past a side weir located in a rectangular channel. The study is confined to the characteristics of side weirs which have zero sill height and a fixed ratio of side weir length to the channel width.The results obtained are based on theorotical, experimental and numerical simulation studies.

Flow separation is generally caused because of the two governing factors, one is the adverse pressure gradient and other is the sudden change in boundary. Flow separation can cause considerable energy losses and it can reduce channel performance sharply. To achieve

optimum performance of machinery or a system, one should clearly understand flow separation characteristics (Chang 1970).

Flow separation can induce vorticity in to the flow. In many cases, prevention of vortices is an essential part of hydraulic design of intake structure, as it can cause non-uniform flow conditions and vibration. Hence, some known structural measures are to be applied to reduce vorticity.

1.2 Thesis Objective:

The primary objective of the present study is to determine the main characteristics of the flow over the side weir placed in a rectangular open-channel (Fig. 1.1). The specific objectives of the study are listed below.

1. To determine all flow characteristics of flow over the side weir. This includes the flow profile, the separation zone, the dividing streamline, the stagnation point on the near wall of the channel, the contraction coefficient of the exiting jet of the side weir. (Fig.1.1).
2. To develop a 3D turbulent model for the rectangular side weir to obtain all the weir flow characteristics and validate the model using present and existing data (Fig.1.1). The RNG k-ε model is chosen for this purpose.
3. To briefly verify the simulation data for the stagnation point using the theoretically determined stagnation point location related to a 2D outlet in which ideal flow occur.

1.3 Thesis outline

In order to discuss the basics of the side weir problem the present thesis is divided into a number of chapters,

Chapter 2 starts with a detailed review of spatially varied flow. The side weir theory is briefly discussed in the next part followed by previous studies carried out to analyze side weir by using experimental and numerical approches.

Present study is divided into two main parts. The first part of the present study is a detailed description of the experimental investigation and the procedures adopted to find the flow characteristics of the side weir including the flow profile, flow separation, and dividing streamline. These are described in chapter 3.

The second part of the present study consists of a 3D turbulence modeling and the procedure adopted to construct the side weir model. This is discussed in the chapter 4. In this chapter, RANS equations are applied to solve the side weir problem in a rectangular open channel. Also, it contains brief information about the procedures of computational fluid dynamics and the RNG k-ε model, the VOF theory and validation of the present side weir model using test data.

Results and discussion are provided in chapter 5. Various methods adopted to verify the results of the present study are discussed. Conclusions based on the present study together with future study topics are addressed in chapter 6.

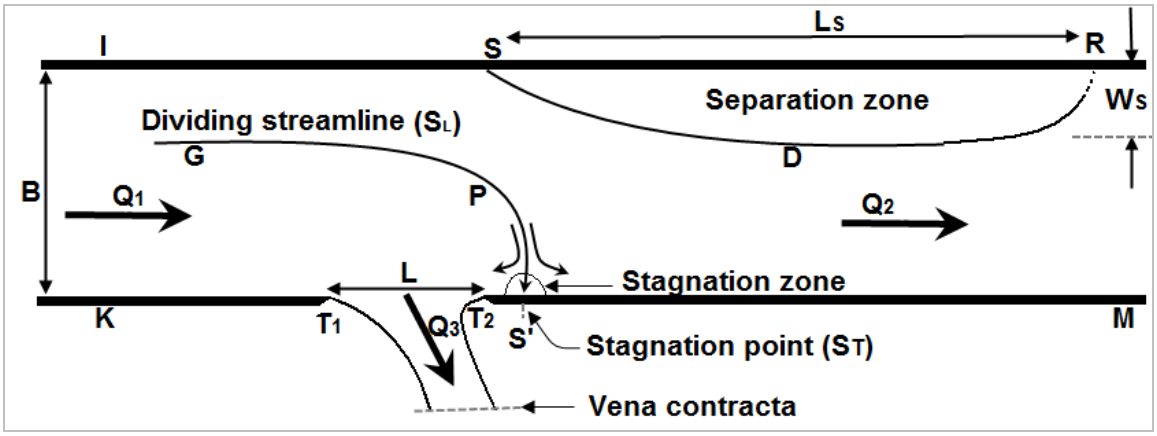

Fig.1.1: Flow characteristics of the rectangular side weir.

CHAPTER 2

LITERATURE REVIEW

2.1 General Remarks

Spatially varied flow, as encountered in open channels, has non-uniform discharge resulting from addition or diminution of water along the flow direction. The following section deals with spatially varied flow with the decreasing discharges. The side weir is also known as the lateral weir because some flow is taken out lateraly from the main channel. Lateral outflow over the side weir is discussed in this chapter.

2.2 Review of spatially varied flow (SVF) equations

The hydraulic behavior of SVF is more complicated than constant discharge flows. SVF can be classified into two types and their hydraulic behavior is different.

i) SVF with increasing discharge (e.g. side channel spillway system)

ii) SVF with decreasing discharge (e.g. side weirs)

Lateral outflow over the side weir is different than the conventional outflow from a basin. Lateral outflow over a side weir is affected by the outflow geometry, the approach velocity of the flow and the direction of outflow structure. The diverted water does not affect the energy head at the upstream of channel. This has been verified in many theoretical and experimental studies. Use of the energy equation is more convenient in solving these types of problems.

General assumptions are (Chow,1959) made in the derivation of spatially varied flow with

decreasing discharge can be summarized as follows:

1. The flow is unidirectional for the approach flow.
2. The pressure distribution is hydrostatic.
3. The velocity distribution across the channel section is constant and uniform.
4. The slope of the channel (S_0) is relatively small.
5. Manning's formula can be used to evaluate the friction loss.
6. The effect of air entrainment is neglected.

2.3 Review of side weir flow

The side-weir is a fixed structure, which is installed on one side or both sides of the main channel to divert a portion of the flow from the open channel. It has been extensively used in hydraulic and environmental engineering applications. Its applications includes flow-diversion and flood control devices widely used in urban drainage, water and wastewater-treatment plants, in combined sewers, in storm drainage and also in the delivery and distribution networks in irrigation systems. Generally side weirs are provided to serve a dual purpose of diverting and measuring discharge.

Side weirs are provided in various sizes and geometrical shapes in open channels that have different types of cross section. The geometrical shape of channel can alter the weir flow characteristics. Hydraulic behavior of each weir is different in such conditions. Because of the large number of geometrical parameters, standardization is essential to quantify features of side weirs. Flow over side weirs is characterized by Froude number of the approach flow, the weir sill height(s), and length of weir (l). Many studies outlined below have been conducted in the past to standardize the hydraulic behavior of side weirs.

2.4 Theoretical considerations

De Marchi (1934) assumed that the total energy of the flow in the main channel remains unchanged along the weir length. De Marchi obtained an empirical equation to find the side weir discharge relation in a rectangular side weir housed in a rectangular channel (Fig 2.1 and Equation 2.1). The dynamic equation of spatially varied flow for outflow over a side weir (Chow 1959) is

$$\frac{dy}{dx} = \frac{S_o - S_f - \left(\frac{\alpha Q}{gA^2}\right)\left(\frac{dQ}{dx}\right)}{1 - \left(\frac{\alpha Q^2 B}{gA^3}\right)} \qquad (2.1)$$

Here, dy/dx is the slope of the water surface with respect to the bed, y is the depth of flow in the main channel, x is the longitudinal direction , S_f is the energy slope, α is the kinetic energy correction coefficient, A is the cross sectional area of flow , g is the acceleration due to gravity.

To derive the above expression (Equation 2.1) the following assumptions are made

1. The channel is rectangular and prismatic.
2. The side weir is short and the specific energy (E) is constant between sections 1 and 2. This is equivalent to assuming (S_o - S_f) = 0 or (S_0 = 0, and S_f = 0).
3. The weir edges are assumed to be sharp with adequate aeration of the nappe.
4. The kinetic energy correction factor (α) is taken to be unity.

Assuming (S_o-S_f) = 0 (constant specific energy across the weir) and α =1

$$q = \frac{dQ_s}{dx_1} = \frac{2}{3} C_m \sqrt{2g} (y_1 - s)^{\frac{3}{2}} \qquad (2.2)$$

Here, Q_s is the total weir discharge, q_s is the weir discharge per unit length, x_1 is the stream wise distance from the upstream edge of the weir , y_1 is depth of flow at T_1 (Fig. 2.1) and C_m is De Marchi coefficient of discharge (Chow 1959).

The De Marchi coefficient of discharge, C_m is expressed in terms of the geometric and hydrodynamic variables of the side weir.

$$C_m = f(F_R, \frac{L}{B}, \frac{s}{y_1}) \qquad (2.3)$$

Where, $F_R = v_1 / \sqrt{g.y_1}$ is upstream Froude number, L and B are length of the side weir and width of a rectangular channel respectively. y_1 is upstream water depth of weir. S is the sill height of side weir. The detailed study done in past on these parameters are discussed in section 2.5.

In practice, subcritical flow is very common in rivers, open channel systems, and irrigation systems in which the side weir is installed. One can observe three types of flow at side weir sections- subcritical flow, supercritical flow and a combination of these flows which involves the hydraulic jump. Hydraulic behavior of subcritical and supercritical flow is different. Hager (1994) described the computational scheme for spatially varied flow. Subcritical flow is governed by a downstream boundary condition (flow depth and discharge) and its computational direction is against the flow direction, while supercritical flow is governed by an upstream boundary condition and its computational flow direction is the same as the flow direction. The portions with subcritical and supercritical flows are separated

by the hydraulic jump. Thus, the flow region is identified by whether the flow is thoroughly subcritical or thoroughly subcritical. A hydraulic jump links these two flow sections.

The focus of the present side weir study is on subcritical approach flow only. Due to decreasing discharge at the side weir, the depth at upstream end of the side weir is less than the normal depth. This is because the flow accelerates as it reaches the crest of the side weir leading to a fall in the water surface. In subcritical flow, the normal depth (y_1) is greater than the critical depth (y_c). The critical flow depth is very important because there is a unique relationship between y_c and rate of flow (q) in the rectangular channel. The surface elevation at the upstream and downstream ends of the weir differentiates subcritical flow in to three different types (Henderson, 1966).

Type 1 (Fig 2.3a): In this case, the flow is subcritical (F_R <1) throughout the length of the side weir. The water level seems to be slightly increasing from the upstream end to the downstream end of the side weir. As a result of this, discharge intensity of the flow at the downstream end is more compared to its value at the upstream end. This condition is generally found in uniform channels and channels with a small slope.

Type 2 (Fig. 2.3.b): In this case, the approach flow is supercritical (F_R > 1) throughout the length of the side weir. Hence the water surface is drops from the upstream end of the side weir to downstream end of side weir. As a result of this, the discharge per unit width (q) of the flow at the upstream end is greater than at the downstream end. This type of flow generally occurs in steep channels.

Type 3 (Fig. 2.2.c): This is a combination of above two types of flow. Initially, flow is

supercritical (F_R >1) which reduces the water surface along the length of side weir. This is Followed by a jump which results in subcritical flow (F_R <1) in the downstream section (Fig. 2.5b). Hydraulic jump found along side weirs is quite different in its characteristics than the traditional hydraulic jump in a straight open channel.

2.5 Previous related studies

The flow out of a 2 dimensional conduit is somewhat similar to the flow out of a side weir. For ideal flow through a 2D conduit (Fig.2.2), Mitchell (1890) presented a general mathematical solution of the problem with plain rigid boundaries using analytical procedures. He used the free streamline theory to solve the problem related to flow past a plane wall having a rectangular aperture. In his study, he solved three different cases of a stream flow past an aperture in two dimensional conduits. One branch of the streamline (S_L-P-S') impinges at S_{TT} on the vertical wall containing the weir (Fig. 2.2). This point (S') is referred as stagnation point (S_{TT}) and corresponding streamline is the dividing streamline. The distance ES' (Fig.2.2) of the stagnation point S_{TT} from the edge of the weir depends on parameters like approach velocity, the jet exit velocity and the jet exit angle (θ). According to the analysis of Michell (1890) the dimensionless distance *l/c* can be denoted in terms of the other variables in Equation 2.4.

$$\frac{l}{c}=\frac{1}{\phi}\left[\frac{v_2^2+v_1v_2+v_1^2}{v_1v_2}\ X\ \frac{v_2-v_1}{v_2+v_1}+\frac{v_1}{v_2}\log\frac{2v_2}{v_2+v_1}+\sqrt{\frac{v_2^2-v_1^2}{v_2^2}}\left(\sin^{-1}\frac{v_1}{v_2}-\frac{\phi}{2}\right)\right] \quad (2.4)$$

Here, ϕ is the width of jet at the vena contracta for the jet emerging out from the side weir. v_1 is the velocity of approach flow, v_2 is velocity of jet, c is the location of stagnation point from downstream end of aperture where streamlines separate, *l* is the length of the aperture.

Most of the earlier weir studies were devoted to the evaluation of the discharge coefficient (C_m) of side weirs having different weir geometries. In the study of a weir located in a rectangular open channel to determine De Marchi weir coefficient C_m, Subramanya and Awasthy (1972) used the Pitot tube to explore internal flow characteristics of a side weir having zero sill height. They measured the velocity distribution and the point gauge to get the water surface profile. Since then, extensive research has been carried out to modify the coefficient C_m for different channel geometries.

Some of the studies on rectangular side weirs were conducted by De Marchi (1934), Collinge(1957), Frazer(1957), Rajaratnam(1967), Subramanya and Awasthy(1972), Carballada (1979), Ranga Raju et al(1979),Ramamurthy and Carballada (1980), Hager(1982 and 1987), Balmforth and Sargasso(1983), Swamee et al(1994), Borghei (1999), Muslu (2001) and Muslu et al(2003), Ramamurthy et al (2006) ,Tadayon (2009). Side weirs in circular channels were investigated by Allen (1957), Uyumaz and Muslu (1985), Hager (1994), Singh et al. (1994), Ramamurthy et al. (1995). El-Khashabad and Smith (1976) and Udoyara (1986) have published results related to trapezoidal side weir flow in trapezoidal channels. Some of the studies are described here.

Experimental Studies:

Borghei et al. (1999) did the experimental analysis to test the effect of the influencing variables on the De Marchi coefficient. However, they also introduced an additional term denoting the slope S_0 of the channel in the weir equation, while using the least-square method. They compared the difference between measured discharge and the theoretical discharge by their numerical model. The addition of slope term S_0 to the list of variables

($F_R, \frac{L}{B}, \frac{s}{y_1}$) improved the results, where slope was a factor.

Hager and Volkart (1986) used a one dimensional approach to examine the spatial flow behavior of the side weir as a distribution channel. He used an axial momentum equation coupled with the appropriate outflow conditions to define the water surface profile and discharge distribution across the side weir. He considered parameters like outflow weir geometry, outflow jet angle and approach velocity. He observed that non-uniform discharge intensity and velocity profile across weir flow. By using geometric constriction of the channel near the side weir, uniform outflow intensity and constant velocity can be achieved. He mentioned that the outflow rate for the side weir is always smaller than the corresponding weir at the end of the channel with the same depth.

Hager (1987) performed experiments to evaluate the discharge coefficient of the side weir having zero sill height. He stated the dynamic flow equation using momentum correction factor and outflow intensity. To calculate the discharge coefficient, he presented an individual equation for each parameter like upstream flow depth, approach velocity, lateral outflow angle, channel shape, lateral outflow intensity. The presented equations were verified for subcritical as well as supercritical flow.

Agaccioglu and Yüksel (1998) performed experiments on a rectangular side weir placed along the 180^0 curved channel. By the velocity measurements and flow visualization, they observed that a stagnation zone existed at the side weir section along the inner side of the bend in a subcritical flow. It occupied almost half the width and extended about halfway along the length of side weirs. The velocity gradient was zero near the surface downstream

of the side weir. The location and size of the separation zone found at depends on Froude number at the upstream of side weir and also on the length of the side weir. The side weir discharge coefficient was found to be depending on the upstream Froude number, the dimensionless weir height, p/y_1 and the dimensionless weir length, L/B. The intensity of the secondary flow (El-Khashab, 1975) due to lateral flow in a curved channel was defined using definition of bend.

Numerical Methods:

Ramamurthy and Carballada (1980) considered parameters $F_R, \frac{L}{B}, \frac{s}{y_1}$ and used the free streamline model of McNown (1951) to analyze the rectangular side weir flow problem. They also presented a different version of the Froude number $F_R = v_1 / \sqrt{g(y-s)}$.

Uyumaz (1997) obtained a numerical model for the flow over side weir in a circular channel using the constant specific energy assumption. He obtained a numerical equation for both subcritical and supercritical flow conditions by using a finite difference method. The water surface profile and the discharge coefficient were found using these numerical equations. They used several hundred combinations of the side weir lengths, sill heights, and the channel slope to obtain the final equations. They validated their equations with experimental results and found they are in good agreement. The curved water surface at the side weir section made considerable effect on the pressure distribution in the flow.

Muslu (2001) used the energy equation as a basis of his investigation to develop a numerical model to find the water surface profile. He verified his model predictions with the results of Subramanya and Awasthy (1972). Further he verified his model predictions for a range of

L/B and s/y_0 ratios while conducting a sensitivity analysis (Muslu 2002). A change in the water surface profile for different ratios were plotted by a curve fitting technique to further find out the variations in the discharge coefficient (C_m).

Ramamurthy et al (2006) used the multivariable nonlinear partial least square method to determine the fourth order polynomial empirical equation for the De Marchi coefficient C_m.

Turbulence modeling of the side weirs:

Qu (2005) simulated flow over a side weir using 3D free surface turbulence model. He used k-ω turbulence model using VOF scheme to capture water surface profile of the side weir for a specific case having L/B ratio of 0.40. The numerical results were validated with experimental data of Subramanya and Awasthy (1972). His simulation captures location of stagnation zone near the downstream edge of the weir.

Tadayon (2009) developed a 3D Reynolds stress transport turbulence model (RSM) for the side weir using the VOF scheme to find the flow rate, water surface profile and the velocity distribution. He validated his model predictions using the experimental results of Hager (1982) related to discharge rate and water surface profile. He also verified his model predictions of velocity distribution using the test data of Subramanya and Awasthy (1972). However the agreement of the test data with model predictions were only approximate in regions where the flow was curved. This disagreement was traced to the inability of the Pitot tube to measure velocities accurately in curvilinear flow.

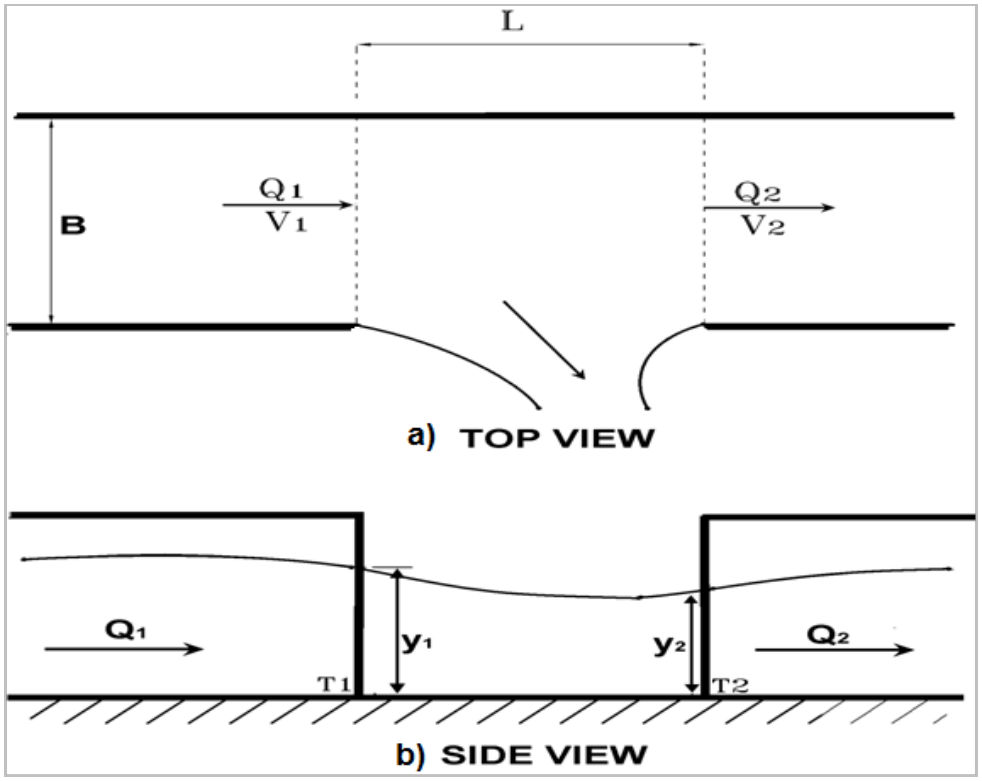

Fig.2.1 Flow over the side weir (sill height=0) a)top view b) side view

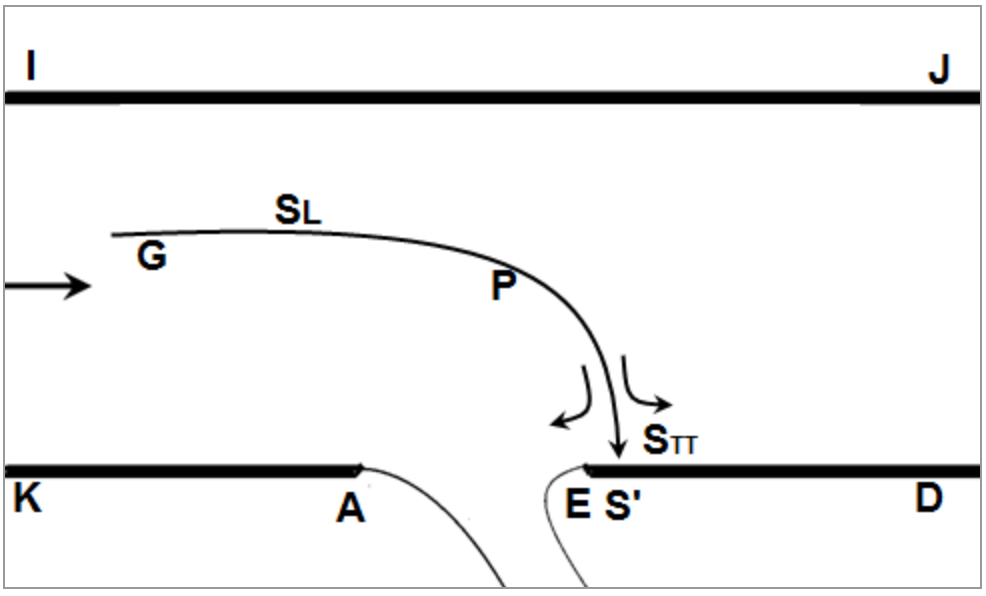

Fig.2.2 Details of dividing streamline GPS' (S_L) and location of theoretical stagnation point S_{TT} at downstream end of the opening.

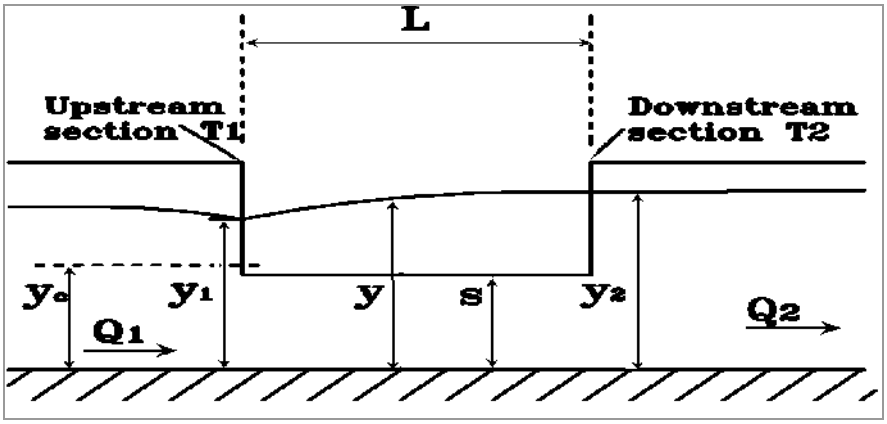

Fig 2.3.a: Water profile along the length of the side weir for subcritical flow

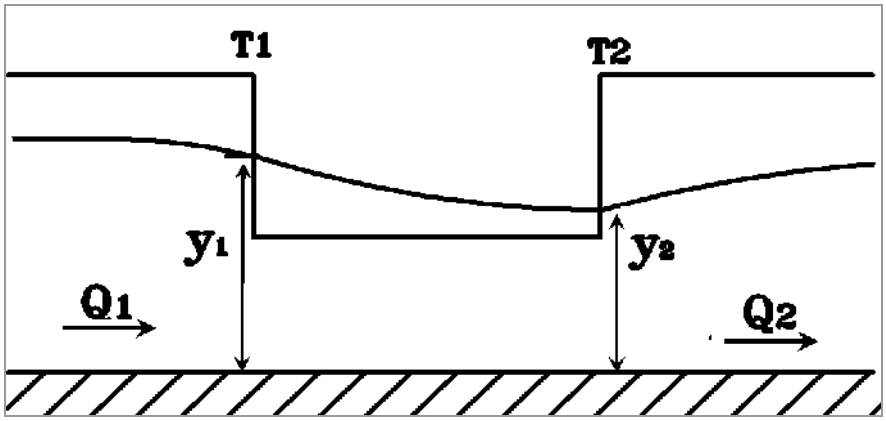

Fig 2.3.b: Water profile along the length of the side weir for supercritical flow.

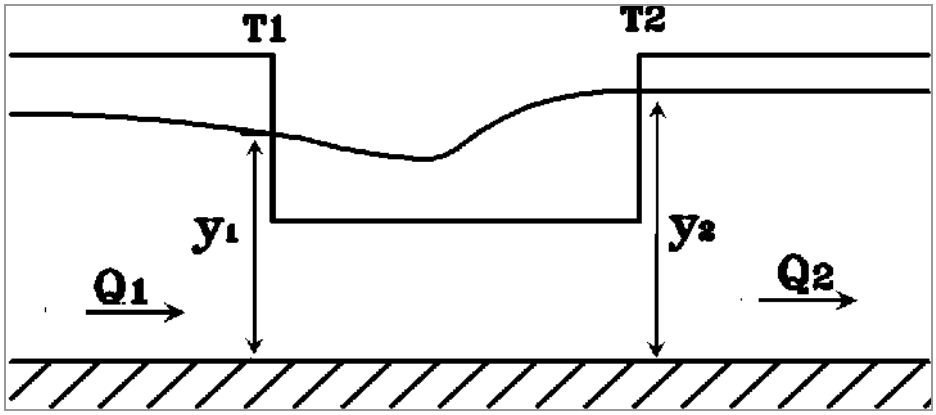

Fig 2.3.c: Water profile along the length of the side weir for hydraulic jump

CHAPTER 3

EXPERIMENTAL SETUP

3.1 Introduction

The experiments were performed in an open channel (fig. 3.1.a) having provision for a side weir at one side of the channel. The main channel is a glass-walled, hydraulically smooth, horizontal channel (Table3.1 and Fig.3.2.b). Channel walls and bed were made up of 12.7 mm Plexiglas plates. The side weir was positioned at a distance 2.82 m from the channel entrance. The length of the channel at upstream part was sufficiently long (Fig. 3.1) to develop a turbulent velocity profile. Machine cut Plexiglas plates were used for side weir. The channel bed was horizontal with no sill height (S) at side weir. The downstream end of the weir was beveled (60^0) to provide a sharp edge at the exit.

The approach flow entered the channel from a constant head tank after passing through a transition section containing a honeycomb and a screen to reduce free turbulence in the channel approach flow. A float was suspended at the entry of the flume dampened surface waves in the approach flow. The depth downstream of the weir was controlled by an end control gate.

3.2Mode of measurements

3.2.1 Discharge

The through discharge of the main channel and the side weir discharge were measured separately by using standard 60^0 V-notch tanks. The total discharge was measured by a

venturimeter located in the 150 mm supply pipeline. The maximum error in the discharge measurement was estimated to be 5%.

3.2.2 Velocity

The laser Doppler Anemometry (LDA) unit by Dantek was used to measure the velocity components of the flow field. The laser power was 300 mW. The focal length of the LDA probe lances were 160 mm and 400 mm. The velocities u and v as and also u and w were measured using two separate orientations of the probe (Fig. 3.2.a and Fig.3.2.b). To measure u and w, the probe was set at right angles to the channel floor while it was set at right angles to the channel sides to measure u and v. The probe was positioned on a 3D automated traverse which could move in steps of 0.006 mm. 1024 samples were used to measure the mean velocities.

At each cross section, the square grid used for velocity measurement was 2 cm x 2cm (fig 3.3). Total 47 cross sections were recorded across the channel for the first run. A detailed grid considered for velocity measurement is shown in fig 3.3. All the flow conditions were kept undisturbed for each run of velocity measurements. Flow conditions were changed only when all the measurements were recorded for that run. Due to the inclined nature of the beams, the v component of the velocity could not be measured very close to the channel floor, while the w component could not be measured close to the side walls. The errors in the velocity measurement were of the order of 1%. The measurement locations are shown in Fig.3.3.

3.2.3 Pressure

The diameter of closely spaced wall pressure taps in the vertical side walls of the flume was 0.5 mm (Fig 3.4). The pressure measurement can be made more accurately by adopting an

inclined manometer.

Point gages were used to measure the water surface elevation to the nearest 0.1 mm to map the water surface profile. Manometer reading represents static pressure head [$(p/\gamma)+z$]. A datum is established at the bottom of the channel to get (p/γ) value.

3.2.4 Non-dimensionalized parameters

The total discharge entering the channel, the flow over the side weir and the flow in the channel downstream of the weir were denoted as Q_1, Q_2, and Q_3 respectively. The parameter Q_3/ Q_2 represented the discharge ratio (Q_R). Three different discharge ratios (Q_3/ Q_2) were selected during the experiment.

All distances X, Y and Z were non-dimensionalized by the channel width B=0.286 m. The non- dimensionalized coordinates were denoted as X*= X/B, Y*=Y/B and Z* =Z/B. The downstream end of weir T_2 (Fig. 3.5) served as the origin for all axial measurements. Hence at T_2, X*=Y*= Z*=0. The mean velocity components in the X, Y, and Z directions were represented by u, v and w, respectively. The corresponding non dimensionalized mean velocity components were denoted by u*, v* and w* by dividing the mean velocity components by the average axial mean velocity ($\bar{u}$) at the cross section. The parameters u`, v` and w` denoting the root mean square (RMS) value of the turbulent velocity components were also measured. These were divided ($\bar{u}$) to yield the non-dimensionalized turbulent intensities u`*= u`/$\bar{u}$, also other two components are, v`*= v`/$\bar{v}$ and w`*= w`/$\bar{w}$.

3.3 Procedures

3.3.1 Tracing dividing streamline:

For purposes of analysis, the flow is considered to be 2D in the region that is away from the weir exit. For 2D flows, an estimate of the streamline location can be made as follows,

- The value $\psi_{far\ wall} = \psi_0 = 0$ is arbitrarily attributed to the streamline denoting the far wall (Fig.3.5), i.e. along MN
- For streamlines OQ and MN space between them = dψ and the discharge $dQ = d\psi$ is passing between the far wall and newly located streamline The volume flow rate dQ (per unit width) passing between OQ and MN streamlines (in 2D flow) can be expressed as, $d\psi = dQ$
- The distance of the streamline OQ from the wall = dy.

  Velocity data at points along the normal to the wall yield dy.

  Thus, dψ = dQ & ψ_1=0 +dψ

  Also, dQ = u.dA = (dψ/dy) (dy x 1)

  Hence, location dy represents the distance where dQ=dψ denotes the point on the streamline for which ψ=ψ1

- Locate similar points along streamline OQ and all other streamlines similarly.
- Since the analysis is based on 2D flow, near the weir where flow is not 2D, the streamline representation is only approximation.
- To locate separation streamline in the zone of separating velocity profile along a normal to wall is determined and the point ‘C‘ where the discharge forward and

reverse denotes the edge of the separation streamline. Join all `C` points along the flow direction, which will give a separation streamline.

- In the flow field, very close to the weir the flow was far from 2D and hence assumption of 2D is not strictly valid.

3.3.2 Finding exiting jet velocity and contraction ratio for the exiting flow of the side weir:

- The upstream approach velocity v_1 of the side weir was taken from experimental LDA data. The jet velocity v_2, the width of the jet at the vena contracta 'ϕ' of the side weir were calculated by taking additional experimental data.

- The vertical section of the free falling three dimensional jet emerging from the side weir was determined at the vena contracta using the point gage. The vena contracta was assumed to be at a of distance of approximately one the side weir width from the weir exit. One may recall that for two dimensional flow out of a sluice gate, the vena contracta occurs at a distance of about one width of the gate opening.

- Cross section of the jet was plotted with respect to the side weir opening and cross sectional area 'A' was calculated as shown in Fig 3.6. The jet velocity v_2 is calculated using the side weir discharge (Q_3).

- The location of the stagnation point S_{TT} on near wall is calculated by Equation 3.4.

- The exiting jet contraction coefficient C_C was calculated by taking ratio of the cross sectional area of the exiting jet in the plane of the side weir section and its area at the vena contracta. Vena contracta was assumed to be located at a distance L, which

denotes width of the weir.

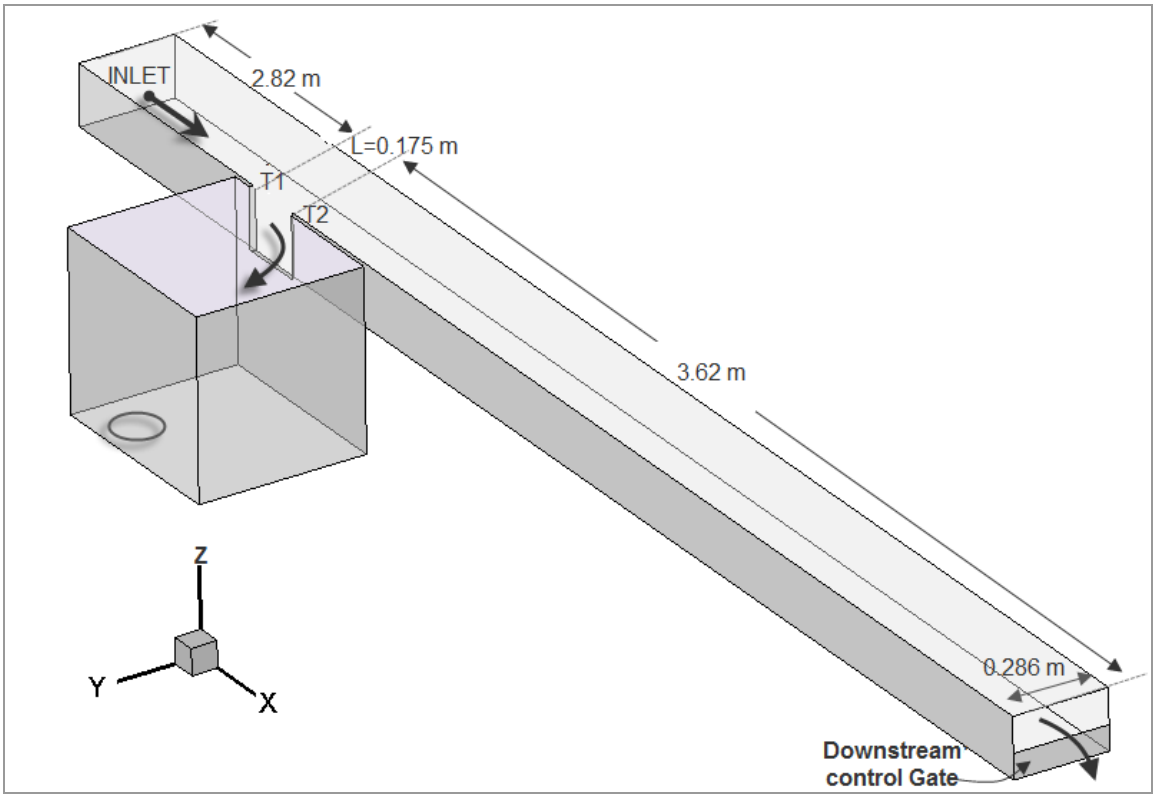

Fig. 3.1.a: Layout of a rectangular side weir flume (sill height=0)

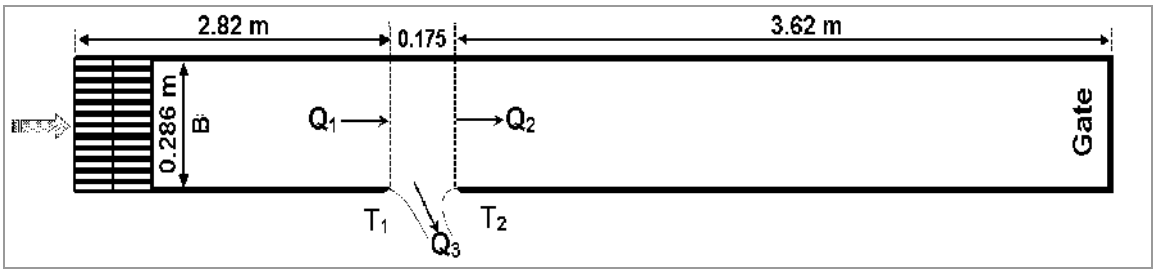

Fig. 3.1.b: Schematic of a rectangular side weir flume (Sill height=0)

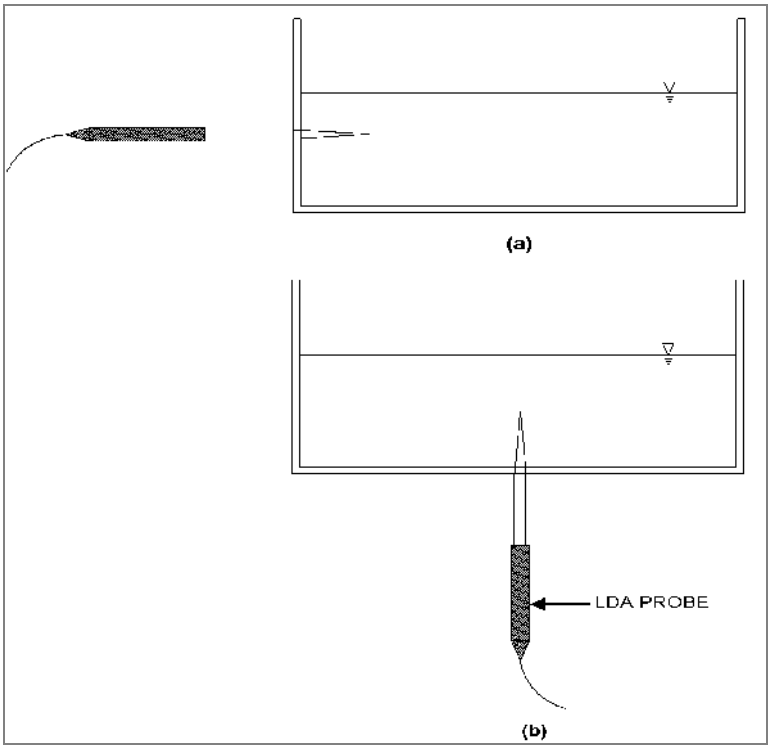

Fig.3.2: Schematic arrangement of LDA probe to measure velocity components. (a) u and v. (b) u and w.

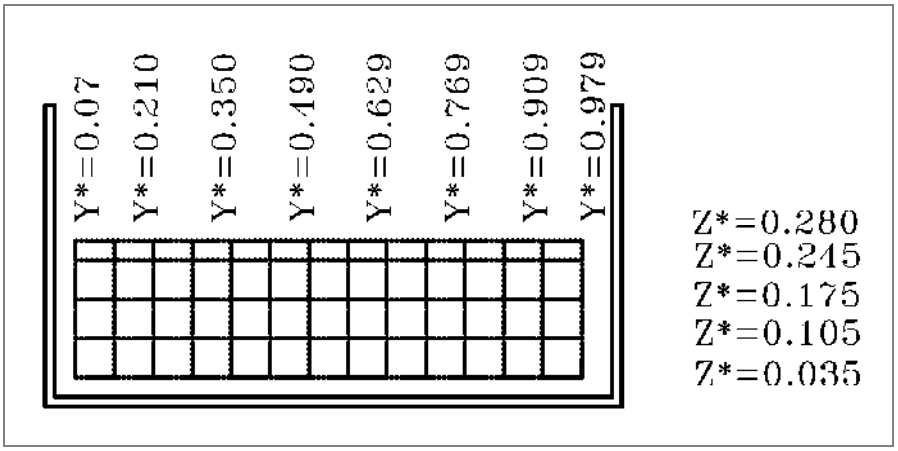

Fig. 3.3: Typical velocity measurement grid points using LDA across the channel section (Y*=Y/B, Z*=Z/B).

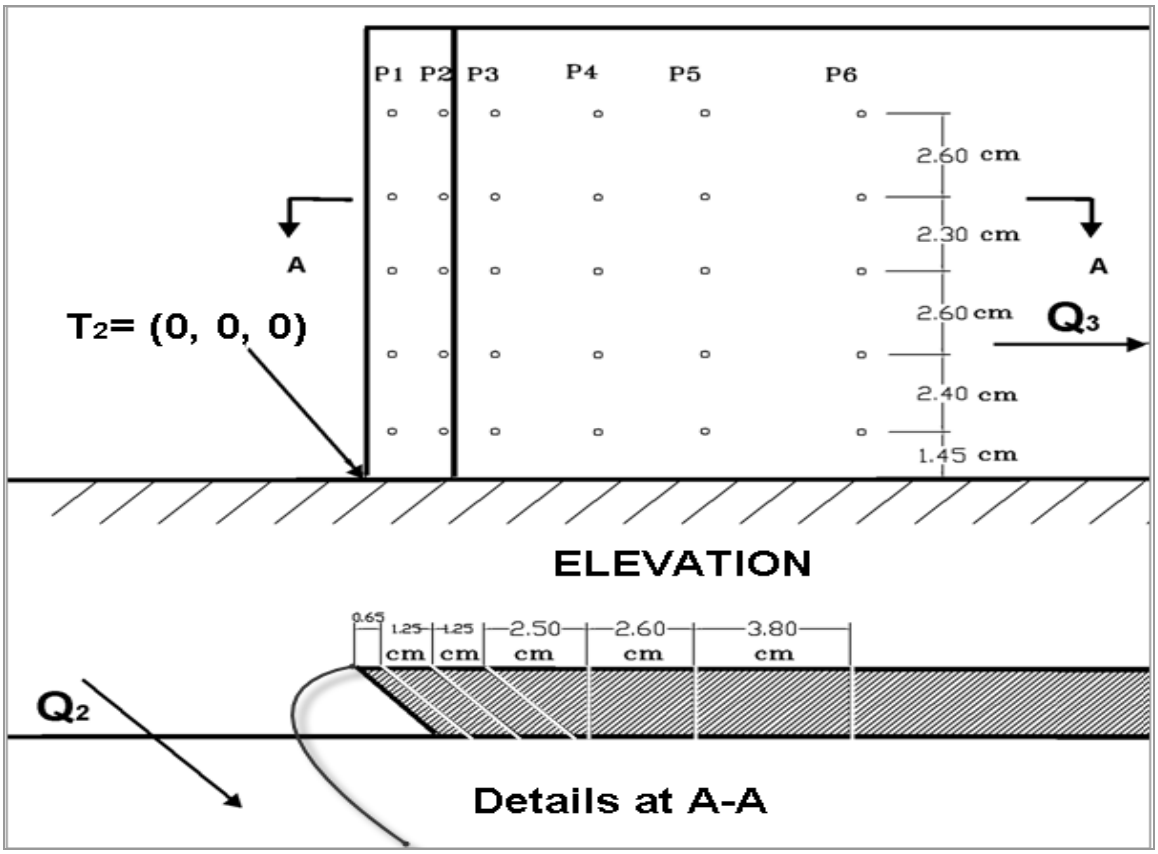

Fig. 3.4: Locations of the pressure taps on the near wall at the downstream end of the side weir T_2.

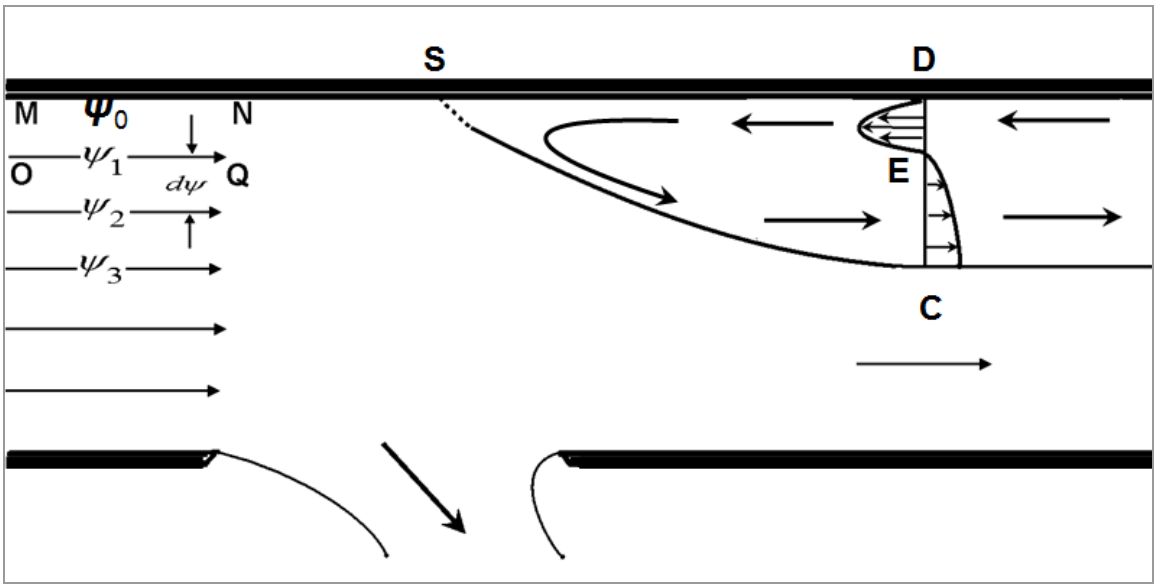

Fig. 3.5: Tracing the streamlines and the separation streamline.

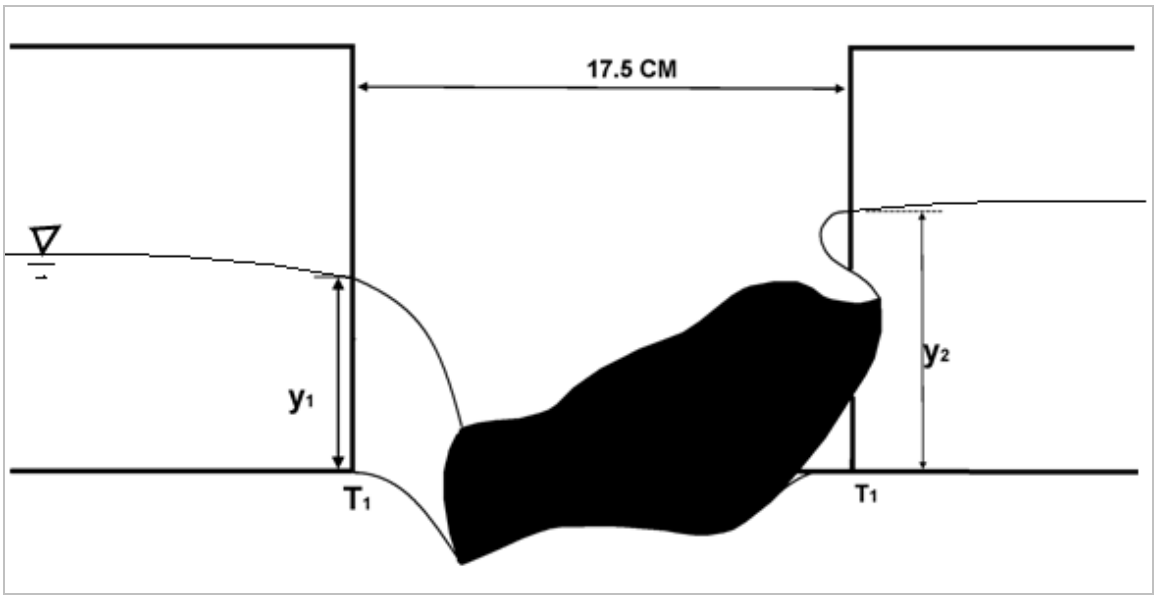

Fig. 3.6: Surface mapping of exiting jet emerging out from the side weir (shaded area) of zero sill height at vena contracta. Coefficient of jet contraction=0.70.

TABLES

Table: 3.1 Experimental Flow configurations for present test and previous test.

Sr. No.	Description	Present Experiments	Subramanya and Awasthy (1972)
1	Overall Length of channel	6.355 m	3.00 m
2	Length of the side weir (L)	0.175 m	0.15 m
3	Width of the channel (B)	0.286 m	0.248 m
4	Upstream flow depth	0.101 m	0.04 m
5	L/B dimensionless ratio	0.611	0.605
6	Upstream length of the channel up to the side weir	2.82 m	--
7	Sill Height (S)	0.00 m	0.00 m

Table: 3.2 Experimental Flow conditions for present test.

Run	u/s depth y_1 (m)	Inlet velocity (m/s)	Reynolds number R_N	Froude Number F_R	Through discharge Q_2 (m^3/sec)	Side weir discharge Q_3 (m^3/sec)	Discharge Ratio Q_R
I	0.101	0.405	40782	0.40	0.002403	0.009172	0.792
II	0.096	0.422	40390	0.434	0.004577	0.006996	0.604
III	0.117	0.347	40477	0.324	0.000608	0.010969	0.940

$F_R = u / \sqrt{g.y}$, $Q_R = Q_3 / Q_1$, $R_N = u.z / \nu$, where ν is kinematic viscosity.

CHAPTER 4

NUMERICAL MODELLING OF SIDE WEIR FLOW

4.1 Numerical modeling using computational fluid dynamics:

Analysis of a numerical model begins with the representation of a physical flow field in terms of a mathematical model. The fundamental properties of a flow field including conservation of mass, momentum, and energy must be satisfied throughout the flow field. Fluid properties are modeled using simple assumptions to make the problem tractable e.g., steady-state, incompressible, inviscid. Appropriate initial and boundary conditions are provided to analyse the flow characteristics.

Computational Fluid Dynamics (CFD) uses numerical methods also called discretization scheme, to develop approximations of the governing equations of the flow regime. CFD is an art of replacing partial derivative equations representing a given flow field with discretized algebraic forms (Veersteeg, 1995). These are solved to obtain a solution for the fluid flow problem at a discrete point in time and/or space. The flow regime is divided into a collection of cells which is termed as a grid. The set of algebraic equations are solved numerically for the flow field variables such as velocity and pressure, at each node or cell. These systems of equations are solved simultaneously to provide the solution representing flow field. The solution is post-processed to extract quantities of interest (e.g. lift, drag, torque, heat transfer, separation, pressure loss, etc.).

4.2 General form of governing equations

The turbulence in the flow field is generated due to various factors. It is convected and dissipated throughout the domain. The fluctuating velocity fields responsible for turbulence, mixes transported quantities such as momentum, energy in momentum transfer or various concentrations in mass transfer. These fluctuations can be of small scale and hence associated with high frequency since one is obliged to use finer grid. So they are computationally expensive to simulate directly in practical engineering calculations. A transport equation defined in terms of turbulent kinetic energy is derived from the Navier-Stokes equation (Hinze, 1975). There are several turbulence models used widely but non of them is superior to deal with all types of flow condition. The choice of turbulence model will depend on considerations such as the flow properties for a specific type of problem, the level of accuracy of the result required, the available computational resources, and the amount of time available for the simulation.

A k-ε model is the frequently used two-equation turbulence model. Here, the partial differential equation for the kinetic energy of turbulence (k) and the dissipation of turbulence (ε) are derived. This two-equation expression yields an eddy viscosity that directly influences the mean flow behavior. It performs well in calculating a wide variety of thin shear layer and recirculating flows with the adjustment of model constants. The turbulent kinetic energy (k) is formulated by adding three normal stresses together.

$$k = \frac{1}{2}[\overline{\sigma_{xx}^{\,2}} + \overline{\sigma_{yy}^{\,2}} + \overline{\sigma_{zz}^{\,2}}] \qquad (4.1)$$

While the Turbulence dissipation rate (ε) is formulated by solving six independent

Reynolds's stresses ($\sigma_{xx}, \sigma_{yy}, \sigma_{zz}, \sigma_{xy}, \sigma_{xz}, \sigma_{yz}$) from the Reynolds's stress tensor σ_{ij}.

$$\sigma_{ij} = \begin{pmatrix} \sigma_{xx} & \sigma_{yx} & \sigma_{zx} \\ \sigma_{xy} & \sigma_{yy} & \sigma_{zy} \\ \sigma_{xz} & \sigma_{yz} & \sigma_{zz} \end{pmatrix} \qquad (4.2)$$

Turbulent dissipation rate (ε), $$\varepsilon = \nu_t \overline{(\frac{\partial u_i'}{\partial x_j})(\frac{\partial u_i'}{\partial x_j})} \qquad (4.3)$$

$$\mu_t = C\rho\ell l = \rho C_\mu \frac{k^2}{\varepsilon} \qquad (4.4)$$

Where, C_μ is a dimensionless constant,

ℓ is the velocity scale and *l* is the length scale of the turbulence.

The kinetic eddy viscosity μ_t is also commonly called the turbulent viscosity. Boussinesq (1877) postulated that the momentum transfer caused by turbulent eddies can be modeled with an eddy viscosity. He assumed the effect of turbulence on the mean flow in the same way as molecular viscosity affects a laminar flow.

Eddy viscosity:

The transfer of momentum caused by the turbulent eddies giving rise to an internal fluid friction, is analogous to the momentum transfer caused by the molecular diffusion (i.e. friction) is modeled with a molecular viscosity. Eddy viscosity is a function of the flow and not of the fluid. It is larger for flows with more turbulence intensity.

Eddy viscosity is also expressed in terms of velocity scale (ℓ) and length scale (*l*) representative of large scale turbulence. These scales are derived from turbulent kinetic energy (k) and dissipation rate (ε). These can also be used to express turbulent Intensity (Versteeg, 1995).

Velocity Scale: $\ell = k^{\frac{1}{2}}$ Length scale: $l = \frac{k^{\frac{3}{2}}}{\varepsilon}$ (4.5)

It is assumed that at high Reynolds's numbers, the rate at which large eddy extract energy from mean flow is equivalent to transfer of energy spectrum to small, dissipating eddies. That's why role of a small eddy variable (ε) is comes into picture in defining large eddy scale (*l*).

4.3 Discretization

The sets of differential equations have to be discretized in space and time by a suitable discretization scheme, which can then be solved using proper software. There are many approaches used commonly to discretize a mathematical model, like finite volume method, finite element method, and finite difference method. Finite Volume Method (FVM) is the robust and inexpensive method commonly used to study open channel flows. In FVM, the spatial domain is discretized into a finite set of control volumes or cells (called as grid or mesh). The general conservation (transport) equations for mass, momentum, energy, etc., are discretized into algebraic equations and then integrated over each control volume as well as solution domain as a whole. The numerical flux is conserved from one discretization cell to its neighbour. The grid can be either unstructured (triangles in 2D, or tetrahedral in 3D) or structured (Meselhe and Sortiropoulos, 2000). Then apply a suitable algorithm on each grid

cell to solve the equations of motion (Euler equations for inviscid and Navier–Stokes equations for viscous flow) to get a discretized conservation equation.

4.4 Convergence

The discretized conservation equations are solved by iterative method. A large number of nested iterations (inner and outer) are usually required to get a converged solution. The inner iterations solve linear equations. In outer iterations, non-linearity of Navier-Stokes equations and coupling of the equations gets solved. A range of physically realistic values can be preset for upper and lower boundaries to get the required converged solution. Convergence is reached when:

- Negligible change occurs in the iterative solution variable from one iteration to the next. Residuals provide a mechanism to help monitor this trend.
- Overall conservation is achieved.

The accuracy and efficiency of a converged solution can be improved by,

- Appropriateness and accuracy of the physical models.
- Grid resolution and independence.
- Selecting suitable Pressure Interpolation Scheme
- Selecting suitable Pressure-Velocity Coupling and Under-Relaxation for the Time-dependent Formulations.

4.5 RNG k-ε model

Renormalization Group Theory (RNG) has been shown by Yakhot and Orszag (1986) to be a powerful tool for turbulence model. *k*- ε equations are derived from the application of a rigorous statistical technique (Renormalization Group Method) to the instantaneous Navier-

Stokes equations. This model renormalizes the Navier-Stokes equations, to account for the effects of smaller scales of motion (Pezzinga, 1994). It is similar in form to the standard k- ε model, but includes the following refinements (Fluent 2002):

- The RNG model has an additional term in its ε equation for interaction between turbulence dissipation and mean shear that significantly improves the accuracy for rapidly strained flows.

- The effect of swirl on turbulence is included in the RNG model, enhancing accuracy for swirling flows.

- While the standard k- ε model is a high-Reynolds-number model, the RNG theory provides an analytically-derived differential formula for effective viscosity that accounts for low-Reynolds-number effects. Effective use of this feature does, however, depend on an appropriate treatment of the near-wall region.

In reality, all scales of motion which occur in the flow will contribute to the turbulent diffusion. This turbulent diffusion is determined in terms of eddy viscosity to represent a numerical model. The transport equations used in RNG k- ε model make an attempt to determine different scales of motion through changes in production term (Choudhary, 1993). While in standard k- ε model the eddy viscosity is determined from a specified single turbulence length scale. RNG k- ε model shows good results for moderately complex behaviour like jet impingement, separating flows, swirling flows, and secondary flows.

The partial differential equations are derived for turbulence kinetic energy, k, and its rate of dissipation, ε .The general form of k or ε equation is represented as follows (Versteeg 1995),

Rate of change of ε or k	+	Transport of ε or k by convection	=	Transport of ε or k by Diffusion	+	Rate of production of ε or k	−	Rate of Destruction of ε or k
(I)		(II)		(III)		(IV)		(V)

Turbulence kinetic energy:

$$\frac{\partial(\rho k)}{\partial t} + div(\rho k U) = div[\alpha_k \mu_{eff}\, grad(k)] + 2\mu_t E_{ij}.E_{ij} - \rho\varepsilon \qquad (4.6)$$

(I) (II) (III) (IV) (V)

Dissipation rate :

$$\frac{\partial(\rho\varepsilon)}{\partial t} + div(\rho\varepsilon U) = div[\alpha_\varepsilon \mu_{eff}\, grad\,\varepsilon] + C_{1\varepsilon}^{*}\frac{\varepsilon}{k}2\mu_t E_{ij}.E_{ij} - C_{2\varepsilon}^{*}\rho\frac{\varepsilon^2}{k} \qquad (4.7)$$

Where,

Eddy viscosity (μ_t) :

$$\mu_{eff} = \mu + \mu_t$$
$$\mu_t = \rho C_\mu \frac{k^2}{\varepsilon} \qquad (4.8)$$

Other auxiliary relations:

$$C_{1\varepsilon}^{*} = C_{1\varepsilon} - \frac{\eta(1-\frac{\eta}{\eta_0})}{1+\beta\eta^3} \qquad \eta = (2E_{ij}.E_{ij})^{\frac{1}{2}}.\frac{k}{\varepsilon} \qquad (4.9)$$

The equation contains five adjustable constants: $\alpha_k, C_\mu, C_{1\varepsilon}, C_{2\varepsilon}, \alpha_\varepsilon$

$C_\mu = 0.0845;$ $C_{1\varepsilon} = 1.42;$ $\beta = 0.012;$

$\alpha_k = \alpha_\varepsilon = 1.39;$ $C_{2\varepsilon} = 1.68;$ $\eta_0 = 4.38$

4.6 Free surface modeling

Most of the free surface modeling problem are solved by VOF (Volume of Fluid) scheme. The VOF is a common technique used in CFD programs based on the finite volume method (Fig. 4.1), in which a local volume fraction is calculated. In FLUENT, the volume of fluid (VOF) model was adopted. The basic assumption made in this scheme is as follows. In this approach, two or more fluids can be modeled by solving one set of momentum equations for all fluids and for turbulent flows; a single set of turbulence transport equation is solved. The Interface tracking scheme is used to locate free surface flow. It is assumed that two or more fluids in the flow domain are not interpenetrating. The Navier Stoke equations are solved in either Cartesian or cylindrical coordinates.

Interface capturing scheme:

The computation is performed on a fixed grid. The motions of the water surface are linked with grid geometry. The shape of a water surface is defined by cells those are filled with fluid (Ferziger, 2002). Each grid cell in the flow domain may represent the same or the combination of phases. The VOF method is based on a function (F) in which, a unit value of F indicates a cell full of fluid, while a zero value indicates that the cell contains no fluid or that the cell is empty. The cells with F values between zero and one must then contain a free boundary (Ferziger and Peric, 2002). The normal direction to the boundary is indicated by the direction in which the value of F changes most rapidly. The function F is defined as follows,

$$F = \frac{\delta\Omega_{water}}{\delta\Omega_{cell}} = \frac{Volume\ of\ cell\ \ filled\ with\ water}{Volume\ of\ computational\ cell}$$

Limitation of VOF:

To locate the exact location of the water surface level, VOF requires a fine mesh near the water surface and the boundary. A coarser mesh near water surface may give wrong results.

4.7 Numerical model validation

A 3D numerical multiphase turbulent side weir model was developed in ANSYS 12 by the volume of fluid (VOF) scheme using a finite volume approach (FVM). The side weir model geometry construction and grid generation was done using ANSYS ICEM CFD 12.0.1 with 298,500 cells. Generation of a good quality grid is the basic part of the numerical modeling and it requires skill. The local density, smoothness in distribution, aspect ratio, and skewness of the cells were checked for all cell configurations. The region of the side weir and some part of the downstream channel were made finer to accommodate dividing streamline, stagnation point and flow separation zone with acceptable accuracy. Grid independence study was done initially for the coarse mesh size. Model was then exported to ANSYS 12 (Fig.4.1 and Fig.4.2).

The viscous model created in the Cartesian coordinate system and is discretized in space and time using second order upwind scheme. A system of differential equations, including continuity equation, energy equation, momentum equation, and turbulence equations are solved. The Renormalized (RNG) k-ε model is employed for the present study. As the flow involves stagnation and separation zone, the PISO algorithm mentioned below was chosen for the pressure discretization over SIMPLE and PRESTO! schemes (Fluent 2002) for the present study .

PISO Algorithm:

The PISO (Pressure Implicit with Splitting of Operators) is a pressure-velocity calculation procedure designed for non-iterative computation of the unsteady flow. The PISO algorithm provides improved performance over SIMPLE and SIMPLEC algorithms. The steady state PISO algorithm has an extra correction step in addition to SIMPLE algorithm which shows a robust convergence and requires less computational effort (Issa, 1986). The PISO algorithm solves the pressure correction equation twice requiring additional storage for calculating the source term of the second pressure correction equation. Although this method involves additional computational effort, it has been found to be efficient and fast.

Non-equilibrium wall function:

Launder and Spalding (1974) provide details of wall functions, which can be classified into the standard equilibrium log-law and non-equilibrium wall functions. A Non-equilibrium wall function is adopted to deal with the severe pressure gradient effect of velocity near smooth vertical walls (Fluent 2002). It has shown improved predictions in complex flows representing, flow separation, flow reattachment, and jet impingement over standard wall functions. Usually, FLUENT computes the near-wall values of the Reynolds stresses and the turbulent dissipation rate, ε from the wall functions. These quantities can be input directly into CFD program or derived from the turbulence intensity and characteristic length. The explicit wall boundary conditions were adopted for the Reynolds stresses by using the log-law and local equilibrium assumptions were specified.

The cells neighbouring the wall are assumed to consist of a viscous sub layer and a fully turbulent layer. The non-equilibrium wall function uses the two-layer concept while computing the turbulence kinetic energy at the wall-adjacent cells, which is needed to solve the k equation at the wall-neighbouring, cells (Fluent 2002).

Boundary Conditions:

Boundary conditions for modeling consist of the inlet boundary, the outlet boundary and the wall boundaries.

The inlet boundary is defined at the inlet section with a known depth of water entering the flow domain with uniform inlet velocity. The channel lengths at upstream and downstream sections used for the experimental investigation can be reduced in order to decrease the computational time. It can be done by introducing exact velocity distribution across the inlet cross section (boundary) by writing user defined functions (UDF). The inlet velocity and inlet water depth measured from the experiment were used as the inlet boundary conditions. The static pressure, total pressure and total temperature were specified at the inlet boundary. The turbulence kinetic energy was adopted as 10% of the inlet kinetic energy and the dissipation length is taken corresponding to hydraulic diameter at the inlet.

The outlet boundary was defined as the pressure outlet used to specify a static gauge pressure at the boundary. The fluid from the flow domain is exited from these outlet boundaries. The rate of production of turbulent kinetic energy k near the free surface is negligible because turbulent eddies gets knocked out near the free surface causing reduction in the velocity fluctuations in the vertical direction.

The flow domain is divided into two phases, air and water. Air was considered as the secondary phase. For the flow domain containing air and water as the phases, the reference pressure location was kept in the portion of the domain filled with air rather than that filled with water, this is because variations in the static pressure are larger in a more dense fluid than in a less dense fluid for the same velocity distribution.

For VOF calculations, the operating density was set as the density of the lightest phase (air) [Hirt and Nicholls, 1981]. The domain was solved using second-order upwind scheme (Buyer et al, 2002). The second order unsteady explicit formulation and standard under-relaxation parameters were considered. In order to achieve convergence, suitable under-relaxation factors have been employed for the governing equations with typical value of, 0.4 for the momentum and 0.3 for pressure. Under relaxation factor of 0.7 was taken for turbulent kinetic energy and turbulent dissipation rate equation.

The numerical solution was considered converged when the residuals of the discretized transport equation reached a value of 1×10^{-5} for all variables including pressure, velocity, turbulent kinetic energy and turbulence dissipation rate or when the solution did not change with further iterations. The iterative numerical solution requires criteria for determining the convergence of the acquired solution. For the simulations with an unsteady solver, the difference in the mass flow rates at the flow inlet and the outlet was monitored to be less than 0.01% in the final solution. The inlet flow domain is patched with inlet velocity along with initialization of turbulence quantities such as turbulence kinetic energy and Turbulence dissipation rate as 1 m^2/s^3.

The flow domain was then computed specifying a minimum number of iterations for chosen

small time steps. The solution was started with a laminar model. After the convergence was ensured for the laminar model, results of the simpler models were used as initial values for more complex turbulence models [Renormalized (RNG) k-ε model]. As before, the convergence criteria for turbulence model was considered converged when the residuals of the discretized transport equation reached a value of 1×10^{-5} for all variables including pressure, velocity, turbulent kinetic energy and turbulence dissipation rate.

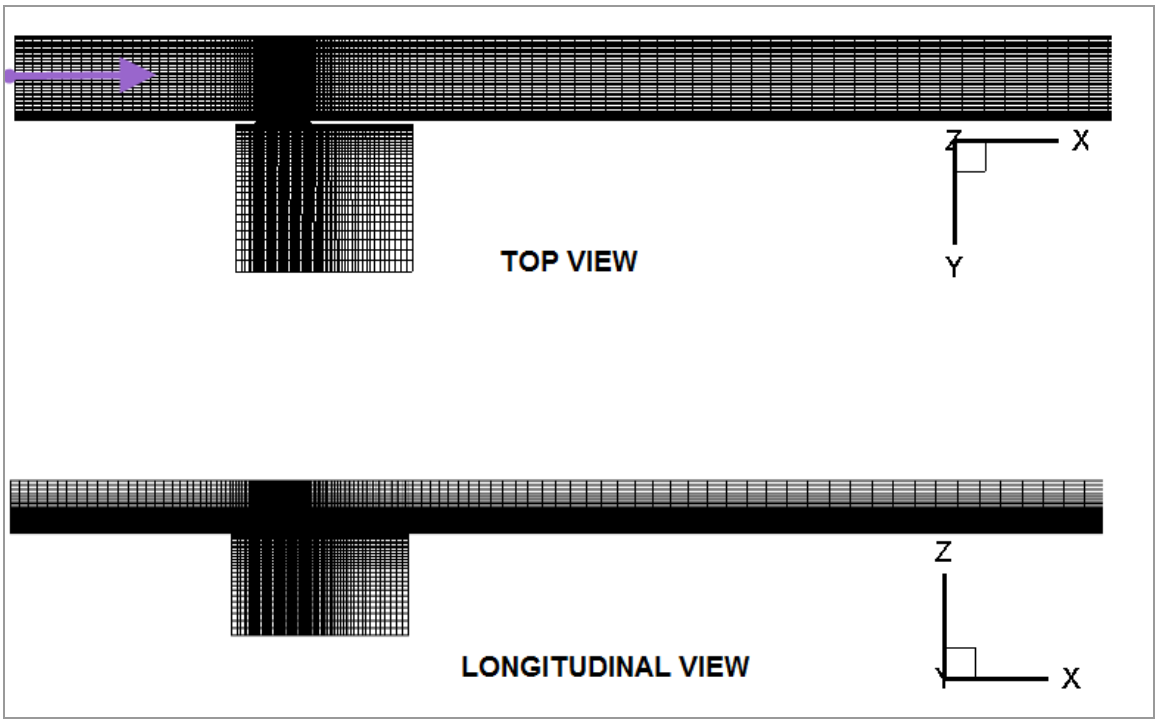

Fig. 4.1: Grid for the rectangular side weir simulation.

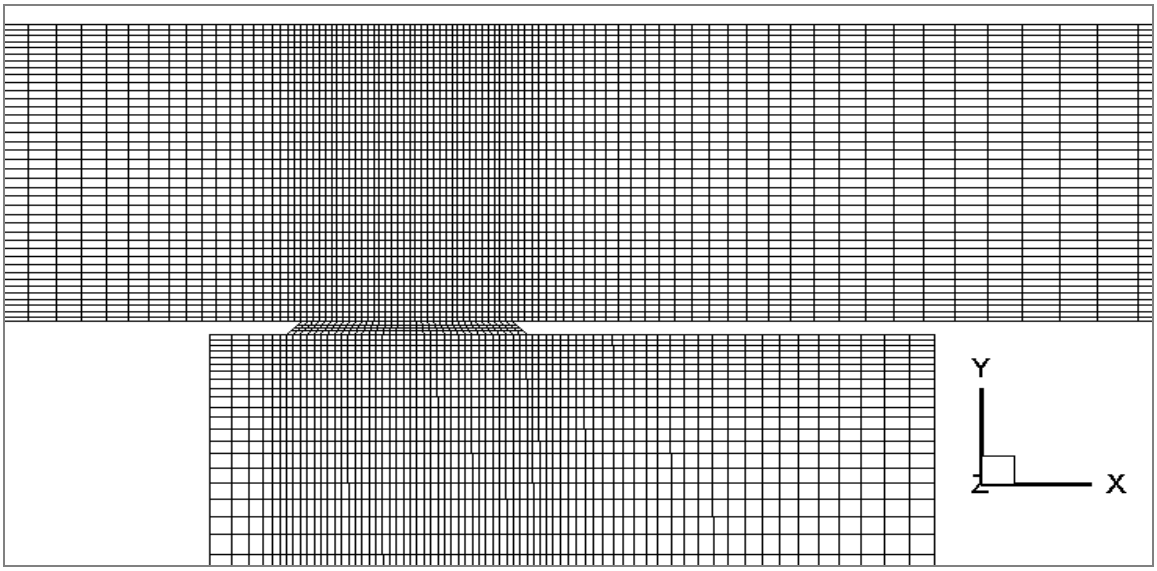

Fig. 4.2: Enlarged grid view at side weir section.

Table 4.1 Computational grid

Software	**Model**	**Grid dimensions**	**Domain size (m^3)**	**Domain**
ICEM ANSYS 12.0	RNG k-ε	260 x 40 x22 = 228,800	4.36 x 0.286 x 0.18 =0.2244 m^3	Main channel
ICEM ANSYS 12.0	RNG k-ε	50 x 2 x22=2,200	0.175x 0.012 x 0.18 =0.0003 m^3	Side weir exit
ICEM ANSYS 12.0	RNG k-ε	75 x 30 x30=67,500	0.45 x 0.5 x 0.5 =0.1125 m^3	Side weir box

CHAPTER 5

RESULTS AND DISCUSSION

The present study deals with the side weir flow parameters such as the location of stagnation point, the stagnation streamline, the separation flow region and the discharge coefficient. These parameters were determined using the following methods for a specific weir flow configuration,

1. Theoretical results: Verification of test data related to stagnation point on side weir wall with the theory proposed by Michell (1890) based on ideal flow theory.

2. Experimental results: The stagnation zone, separation zone, dividing streamline and the exiting jet contraction coefficient for the exiting jet were determined for a specific flow configuration.

3. Numerical modeling: Some of the flow parameters are also determined using 3D RNG k-ε turbulence modeling. The free surface was determined by using the VOF scheme. The commercial software used was ANSYS 12.

4. Flow visualization methods based on dye injection tests.

5.1 Experimental verification of the prediction of stagnation points

5.1.1 Experimental approach:

Some part of the flow approaching the weir is taken out from the side weir while the through flow moves forward in the downstream channel (Fig. 5.1). The exiting flow slightly overshoots the dividing streamline S_LPS' of (Fig.2.2) separates the through flow and the weir

flow. Test data indicated that position of the stagnation point (S_{TE}) of Fig.5.11.b varies slightly along the depth of the flow as the flow is 3D. As such, the location of S_{TT} is not very precise.

For purposes of analysis, the flow is considered to be 2D to locate the approximate position of the streamlines in the flow field. Very close to the weir the flow was far from 2D and hence the assumption of 2D is not strictly valid there. The procedure discussed in section 3.3 is adopted to trace the stagnation streamline. The stagnation streamline meets the near wall at the theoretical stagnation point (S_{TT}) in Fig. 2.2. At S_{TT}, the velocity is zero. For the flow configuration shown in Fig. 2.2, flow on the right side of the streamline $\mathbf{S_L}$ (facing downstream) emerges out from the side weir, while the flow from the left side of $\mathbf{S_L}$ to denote the through flows. The latter continues to flow in the channel downstream of the weir. As mentioned earlier flow very close to the weir is not 2D and hence streamline patterns in these zones are not very accurate and as such they are shown in dashed lines.

5.1.2 Verification of stagnation point using Michell's Mathematical equation

The location of the stagnation point S_{TT} at Z=6 cm on the wall was estimated to be at a distance X*=0.060 from the edge T_2 of the 2D outlet (Fig. 2.2). This value was computed using eqn. 2.4 proposed by Michell (1890). This result is in a good agreement with the experimentally estimated value of X*=0.076 for the distance of the stagnation point from the edge T_2 of the weir outlet (Fig. 5.9). The discrepancy in these two estimates can be traced to the following facts,

- Flow in the test flume has a free and the flow is strictly not 2D near the side weir.
- The theoretical estimate is based on ideal flow theory for a 2D outlet.

The contraction ratio for the jet exiting the weir outlet was observed to be 0.70.

5.2 Comparison of experimental results with numerical model predictions

5.2.1 Water surface profiles:

Table 3.1 provides the details related to the specific flow configuration. Fig. 5.1.a shows the cross sections near the side weir regions where the water surface profiles were determined. Figs. 5.3 a, b and c show the non-dimensional flow depth z/B as a function of the non-dimensional distance y/B at three different channel cross sections AC, GH and ED (Fig.5.2). Figs.5.4. a and b show the water surface profiles along the weir length AGE and BIJF (Fig.5.2). These results show that the predictions of the present numerical simulation compare well with the present series of test results and those of Subramanya and Awasthy (1972) for water surface profiles. The experimental channels in the two series of tests were geometrically similar. The water surface profiles were taken across three cross sections and along the two longitudinal sections of the channel (Fig.5.2.a). These data are in very good agreement with the numerical model predictions marked by solid lines (Fig. 5.3 and Fig. 5.4).

Fig. 5.5.b shows the contour plot of the measured water surface profile for the side weir problem with a discharge ratio of Q_R=0.792. It shows the overall variation of the water surface. There is a qualitative agreement between the experimental value and model prediction. For instance, the depth of the approach flow remains nearly unaltered until X*=1.60 in the simulation compared to X*=1.40 in experiment. Similarly, for the far wall, flow depth remains unaltered till X*=0.25 and X*= -0.80 for simulation and experiments respectively. The flow across the weir varies from 0.27 to 0.35 in both cases. As mentioned

earlier, as flow approaches the weir it loses it's two dimensionality.

For subcritical flow (F_R<1), along the near wall AG, the water surface profile rises from the upstream edge T_1 to the downstream edge T_2 of the side weir. Near the entrance of the weir (Fig. 5.2.a), the flow accelerates and hence the depth decreases at T_1. Since the discharge per foot width in the downstream section is much less, the depth in the downstream channel increases. As such, the depth at the end of the weir T_2 is higher than at the entry of the weir T_1 (Fig. 5.4.b). As mentioned earlier the flow exiting the weir is 3D and tends to become 2D in the channel downstream. As the flow expands in the channel downstream of the weir, the resulting adverse pressure gradient causes the flow to separate from the far wall (Fig. 5.10). In fact, in the vicinity of the far wall, velocity data indicated that, a separation zone is formed in this region (Fig. 5.9). The details of determining the separation zone are provided in section 3.3. Since the flow is very unsteady near the reattachment point R on the far wall, the estimate of the length "Ls" of the separation zone is not very accurate. It is estimated that the errors in determining "Ls" is in the order of 6%. The width w of the separation zone was estimated by determining the maximum width of this zone (Fig.5.9).

5.2.2 Velocity profile:

In Fig. 5.2.b, the nine grid locations a to i for velocity measurements are indicated. They correspond to three cross sections located at X*=X/B=1.171, 0.751, 0.297. Besides these three longitudinal sections at Y*= Y/B =0.839, 0.490, 0.140 were also chosen for velocity measurement. Figs. 5.6 a to i show the experimental velocity profiles at these selected locations it terms of the variable $u^* = u / \bar{u}$ as a function of Z/B. The earlier data of Subramanya and Awasthy (1972), corresponding to tests in a geometrically similar model is

also presented in fig 5.6. It may be recalled that they used Pitot tube for velocity measurements. There is a good agreement between the present model predictions and the experimental data based on present and earlier tests.

Vector plot (u and w):

Fig. 5.7.a show the vector plot denoting the resultant of the axial velocity of u and the lateral velocity w at the horizontal plane z = 6cm. Location of the stagnation point was observed at X*=0.076 from the downstream edge T_2 of the side weir at Z*=0.209. As stated earlier, location of the stagnation point for a 2D outlet was 0.060 obtained from equation 3.4. The corresponding value for X* was 0.091 in the numerical model. Fig. 5.8.a show the vector plot denoting the resultant of the axial velocity of u and the lateral velocity w at the horizontal plane z = 7cm. Location of the stagnation point was observed at X*=0.070 from the downstream edge T_2 of the side weir at Z*=0.244 (Fig. 5.8.a).

5.2.3 Dividing streamline and Stagnation point

The envelopes of the vectors yield the streamlines (Fig.5.9 and Fig.5.10). The particular streamline separating the through flow and the weir flow denotes the dividing streamline. This dividing streamline GPS' divides the weir flow and the through flow. Extrapolating the dividing streamline up to the wall provides the stagnation point S_{TS} based on simulation. This procedure was also used to locate the stagnation point S_{TE} based on experimental data (Fig.5.9). As mentioned earlier, procedure for locating streamline is based on two dimensional flow. Further, the flow was observed to be slightly unsteady near the stagnation zone, as observed during dye injection tests. As such, near the weir outlet where the flow deviates from two dimensionality, some errors are present in determining S_{TS}. Hence, only an

approximate location of the stagnation point S_{TS} (Fig. 5.9) is obtained on the basis of streamline analysis. However, there is a reasonable agreement between the experimental, theoretical and simulation values of the stagnation point location (Fig. 5.11.b and Table 5.4). Figs. 5.9 and Fig. 5.11 a to d provide the streamline pattern developed on the basis of experimental data and model for different horizontal planes at a fixed discharge ratio.

The dividing streamline is strikes the near wall of the channel at the stagnation point. The location of the stagnation point is verified by experimental, theoretical and simulation results and they are represented as S_{TE}, S_{TT} and S_{TS} respectively. Fig. 5.9 shows the location of the stagnation point (S_{TE}) striking on the downstream side weir wall at X/B= 0.076. Fig.5.10.b shows the location of the stagnation point (S_{TE}, S_{TT} and S_{TS}) by three methods. The theoretical location of the stagnation point S_{TT} is observed in good agreement with the experimental value. Table 5.1 shows the comparison of values obtained from different methods. The simulation value of the stagnation point is found to be slightly downstream than the experimental value X*=0.091 (Fig. 5.11.b). The locations of the stagnation points at different depths are not along a vertical line. Compared to its location at the channel bed (0.084), the distance of the stagnation point is slightly closer to the end of the weir at the free surface (0.063).

5.2.4 Separation zone:

The procedure discussed in section 3.3 was adopted to trace the separation streamline and identify the flow separation region SDR in Fig. 5.9. The recirculation region (C_R) starts from the separation point 'S' which is on the far wall and terminates at the reattachment point 'R'. Location of R was estimated by noting the region where the velocity was zero. The flow was

slightly unsteady near the reattachment region. Location of the reattachment point was confirmed using flow visualization. At the location of reattachment point, the injected dye had a tendency to move forward or backward. The length of the separation zone L_S was approximately three times the width B of the channel. The width of the separation zone W_S is as 0.3B.

Fig 5.12 shows three dimensional view of the separation zone determined by the trace of streamlines. As mentioned earlier, the flow loses its 3 dimensionality in the zone of separation and in the vicinity of the weir. As such, the dimensions of the separation zone determined on the basis of streamline analysis are rough estimates.

In the separated region, backflow covers considerable distance/height from the bottom surface and extends almost the total length of the separation zone. Turbulence and shear stress increases downstream in the mixing region.

5.3 Turbulence modeling:

Results of the experimental investigation are compared with the predicted results of the RNG k- ε model in ANSYS commercial software.

The solid lines in Figs.5.3 a to c and Figs.5.4 a and b show the water surface profiles obtained from numerical simulation. The agreement between predicted values and experiment value are very good for all the sections considered. Fig. 5.5.a presents the contour plots of the predicted water surface level from VOF model. Compared to experiment depth data, the maximum error in prediction of depth from numerical simulation was of the order of 5% (Fig.5.6).

Solid lines in Figs. 5.6 a to i show the velocity distribution obtained from numerical simulation. The velocity vector plots of the resultant of u and w (Fig. 5.7.b and Fig. 5.8.b) show that the model was able to predict the measured test data with reasonable accuracy. The dividing streamline configuration based on experimental data is quite similar to model predictions (Fig.5.9 a and b). In simulation, the zone of separation was observed near the far wall as in the experiment. However the RNG k- ε model was not able to locate the reattachment point (Fig.5.10). Only the width W_S of the separation zone could be determined by the model. Its value was close to the experimental value of 0.3B (Table 5.1).

Fig. 5.11 a, b, c and d presents streamline layout in a horizontal plane. Streamlines are originated from the inlet section of the weir. The channel width is divided into 27 number of stream channels and it is observed that around 80% of the flow was taken out from the side weir and remaining through flow towards downstream end of the channel. The stagnation streamlines from Fig.5.13 are originated from different Y* values. The distance of the stagnation point from the downstream edge of the weir was slightly different at different depths. This indicates deviation of the flow from two-dimensionality in the vicinity of the weir.

5.4 Flow Visualization

The locations of the dividing streamline, stagnation point and the separation zone were also confirmed by flow visualization tests. At the reattachment point, the injected dye had a tendency to move forward or backward and the flow was generally unsteady. As such, only an estimate of the reattachment point could be made. However the data indicated that the estimate was reasonable (Table 5.2).

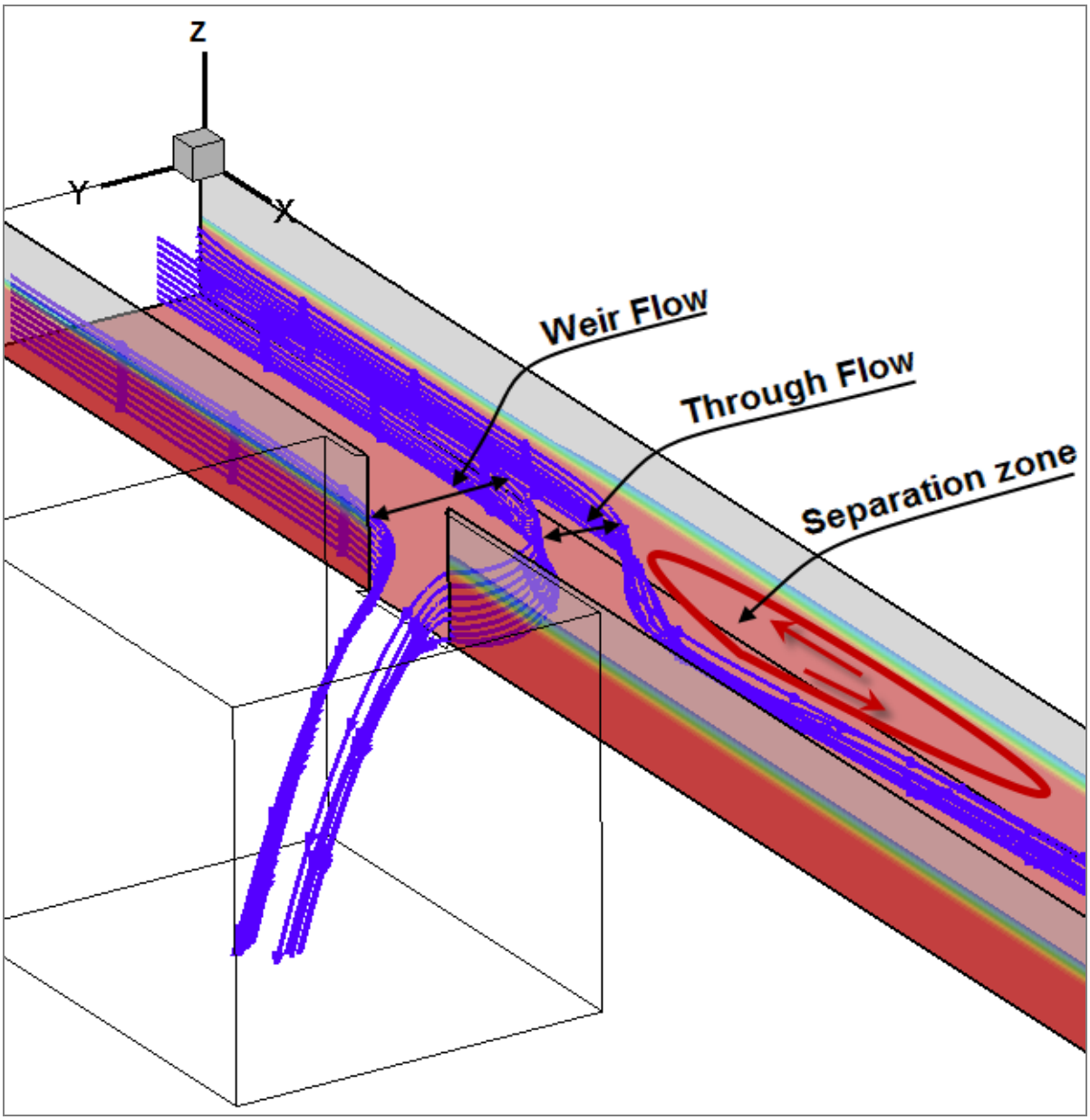

Fig. 5.1: Trace of streamlines in the planes (z= 0 to 0.1m) showing the downstream and the through flow weir flow forming a separation zone

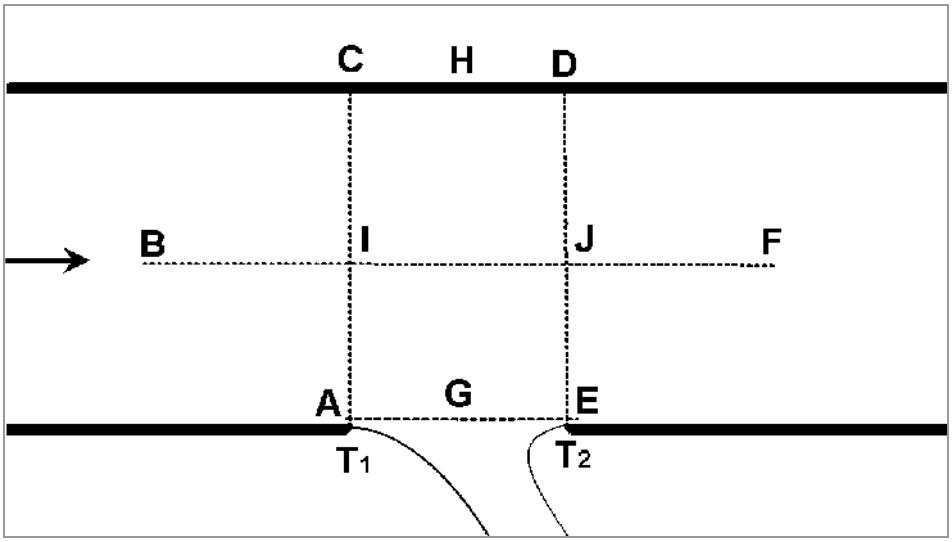

Fig. 5.2.a: Selected measuring locations for water surface profiles

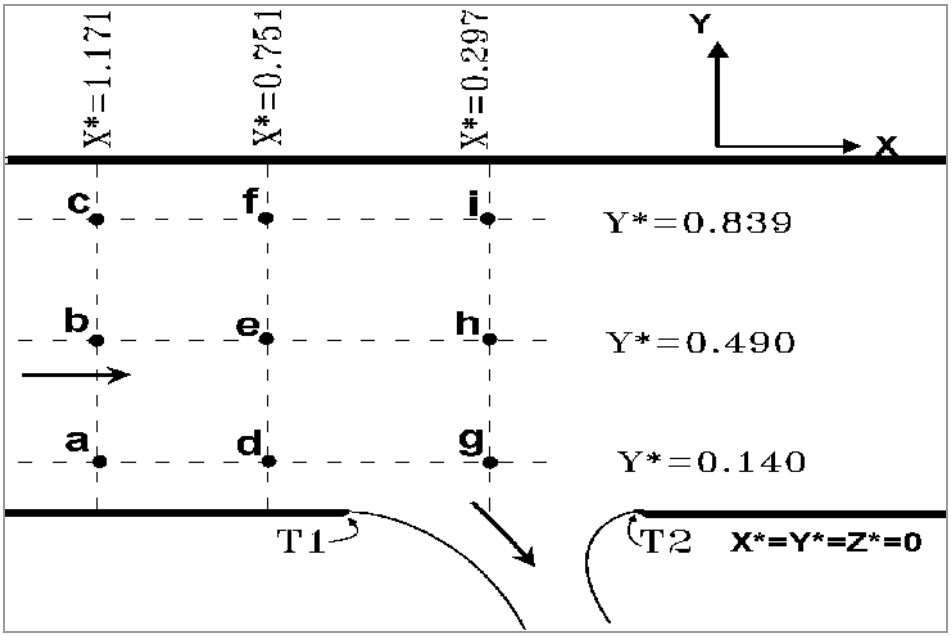

Fig. 5.2.b: Selected measuring locations for velocity profiles, X*=X/B, B=0.286m.

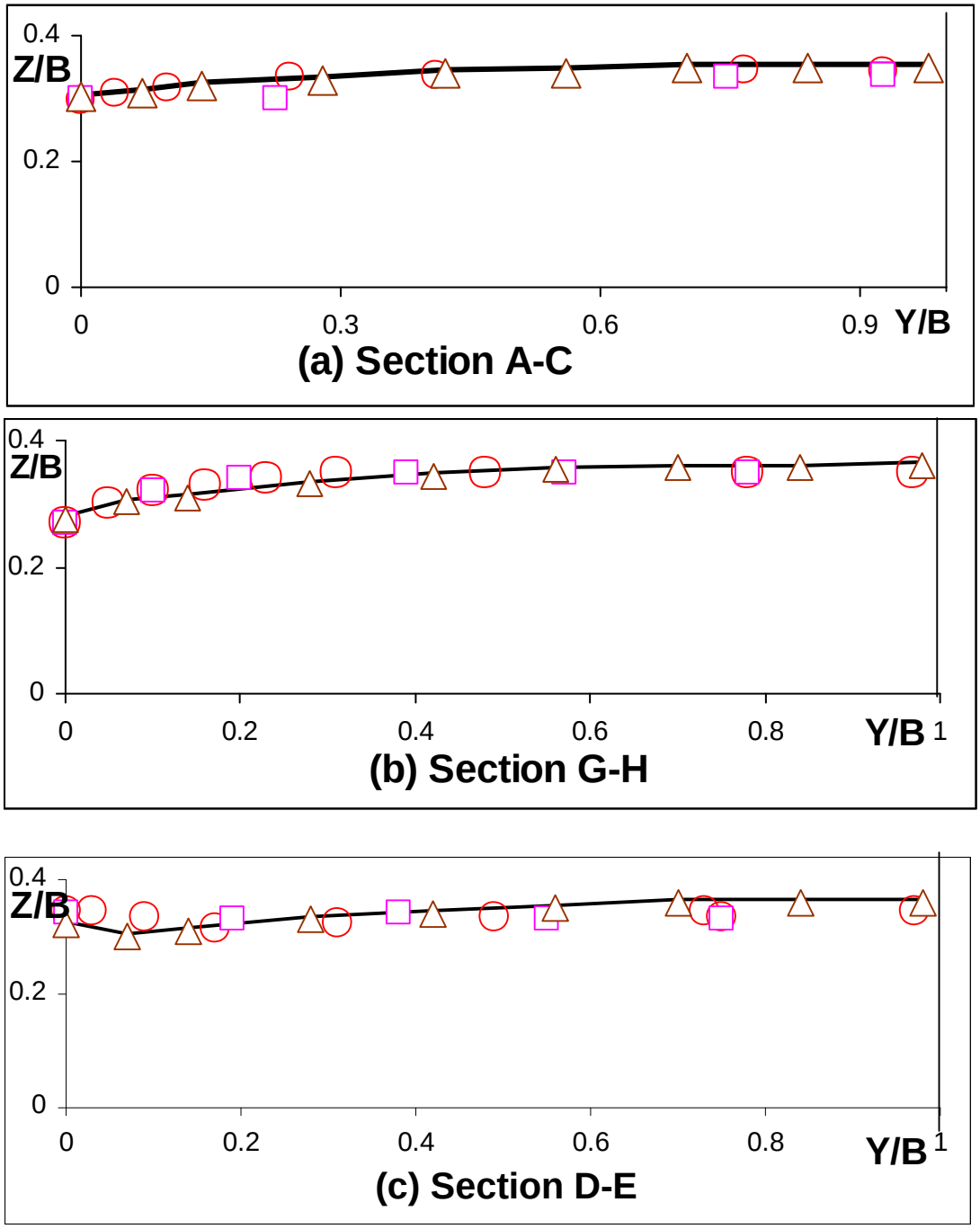

Fig. 5.3: Water surface profiles across the channel, (Q_R=0.792), F_R =0.40 a) AC (weir entry), b) GH (weir center), c) DE (end of weir) ○ Qu- simulation (2005) △ Present test □ Subramanya and Awasthy- test (1972) —— Present simulation.

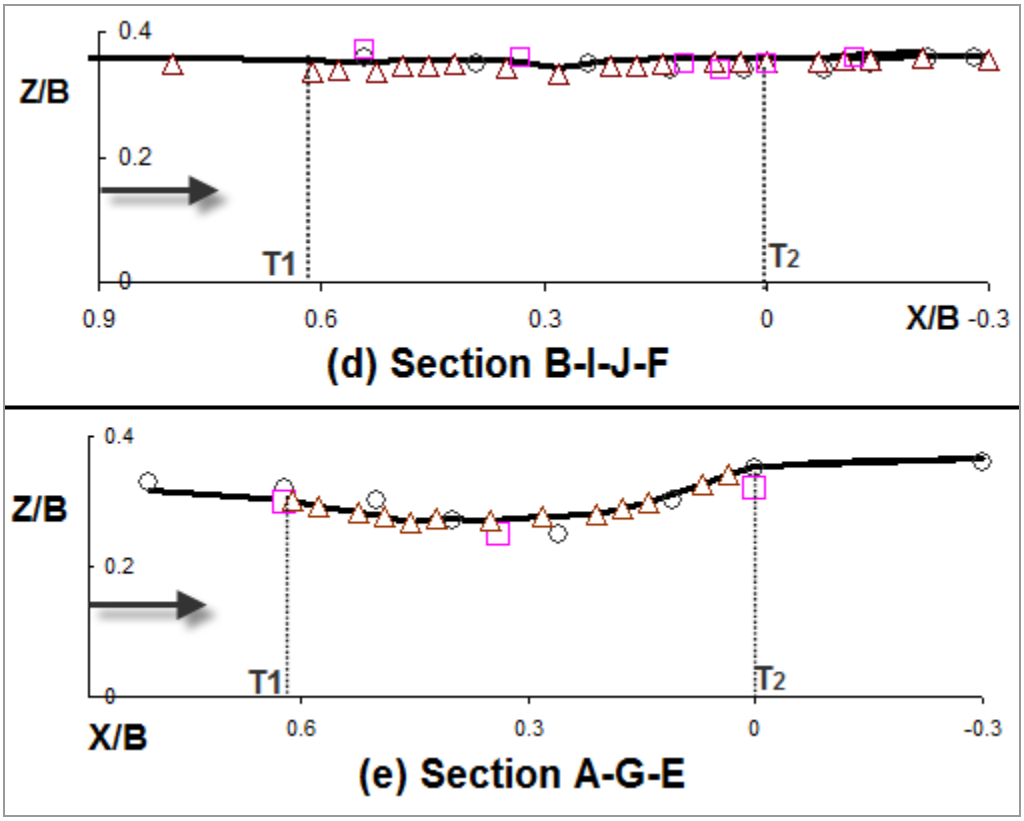

Fig. 5.4: Water surface profiles along the length of the channels.

a) BIJF (along centerline of channel) b) AGE (along near wall)

○ Qu- simulation (2005) △ Present test

□ Subramanya and Awasthy- test (1972)

—— Present simulation.

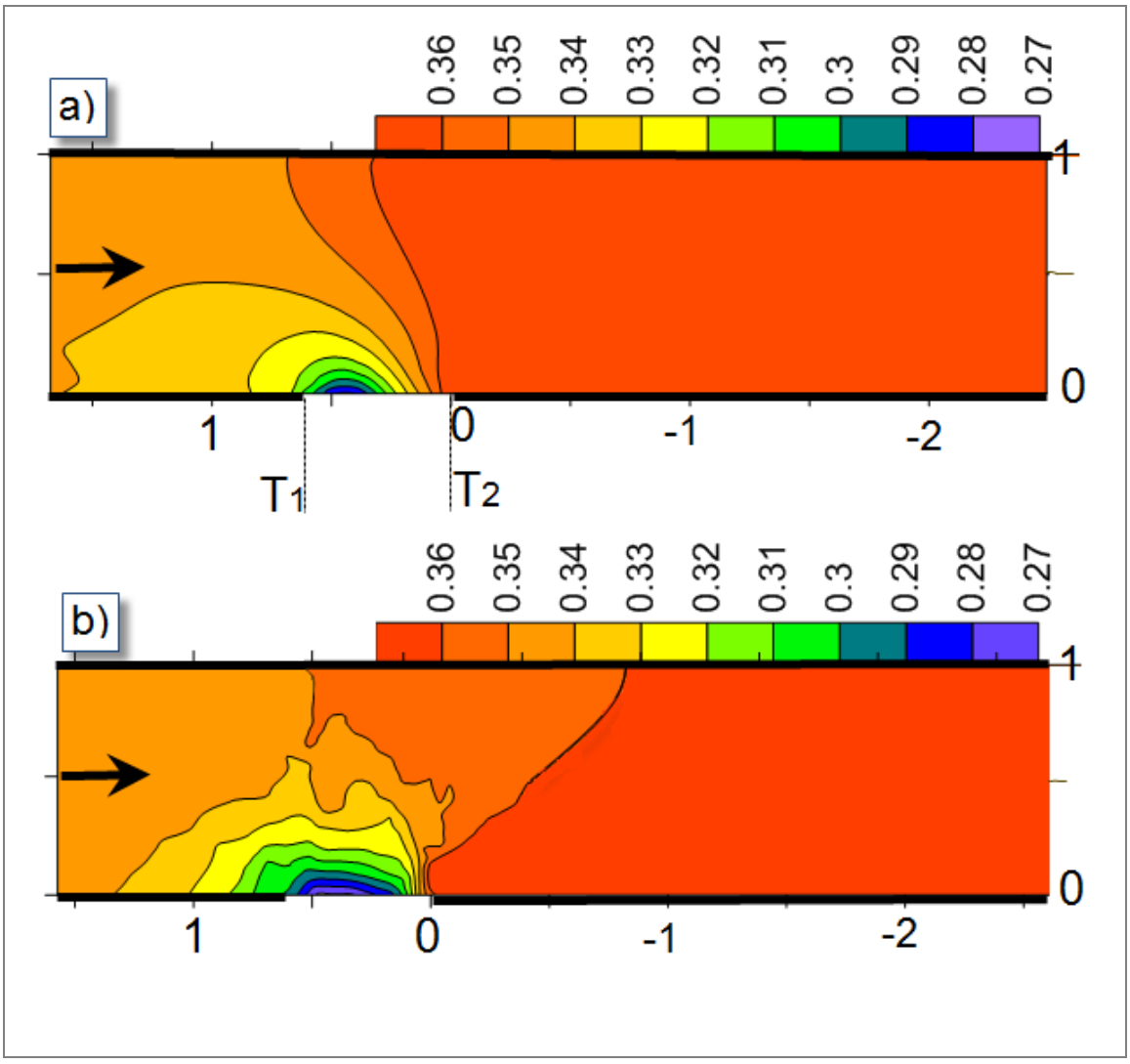

Fig.5.5 Water surface profile contours for the side weir (Q_R=0.792).

(a) Numerical simulation result (b) Experimental result

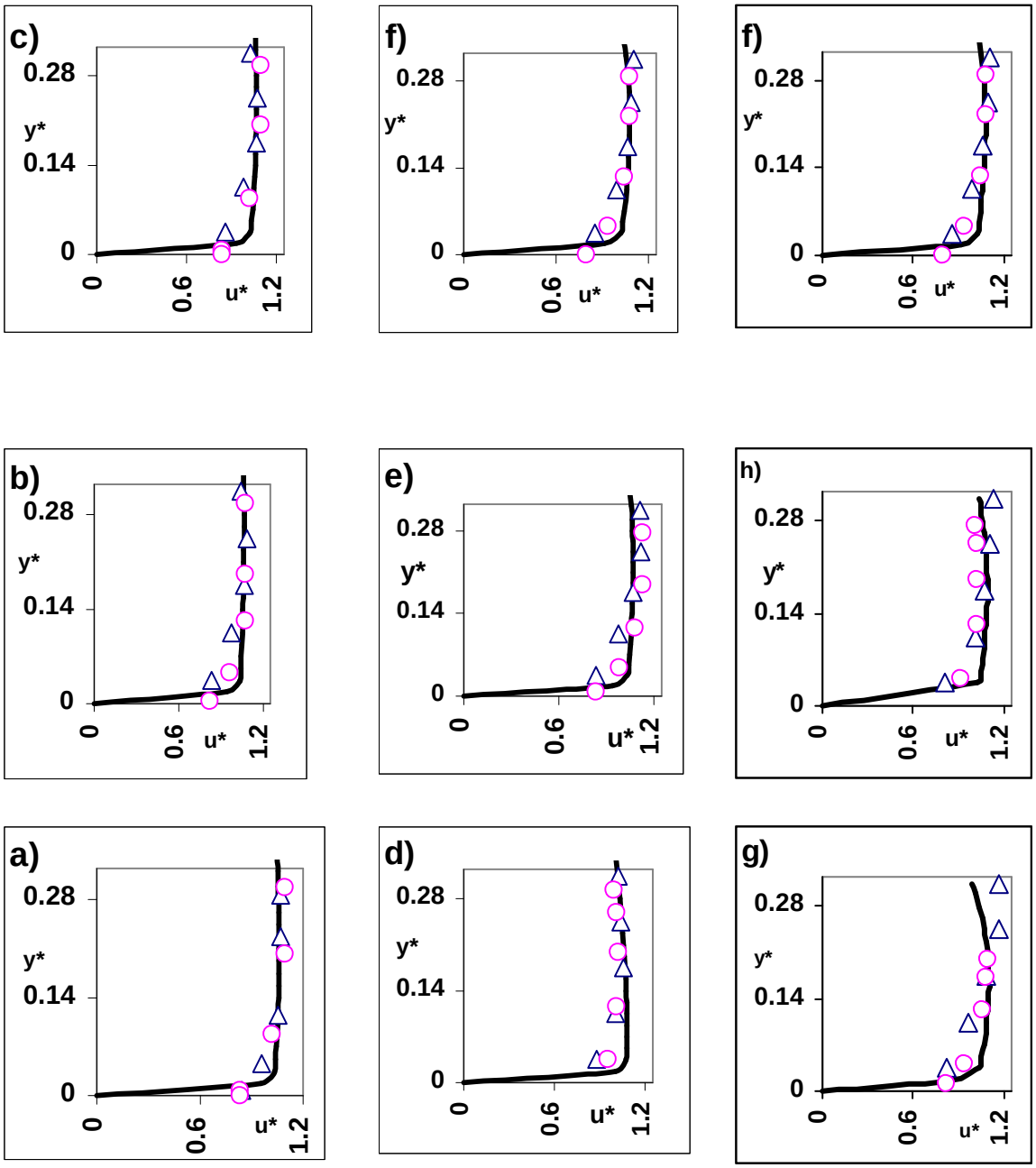

Fig. 5.6 Velocity distribution at selected cross sections, u*=u/ū

△ **Present test results**

○ **Subramanya and Awasthy test results (1972)**

——Present simulation results.

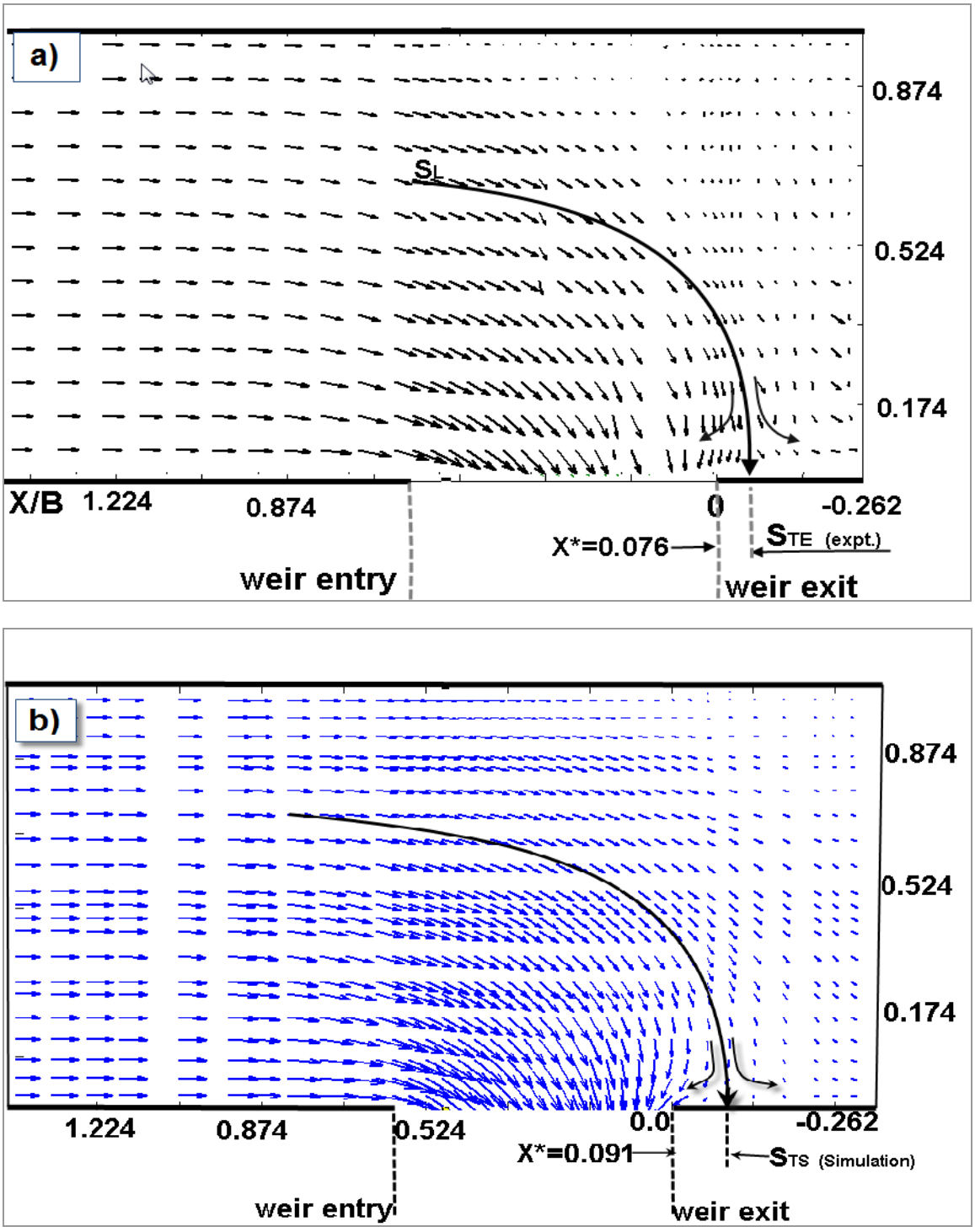

Fig. 5.7: Velocity vector plot of the resultant of u and w (F_R=0.4 and Z*=0.209) a) Experimental data-Q_R=0.792 b)Numerical simulation- Q_R=0.811

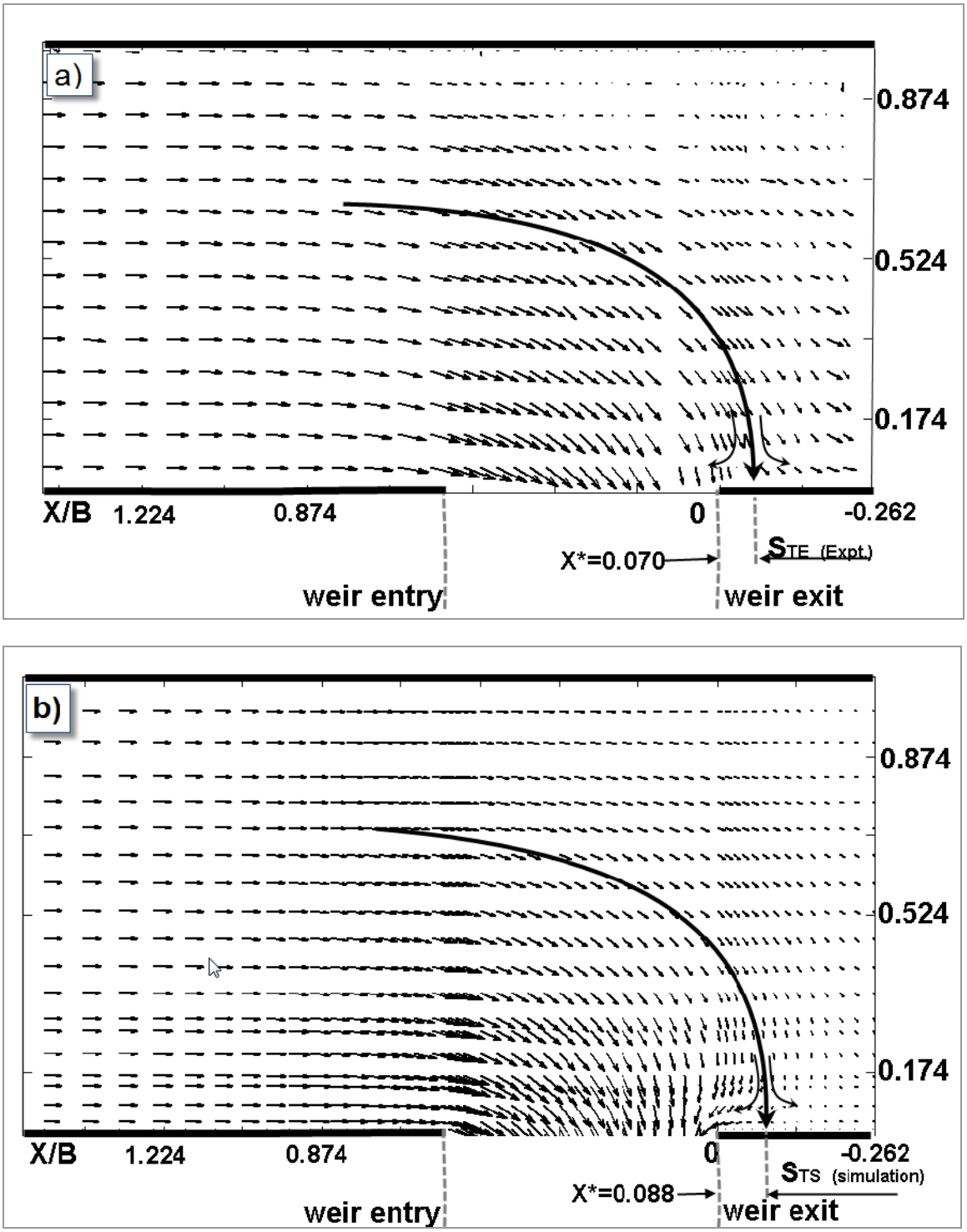

Fig. 5.8: Velocity vector plot of the resultant of u and w (F_R=0.4 and Z*=0.244) a) Experimental data-Q_R=0.792 b) Numerical simulation- Q_R=0.811

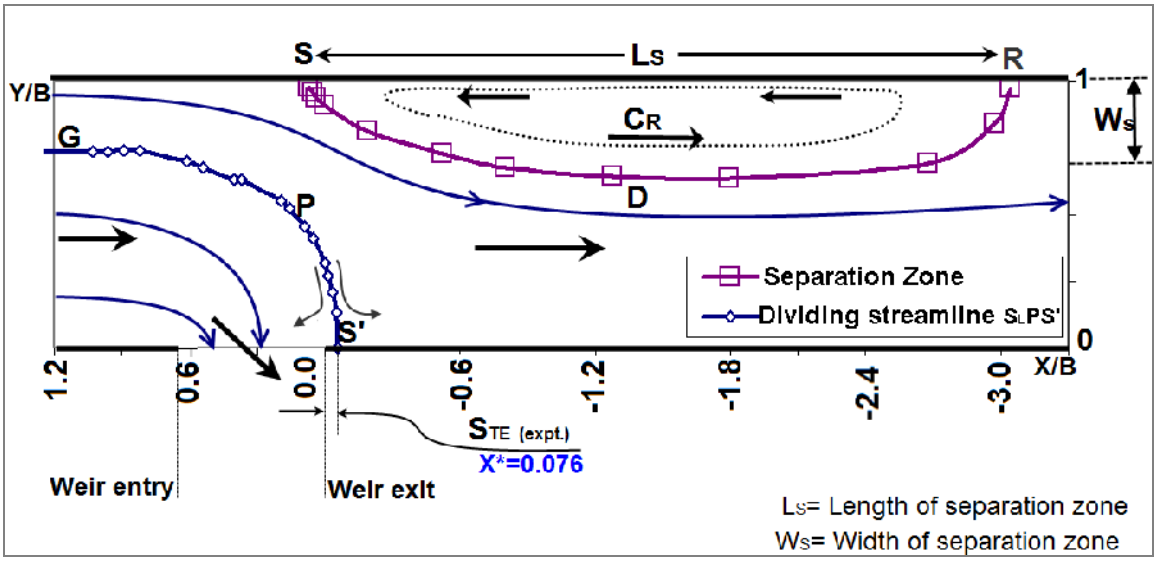

Fig. 5.9: Experimental results: Stagnation point S_{TE} at z*=0.209, Q_R=0.792, F_R=0.40 (expt.) and separation zone SDR.

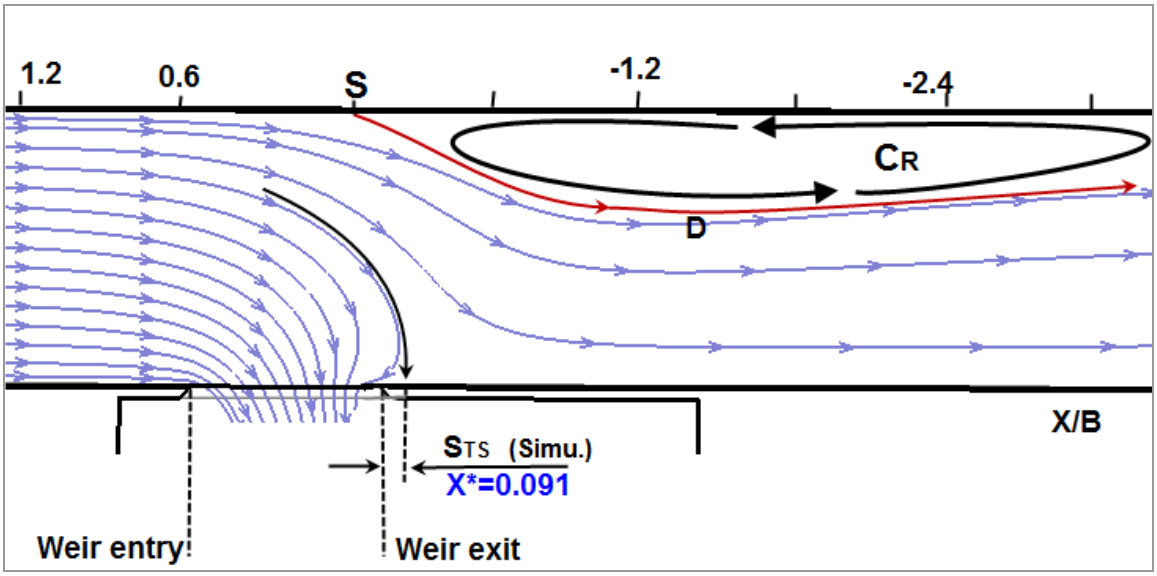

Fig 5.10: Simulation results: Layout of streamlines near side weir and formation of separation zone at z*=0.209, Q_R=0.811, F_R=0.40.

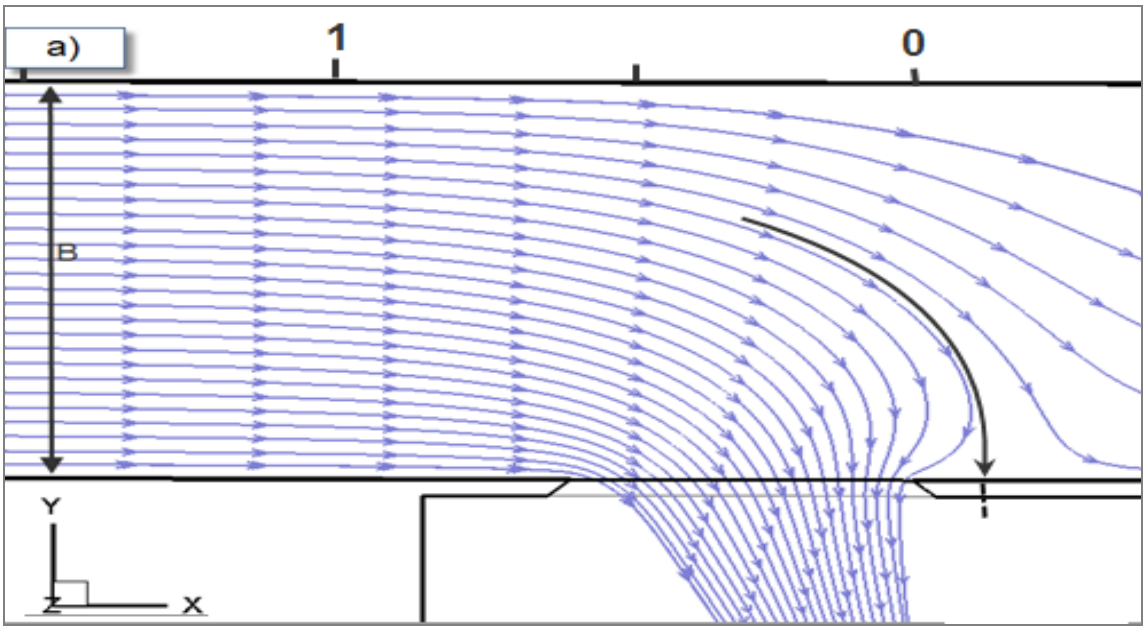

Fig.5.11.a: Streamlines layout at horizontal plane , Z=0.03 m.

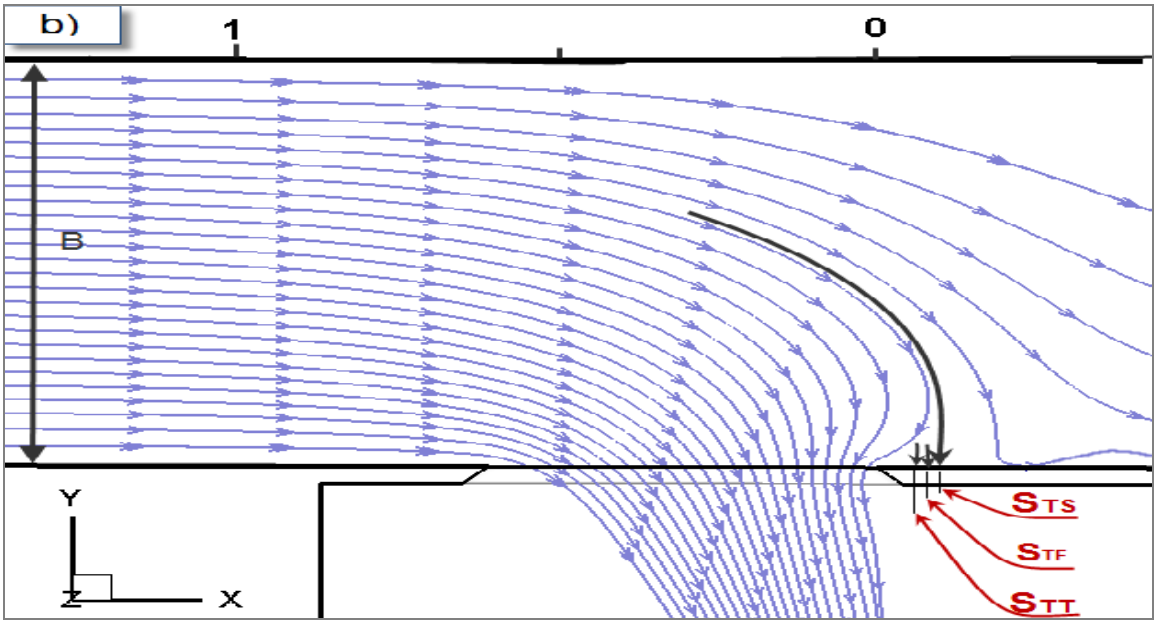

Fig.5.11.b: Streamline layout indicating location of stagnation points (Ideal flow, Experimental, Simulation), Q_R=0.811 F_R=0.40, at Z=0.06 m.

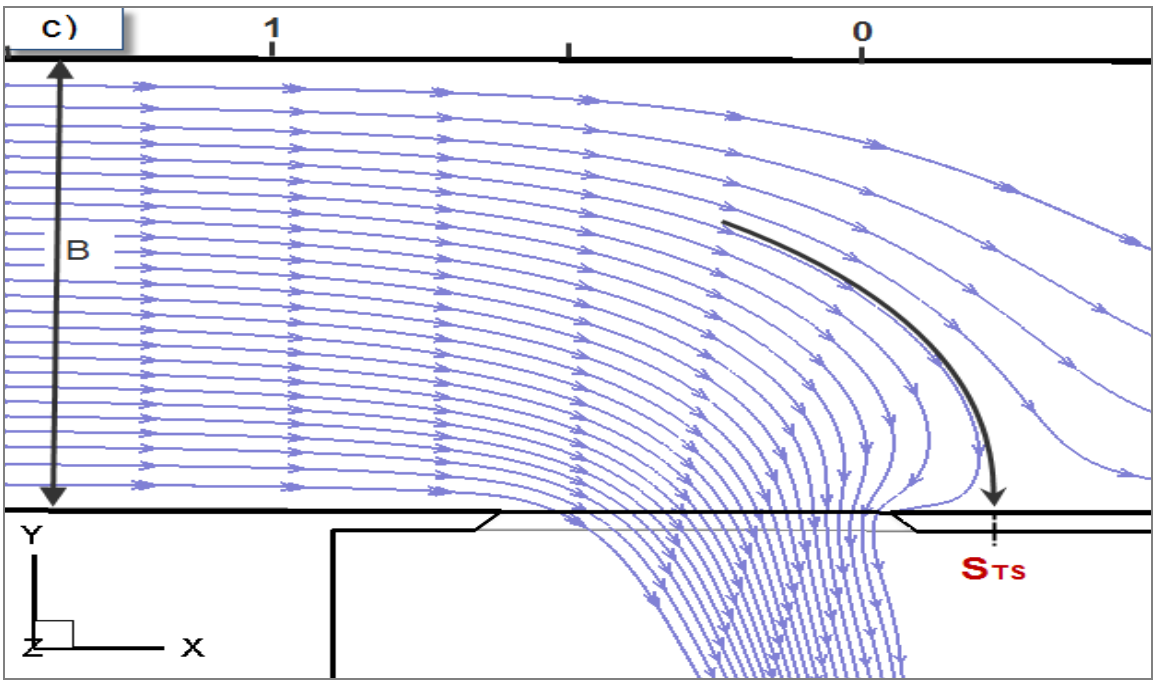

Fig.5.11.c : Streamlines layout at horizontal plane, Q_R=0.811, F_R=0.40,Z=0.07m.

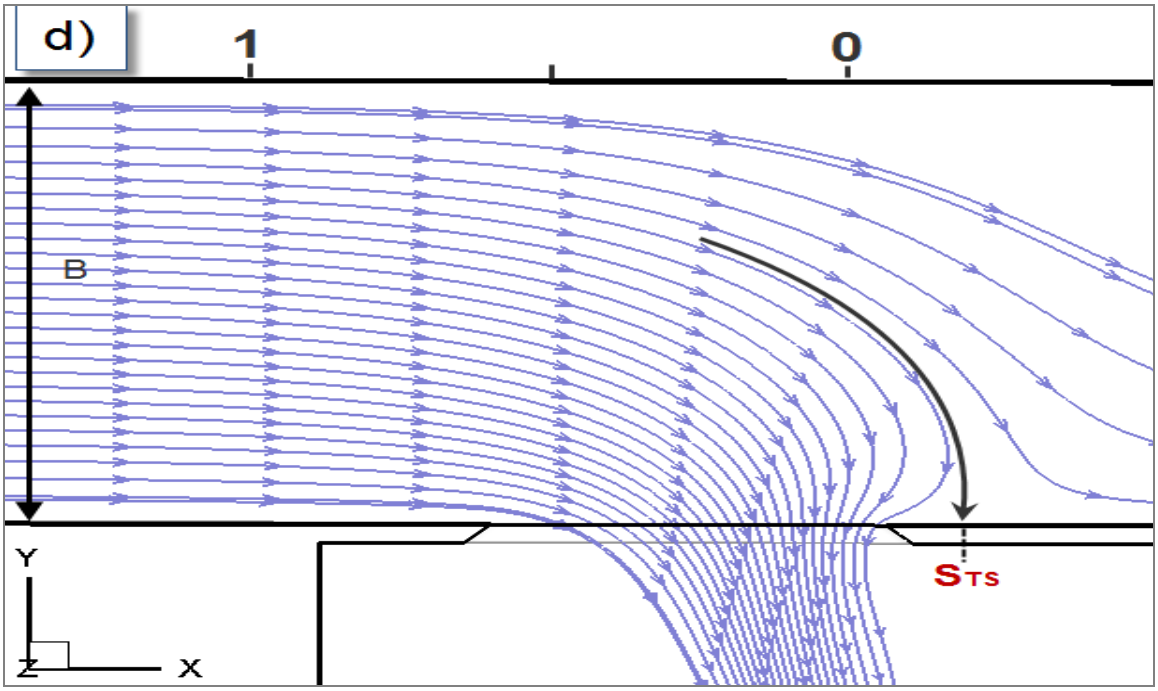

Fig.5.11.d: Streamlines layout at horizontal plane , Q_R=0.811, F_R=0.40,Z=0.09 m

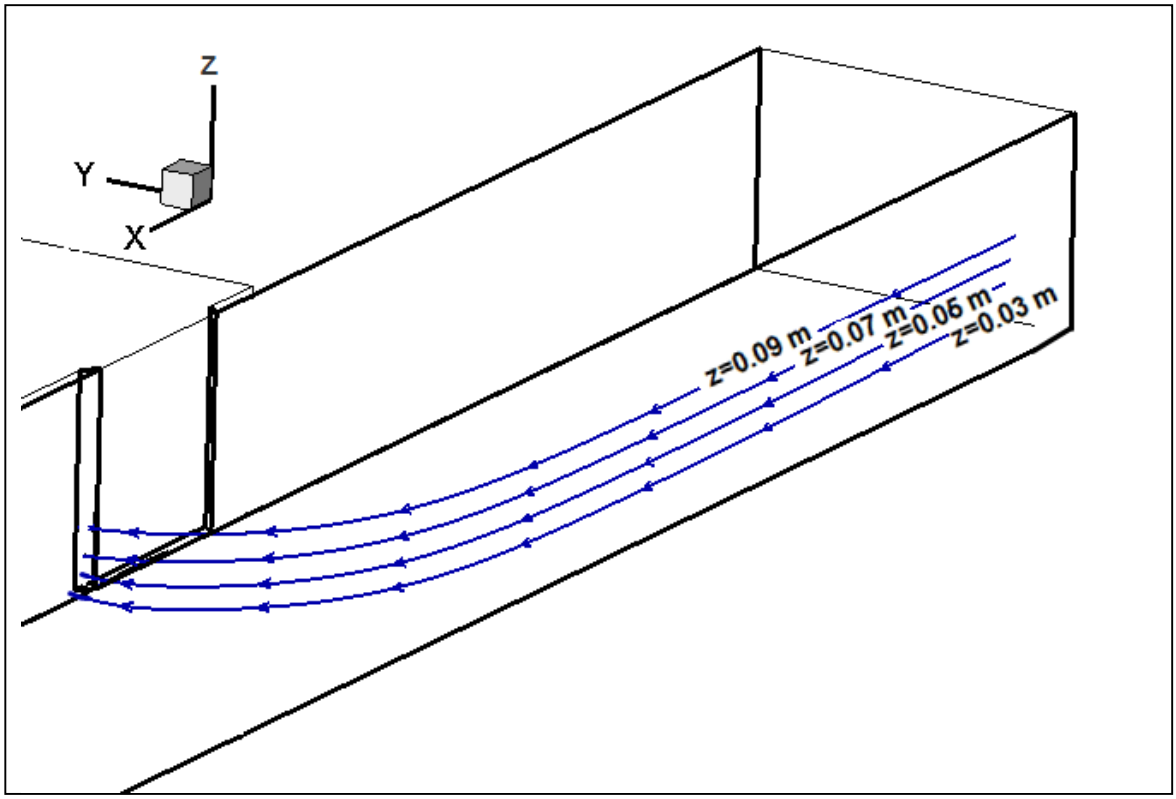

Fig. 5.12: Trace of dividing streamlines in the planes, z=0.09 m, z=0.07 m, z=0.06m and z=0.03 m reaching near wall at stagnation points in inclined plane (Q_R=0.792).

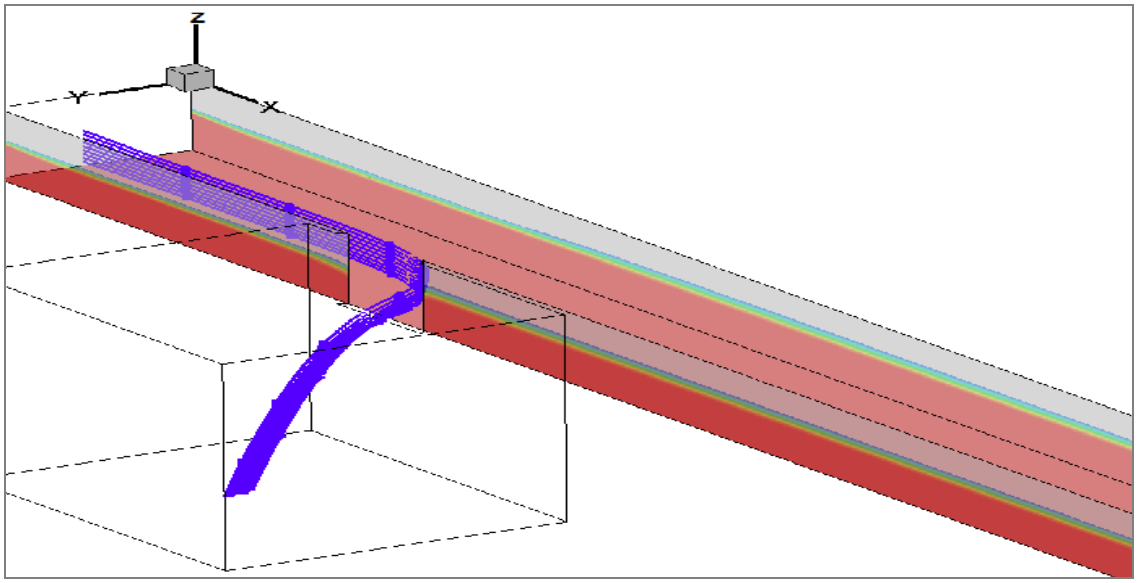

Fig. 5.13: Trace of streamlines emerging out of the side weir.

TABLES

Table 5.1 Measured and predicted flow configuration

#	Description	Units	Simulation Results	Experimental Results
1	Downstream end (Through) discharge (Q_2)	m^3/sec	0.00212	0.00240
2	Discharge over side weir (Q_3)	m^3/sec	0.00928	0.00917
3	Discharge Ratio	--	0.811	0.792
4	Froude Number	--	0.40	0.40
5	Upstream water depth	m	0.101	0.101

Table 5.2 Characteristics of side weir flow (Fig. 1.1)

Channel width B= 0.286 m, X*=X/B.

#	Description	Nota-tion	Value	Fig.
1.a	Length of Separation (Experimental-LDA)	L_{SE}	3.00 B	Fig. 5.8
1.b	Length of Separation (Visualization) Uncertainty = ± 0.07 B	L_{SV}	2.80 B	--
2.a	Width of separation (Experimental-LDA)	W_{SE}	0.30 B	Fig. 5.8
2.b	Width of separation (Visualization) Uncertainty = ± 0.02 B	W_{SV}	0.31 B	--
2.c	Width of separation (Simulation)	W_{SS}	0.33 B	Fig. 5.9
3.a	Distance X* of stagnation from weir end T_2: (Experimental) Z* = 0.209	S_{TE}	0.076	Fig. 5.6.a
3.b	Distance X* of stagnation from weir end T_2:(Visualization) Uncertainty = ± 0.025 B	S_{TV}	0.073	--
3.c	Distance X* of stagnation from weir end T_2: (Simulation) Z* = 0.209	S_{TS}	0.091	Fig. 5.6.b
3.d	Distance X* of stagnation from weir end T_2: (Eq. 3.4)	S_{TT}	0.060	Fig.5.10.b
4.a	Exiting jet contraction ratio (Experimental)	C_{CE}	0.70	--
4.b	Exiting jet contraction ratio (Simulation)	C_{CS}	0.68	--

CHAPTER 6

SUMMARY, CONCLUSIONS AND SCOPE FOR FUTURE STUDIES

6.1 Summary:

The present study deals with the determination of the flow characteristics of a side weir located in a rectangular channel for a specific flow configuration. The numerical model based on RNG k-ε turbulence model provided the predictions for the weir flow configuration considered. The VOF scheme was considered to trace the water surface profile. Test data based on LDA velocity measurements provided test data to validate the model predictions. The properly validated model can be used to determine the flow characteristics for other flow configurations and rectangular channel geometries. The stagnation point was also determined using theoretical method base on ideal flow theory.

6.2 Conclusions:

1. Experimental results yielded weir flow parameters such as the water surface profiles, the velocity vector pattern, the streamline pattern, the dividing streamline and the stagnation on the near wall, length and width of the separation zone, and the exiting jet contraction coefficient.
2. The VOF approach with the RNG k- ε turbulence model can be used to predict the various characteristics of the side weir flow.
3. A properly validated model can be used for knowing the side weir characteristics for other flow configurations and similar channel geometries.
4. Results based on LDA measurements and flow visualization tests provided the test

data which validated the numerical model predictions.

5. Experimental and simulation results were found to be in agreement.

6. The theoretically determined stagnation point found on the basis of ideal flow theory was in qualitatively agreement with the experimentally determined values and model predictions.

7. RNG k- ε turbulence model failed to predict the location of reattachment point R of the separation zone for the side weir flow.

8. The flow very close to the side weir region is three dimensional and hence it introduces some errors in tracing the streamlines.

6.3 Scope for future studies

- The numerical model may be developed for different geometrical shapes of the side weir in different channel geometry with a wide range of hydraulic and geometric design parameters such as L/B, s/y_1 and $F_{R.}$

- The present study is focused on RNG k-ε model. More advanced turbulence model such as k-ω, RSM, LES; may be developed to obtain improved and additional turbulence quantities which current model is unable to predict.

- To find the exact generalized equation for the discharge over the side weir using different combinations and range of the hydraulic parameters like $F_R, \frac{L}{B}, \frac{s}{y_1}$.

APPENDIX 1

REFERENCES

1. Agaccioglu, H. and Yüksel, Y. (1998). "Side-weir flow in curved channels", Journal of Irrigation and Drainage Engineering, vol.124, n 3, pp.163-175.

2. Balmforth, D.J.; Sargasso, E.J.(1983). "Effects of curvature in supercritical side weir flow", Journal of Hydraulic Research, vol. 21, n 5, pp. 333-343.

3. Borghei, S.M., Jalili, M.R. and Ghodsian M. (1999). "Discharge coefficient for sharp-crested side weirs in subcritical flow", Journal of the Hydraulic Division, ASCE, Vol.125 (10), pp. 1051-1056.

4. Buyer, M., Vazquez, J., Bremond, B. (2002). "Modeling of the low crested prismatic sewer side weir", Global Solutions for Urban Drainage, pp. 1-18.

5. Carballada, L.B. (1979). "Some characteristics of lateral flow", PhD thesis, Concordia University, Montreal, Canada.

6. Chang, P. K. (1970). "Separation of Flow", Pergamon Press, Oxford, New York.

7. Choudhary, D. (1993). "Introduction to the Renormalization Group Method and Turbulence Modeling", Technical Memorandum, Fluent Inc, TM-107.

8. Chow, V.T. (1959). "Open Channel Hydraulics", McGraw-Hill, New York.

9. Collinge, V.K. (1957). "The Discharge capacity of side weirs", Proceedings of the Institution of Civil Engineers, London, England, Vol.6, pp. 288-304.

10. DeMarchi, G. (1934). "Saggio di teoria di funzionamente degli stramazzi laterali", L'Energia Elettrica, Milano, Italy, vol.11, pp. 849-860(in Italian).

11. El-Khashabad and Smith, K. (1976). "Experimental investigation of flow over side weirs", Journal of Hydraulic. Eng., ASCE, vol.102, pp.1255-1268.

12. Ferziger, J.H. and Peric, M. (2002). "Computational method for CFD", 3rd edition, Springer.

13. Fluent Inc. (2006). "FLUENT 6.3 User's guide", Lebanon, New Hampshire.

14. Frazer, W. (1957). "The Behavior of side weirs in prismatic Rectangular channels", Proceedings of the Institution of Civil Engineers, London, England, vol.6, pp.305-328.

15. Gerald, C. F. and Wheatley, P. O. (1994). "Applied numerical analysis", 5th edition, Addison-Wesley Publishing Company.

16. Hager, W.H. (1982). “Die Hydraulik von Verteilkanaelen”, Teil 1-2, Mitteilung Nr.55-56, Versuchanstalt fur Wasserbau, Hydrologie und Glaziologie, ETh, Zurich (in German).

17. Hager, W.H. (1985), “Critical flow condition in open channel hydraulics”, Acta Mechanica, vol.54, pp.157-179.

18. Hager, W. H. and Volkart, P. U. (1986). “Distribution channels” Journal of Hydraulic Engineering, Vol. 112, No. 10.

19. Hager, W.H. (1987), “Lateral outflow over side weirs”, Journal of Hydraulic Engineering, ASCE, vol.113, pp.491-504.

20. Hager, W. H. (1994). “Wastewater hydraulics: theory and practice”, Springer-Verlag Berlin Heidelberg.

21. Hager, W. H.(1994).“Supercritical flow in circular-shaped side weir”, Journal of Irrigation and Drainage Engineering, vol. 120, n 1, pp.1-12.

22. Henderson, F.M. (1966). “Open channel flow”, McMillan & Co., New York.

23. Hinze, J. O. (1975). “Turbulence”, Second Ed., McGraw-Hill, New York.

24. Hirt, C.W. and Nicholls, B.D. (1981). “Volume of Fluid (VOF) method for dynamics of free boundaries”, J. Computational Physics, 39, pp. 201-221.

25. Issa, R.I. (1986), "Solution of the implicitly discretized fluid flow equations by operator splitting", J. Computational Physics, 62, pp.40-65.

26. Kandaswamy, P.R. and Rouse, H. (1957). “Characteristics of flow over terminal weirs and sills”, Journal of the Hydraulic Division, ASCE, vol.83, No. HY4, pp. 1-13.

27. Lander, B.E. and Spalding, D.B. (1974). “The numerical computation of turbulent flows”, Computational methods for Applied Mechanical Engineering, vol.3, pp. 269-289.

28. Michell, J.M. (1890). “On the theory of the free stream lines”, Philosophical Transactions of the Royal Society, London, vol.A181, pp.389-431.

29. McNown, J.S. and Hsu, E. (1951). “Application of conformal mapping to dividing flow”, Proc. Midwestern Conf. on Fluid Dynamics, J.W. Edwards, Ann Arbor Mich., pp. 143-155

30. Meselhe, E.A. and Sortiropoulos, F. (2000). “Three-dimensional numerical model for open channels with free surface variations”, Journal of Hydraulic Research, IHAR, vol.38 (2), pp. 115-121.

31. Muslu, Y. (2001). “Numerical analysis for lateral weir flow”, Journal of Irrigation and Drainage Engineering, ASCE, vol.127 (4), pp. 246–253.

32. Muslu, Y., Tozluk, H. and Yuksel, E. (2003a). “Effect of lateral water surface profile on side

weir discharges", Journal of Irrigation and Drainage Engineering, ASCE, vol.129 (5), pp.371–375.

33. Muslu, Y and Tozluk, H. (2003b). "Transition effects in flow over side weirs", Journal of Irrigation and Drainage Engineering, ASCE, vol.130 (1), pp. 92–95.

34. Pezzinga, G. (1994). "Velocity distribution in compound channel flows by numerical modeling", J. Hydraulic Engineering, ASCE, vol.120 (10), pp.1176–1198.

35. Qu, J.(2005), " Three dimensional turbulence modeling for free surface flows", PhD thesis, Concordia University, Montreal, Quebec, Canada.

36. Rajaratnam, N. and Murlidhar, D. (1968). "Characteristics of the rectangular free overfall", Journal of hydraulic research, IAHR, vol.6 (3), pp.233-258.

37. Ramamurthy, A.S., Zhu W. M. and Carballada, L.B. (1994). "Flow past a 2D lateral slot", Journal of environmental Engineering, ASCE, vol.120 (6), pp.1632-1638.

38. Ramamurthy, A.S. and Carballada, L.B. (1979). "Lateral flow past a barrier", Journal of Fluid Engineering, ASME, vol.101 (4), pp.449-452.

39. Ramamurthy, A.S. and Carballada, L.B. (1980). "Lateral weir flow model", Journal of the Irrigation and Drainage Division, ASCE, vol.106 (1), pp.9-25.

40. Ramamurthy, A.S., Zhu, W. and Vo, D. (1995). "Rectangular lateral weirs in circular open channels", Journal of Hydraulic Engineering, ASCE, vol.121 (8), pp. 608-612.

41. Ramamurthy, A.S., Qu, J. And Vo, D. (2005). "Volume of fluid model for an open channel flow problem", Canadian Journal of Civil Engineering, vol. 32, n 5, pp.996-1001.

42. Ramamurthy, A.S., Qu, J., and Vo, D. (2006). "VOF model for simulation of a free overfall in trapezoidal channels", Journal of Irrigation and Drainage Engineering, ASCE, Vol. 132(4), pp.425-428.

43. Singh, R., Manivannan, D. and Satyanarayana, T. (1994). "Discharge coefficient of rectangular side weirs", Journal of Irrigation and Drainage Engineering, ASCE, vol.120 (4), pp.814-819.

44. Subramanya, K. and Awasthy, S. C. (1972). "Spatially varied flow over side weirs", Journal of Hydraulic Division, ASCE, vol.98 (HY1), pp.1–10.

45. Subramanya k. (1997). "Flow in open channels", 2nd edition, Tata McGraw Hill, New Delhi.

46. Swamee, P. K., Pathak, S. K. ,Agrawal, S. K., Ali, M. S. (1994). "Subcritical flow over rectangular side weir", Journal of Irrigation and Drainage Engineering, vol. 120, n 1, pp. 212-217, Jan-Feb 1994

47. Swamee, P. K. , Pathak, S. K., Ali, M.S. (1994). "Side-weir analysis using elementary discharge coefficient", Journal of Irrigation and Drainage Engineering, v 120, n 4, p 742-755.

48. Ranga Raju, Prasad, K.G. and Gupta, S.K. (1979), "Side weir in rectangular channel", Journal of Hydraulic Division, ASCE, vol.105 (5), pp.547-554.

49. Tadayon, R. (2009), "Modelling curvilinear flows in hydraulic structures", PhD thesis, Concordia University, Montreal, Quebec, Canada.

50. Udoyara, T. (1986). "Characteristics of some hydraulic structures used for flow control and measurement in open channels", PhD thesis, Concordia University, Montreal, Quebec, Canada.

51. Uyumaz, A. and Muslu, Y. (1985). "Flow over side weirs in circular channels", Journal of Hydraulic Engineering, ASCE, vol. 111(1), pp.144-160.

52. Uyumaz, Ali. (1992). "Side weir in triangular channel", Journal of Irrigation and Drainage Engineering, vol.118, n.6, pp.965-970.

53. Uyumaz, Ali. (1997). "Side weir in U-shaped channels", Journal of Hydraulic Engineering, vol.123, n 7, pp. 639-646.

54. Versteeg, H. K. and Malalsekara, W. (1995). "An introduction to computational fluid dynamics: The finite volume method", Longman Group Limited, Essex, London.

55. Wilcox, D.C. (1994). "Simulation of transition with a two-equation turbulence model", AIAA J., vol.32 (2), pp.247-255.

56. Wilcox, D. C. (2000). "Turbulence modeling for CFD", 3rd edition, DCW Industries, Inc.

57. Yakhot, V. and Orszag, S.A. (1986), "Development of turbulence model for shear flows by a double expansion technique", Physics of fluids A, Vol.4, No.7, pp.1510-1520.

58. Yu-Tech, L. (1972). "Discussion of 'Spatially varied flow over side weirs' by Subramanya, K. and Awasthy, S.C.", Journal of Hydraulic Division, ASCE, vol. 98(1), pp.2046-2048.

59. Zhai, C. (2003). "Hydrodynamic principles applied to flow measurement.", M.A.Sc. Thesis, Concordia University, Montreal, Canada.

Appendix 2.1 Water surface profile readings for the side weir flows in open channel, RUN-I (Q_R=0.792), Details are provided in Table 3.2.

X*=X/B , Y*=Y/B, Z*=Z/B, B=0.286 m

X*	Y*	Z*
5.944	0.07	0.35
5.944	0.14	0.35
5.944	0.21	0.35
5.944	0.28	0.35
5.944	0.35	0.35
5.944	0.42	0.349
5.944	0.49	0.348
5.944	0.559	0.347
5.944	0.629	0.346
5.944	0.699	0.346
5.944	0.769	0.345
5.944	0.839	0.345
5.944	0.909	0.345
5.944	0.979	0.345
5.594	0.07	0.349
5.594	0.14	0.35
5.594	0.21	0.351

X*	Y*	Z*
5.594	0.28	0.35
5.594	0.35	0.35
5.594	0.42	0.347
5.594	0.49	0.346
5.594	0.559	0.346
5.594	0.629	0.345
5.594	0.699	0.345
5.594	0.769	0.344
5.594	0.839	0.345
5.594	0.909	0.342
5.594	0.979	0.342
5.245	0.07	0.35
5.245	0.14	0.35
5.245	0.21	0.35
5.245	0.28	0.351
5.245	0.35	0.351
5.245	0.42	0.349

X*	Y*	Z*
5.245	0.49	0.349
5.245	0.559	0.348
5.245	0.629	0.349
5.245	0.699	0.348
5.245	0.769	0.352
5.245	0.839	0.349
5.245	0.909	0.35
5.245	0.979	0.35
4.895	0.07	0.35
4.895	0.14	0.35
4.895	0.21	0.35
4.895	0.28	0.35
4.895	0.35	0.35
4.895	0.42	0.35
4.895	0.49	0.348
4.895	0.559	0.347
4.895	0.629	0.346

X*	Y*	Z*
4.895	0.699	0.345
4.895	0.769	0.343
4.895	0.839	0.344
4.895	0.909	0.344
4.895	0.979	0.344
4.545	0.07	0.353
4.545	0.14	0.352
4.545	0.21	0.351
4.545	0.28	0.35
4.545	0.35	0.348
4.545	0.42	0.347
4.545	0.49	0.347
4.545	0.559	0.347
4.545	0.629	0.347
4.545	0.699	0.346
4.545	0.769	0.345
4.545	0.839	0.345

Appendix 2.1 Water surface profile readings for the side weir flows in open channel (Q_R=0.792) Contd.

X*	Y*	Z*
4.545	0.909	0.345
4.545	0.979	0.345
4.196	0.07	0.35
4.196	0.14	0.35
4.196	0.21	0.35
4.196	0.28	0.346
4.196	0.35	0.347
4.196	0.42	0.347
4.196	0.49	0.347
4.196	0.559	0.347
4.196	0.629	0.347
4.196	0.699	0.347
4.196	0.769	0.347
4.196	0.839	0.347
4.196	0.909	0.347
4.196	0.979	0.348
3.846	0.07	0.351

X*	Y*	Z*
3.846	0.14	0.35
3.846	0.21	0.353
3.846	0.28	0.35
3.846	0.35	0.35
3.846	0.42	0.349
3.846	0.49	0.348
3.846	0.559	0.347
3.846	0.629	0.346
3.846	0.699	0.344
3.846	0.769	0.343
3.846	0.839	0.342
3.846	0.909	0.343
3.846	0.979	0.342
3.497	0.07	0.35
3.497	0.14	0.352
3.497	0.21	0.353
3.497	0.28	0.35

X*	Y*	Z*
3.497	0.35	0.349
3.497	0.42	0.351
3.497	0.49	0.349
3.497	0.559	0.347
3.497	0.629	0.348
3.497	0.699	0.346
3.497	0.769	0.346
3.497	0.839	0.345
3.497	0.909	0.347
3.497	0.979	0.347
3.147	0.07	0.346
3.147	0.14	0.346
3.147	0.21	0.347
3.147	0.28	0.346
3.147	0.35	0.346
3.147	0.42	0.346
3.147	0.49	0.346

X*	Y*	Z*
3.147	0.559	0.346
3.147	0.629	0.347
3.147	0.699	0.347
3.147	0.769	0.346
3.147	0.839	0.347
3.147	0.909	0.346
3.147	0.979	0.347
2.797	0.07	0.346
2.797	0.14	0.346
2.797	0.21	0.346
2.797	0.28	0.345
2.797	0.35	0.345
2.797	0.42	0.345
2.797	0.49	0.344
2.797	0.559	0.343
2.797	0.629	0.343
2.797	0.699	0.342

Appendix 2.1 Water surface profile readings for the side weir flows in open channel (Q_R=0.792) Contd.

X*	Y*	Z*
2.797	0.769	0.342
2.797	0.839	0.342
2.797	0.909	0.34
2.797	0.979	0.339
2.448	0.07	0.348
2.448	0.14	0.348
2.448	0.21	0.347
2.448	0.28	0.348
2.448	0.35	0.351
2.448	0.42	0.348
2.448	0.49	0.348
2.448	0.559	0.347
2.448	0.629	0.348
2.448	0.699	0.348
2.448	0.769	0.348
2.448	0.839	0.348
2.448	0.909	0.348

X*	Y*	Z*
2.448	0.979	0.348
2.273	0.07	0.346
2.273	0.14	0.346
2.273	0.21	0.346
2.273	0.28	0.346
2.273	0.35	0.345
2.273	0.42	0.346
2.273	0.49	0.346
2.273	0.559	0.346
2.273	0.629	0.345
2.273	0.699	0.343
2.273	0.769	0.342
2.273	0.839	0.345
2.273	0.909	0.344
2.273	0.979	0.344
2.098	0.07	0.346
2.098	0.14	0.346

X*	Y*	Z*
2.098	0.21	0.346
2.098	0.28	0.347
2.098	0.35	0.346
2.098	0.42	0.346
2.098	0.49	0.344
2.098	0.559	0.342
2.098	0.629	0.345
2.098	0.699	0.344
2.098	0.769	0.344
2.098	0.839	0.345
2.098	0.909	0.344
2.098	0.979	0.344
1.748	0.07	0.347
1.748	0.14	0.347
1.748	0.21	0.348
1.748	0.28	0.346
1.748	0.35	0.347

X*	Y*	Z*
1.748	0.42	0.346
1.748	0.49	0.347
1.748	0.559	0.347
1.748	0.629	0.346
1.748	0.699	0.346
1.748	0.769	0.345
1.748	0.839	0.346
1.748	0.909	0.346
1.748	0.979	0.345
1.573	0.07	0.346
1.573	0.14	0.345
1.573	0.21	0.346
1.573	0.28	0.346
1.573	0.35	0.345
1.573	0.42	0.346
1.573	0.49	0.344
1.573	0.559	0.343

Appendix 2.1 Water surface profile readings for the side weir flows in open channel (Q_R=0.792) Contd.

X*	Y*	Z*
1.573	0.629	0.346
1.573	0.699	0.346
1.573	0.769	0.345
1.573	0.839	0.345
1.573	0.909	0.344
1.573	0.979	0.342
1.101	0.07	0.336
1.101	0.14	0.338
1.101	0.21	0.338
1.101	0.28	0.342
1.101	0.35	0.347
1.101	0.42	0.348
1.101	0.49	0.348
1.101	0.559	0.346
1.101	0.629	0.348
1.101	0.699	0.353
1.101	0.769	0.354

X*	Y*	Z*
1.101	0.839	0.355
1.101	0.909	0.355
1.101	0.979	0.353
1.031	0.07	0.334
1.031	0.14	0.337
1.031	0.21	0.337
1.031	0.28	0.341
1.031	0.35	0.343
1.031	0.42	0.348
1.031	0.49	0.35
1.031	0.559	0.352
1.031	0.629	0.355
1.031	0.699	0.356
1.031	0.769	0.355
1.031	0.839	0.355
1.031	0.909	0.356
1.031	0.979	0.356

X*	Y*	Z*
0.962	0.07	0.329
0.962	0.14	0.333
0.962	0.21	0.336
0.962	0.28	0.338
0.962	0.35	0.34
0.962	0.42	0.344
0.962	0.49	0.345
0.962	0.559	0.348
0.962	0.629	0.35
0.962	0.699	0.349
0.962	0.769	0.352
0.962	0.839	0.353
0.962	0.909	0.355
0.962	0.979	0.357
0.892	0.07	0.326
0.892	0.14	0.327
0.892	0.21	0.329

X*	Y*	Z*
0.892	0.28	0.337
0.892	0.35	0.338
0.892	0.42	0.343
0.892	0.49	0.345
0.892	0.559	0.348
0.892	0.629	0.35
0.892	0.699	0.354
0.892	0.769	0.355
0.892	0.839	0.356
0.892	0.909	0.356
0.892	0.979	0.359
0.822	0.07	0.323
0.822	0.14	0.324
0.822	0.21	0.328
0.822	0.28	0.334
0.822	0.35	0.337
0.822	0.42	0.341

X*	Y*	Z*
0.822	0.49	0.343
0.822	0.559	0.348
0.822	0.629	0.35
0.822	0.699	0.352
0.822	0.769	0.355
0.822	0.839	0.359
0.822	0.909	0.361
0.822	0.979	0.362
0.752	0.07	0.314
0.752	0.14	0.319
0.752	0.21	0.327
0.752	0.28	0.331
0.752	0.35	0.336
0.752	0.42	0.341
0.752	0.49	0.344
0.752	0.559	0.348
0.752	0.629	0.351

X*	Y*	Z*
0.752	0.699	0.36
0.752	0.769	0.358
0.752	0.839	0.357
0.752	0.909	0.358
0.752	0.979	0.362
0.682	0.07	0.304
0.682	0.14	0.308
0.682	0.21	0.32
0.682	0.28	0.327
0.682	0.35	0.337
0.682	0.42	0.34
0.682	0.49	0.342
0.682	0.559	0.348
0.682	0.629	0.358
0.682	0.699	0.359
0.682	0.769	0.359
0.682	0.839	0.361

X*	Y*	Z*
0.682	0.909	0.362
0.682	0.979	0.363
0.612	0	0.299
0.612	0.07	0.308
0.612	0.14	0.313
0.612	0.21	0.32
0.612	0.28	0.328
0.612	0.35	0.331
0.612	0.42	0.333
0.612	0.49	0.23
0.612	0.559	0.34
0.612	0.629	0.34
0.612	0.699	0.349
0.612	0.769	0.35
0.612	0.839	0.348
0.612	0.909	0.348
0.577	0	0.294

X*	Y*	Z*
0.577	0.07	0.301
0.577	0.14	0.31
0.577	0.21	0.32
0.577	0.28	0.327
0.577	0.35	0.331
0.577	0.42	0.336
0.577	0.49	0.337
0.577	0.559	0.34
0.577	0.629	0.34
0.577	0.699	0.347
0.577	0.769	0.349
0.577	0.839	0.35
0.577	0.909	0.35
0.524	0	0.28
0.524	0.07	0.295
0.524	0.14	0.304
0.524	0.21	0.318

Appendix 2.1 Water surface profile readings for the side weir flows in open channel (Q_R=0.792) Contd.

X*	Y*	Z*
0.524	0.28	0.325
0.524	0.35	0.331
0.524	0.42	0.332
0.524	0.49	0.337
0.524	0.559	0.337
0.524	0.629	0.353
0.524	0.699	0.35
0.524	0.769	0.348
0.524	0.839	0.346
0.524	0.909	0.349
0.49	0	0.269
0.49	0.07	0.29
0.49	0.14	0.308
0.49	0.21	0.318
0.49	0.28	0.328
0.49	0.35	0.335
0.49	0.42	0.343

X*	Y*	Z*
0.49	0.49	0.344
0.49	0.559	0.346
0.49	0.629	0.351
0.49	0.699	0.349
0.49	0.769	0.352
0.49	0.839	0.351
0.49	0.909	0.348
0.455	0	0.266
0.455	0.07	0.292
0.455	0.14	0.311
0.455	0.21	0.324
0.455	0.28	0.33
0.455	0.35	0.34
0.455	0.42	0.343
0.455	0.49	0.345
0.455	0.559	0.346
0.455	0.629	0.346

X*	Y*	Z*
0.455	0.699	0.352
0.455	0.769	0.351
0.455	0.839	0.354
0.455	0.909	0.357
0.42	0	0.269
0.42	0.07	0.292
0.42	0.14	0.309
0.42	0.21	0.324
0.42	0.28	0.328
0.42	0.35	0.341
0.42	0.42	0.345
0.42	0.49	0.346
0.42	0.559	0.346
0.42	0.629	0.347
0.42	0.699	0.348
0.42	0.769	0.35
0.42	0.839	0.354

X*	Y*	Z*
0.42	0.909	0.354
0.35	0	0.267
0.35	0.07	0.294
0.35	0.14	0.31
0.35	0.21	0.323
0.35	0.28	0.331
0.35	0.35	0.339
0.35	0.42	0.339
0.35	0.49	0.342
0.35	0.559	0.344
0.35	0.629	0.346
0.35	0.699	0.35
0.35	0.769	0.35
0.35	0.839	0.353
0.35	0.909	0.355
0.28	0	0.273
0.28	0.07	0.299

Appendix 2.1 Water surface profile readings for the side weir flows in open channel (Q_R=0.792) Contd.

X*	Y*	Z*
0.28	0.14	0.311
0.28	0.21	0.323
0.28	0.28	0.33
0.28	0.35	0.334
0.28	0.42	0.33
0.28	0.49	0.341
0.28	0.559	0.347
0.28	0.629	0.346
0.28	0.699	0.353
0.28	0.769	0.354
0.28	0.839	0.358
0.28	0.909	0.358
0.21	0	0.283
0.21	0.07	0.304
0.21	0.14	0.316
0.21	0.21	0.326
0.21	0.28	0.329

X*	Y*	Z*
0.21	0.35	0.334
0.21	0.42	0.342
0.21	0.49	0.345
0.21	0.559	0.348
0.21	0.629	0.352
0.21	0.699	0.354
0.21	0.769	0.358
0.21	0.839	0.359
0.21	0.909	0.36
0.175	0	0.285
0.175	0.07	0.307
0.175	0.14	0.318
0.175	0.21	0.324
0.175	0.28	0.327
0.175	0.35	0.33
0.175	0.42	0.343
0.175	0.49	0.347

X*	Y*	Z*
0.175	0.559	0.348
0.175	0.629	0.352
0.175	0.699	0.355
0.175	0.769	0.355
0.175	0.839	0.356
0.175	0.909	0.359
0.14	0	0.294
0.14	0.07	0.308
0.14	0.14	0.318
0.14	0.21	0.324
0.14	0.28	0.33
0.14	0.35	0.34
0.14	0.42	0.346
0.14	0.49	0.349
0.14	0.559	0.352
0.14	0.629	0.353
0.14	0.699	0.355

X*	Y*	Z*
0.14	0.769	0.355
0.14	0.839	0.357
0.14	0.909	0.359
0.07	0	0.322
0.07	0.07	0.324
0.07	0.14	0.332
0.07	0.21	0.34
0.07	0.28	0.344
0.07	0.35	0.344
0.07	0.42	0.349
0.07	0.49	0.351
0.07	0.559	0.353
0.07	0.629	0.353
0.07	0.699	0.357
0.07	0.769	0.358
0.07	0.839	0.357
0.07	0.909	0.358

Appendix 2.1 Water surface profile readings for the side weir flows in open channel (Q_R=0.792) Contd.

X*	Y*	Z*
0.035	0	0.349
0.035	0.07	0.349
0.035	0.14	0.344
0.035	0.21	0.345
0.035	0.28	0.349
0.035	0.35	0.349
0.035	0.42	0.349
0.035	0.49	0.35
0.035	0.559	0.354
0.035	0.629	0.358
0.035	0.699	0.36
0.035	0.769	0.359
0.035	0.839	0.36
0.035	0.909	0.361
0	0.07	0.369
0	0.14	0.363
0	0.21	0.35

X*	Y*	Z*
0	0.28	0.348
0	0.35	0.346
0	0.42	0.348
0	0.49	0.349
0	0.559	0.351
0	0.629	0.351
0	0.699	0.353
0	0.769	0.355
0	0.839	0.356
0	0.909	0.353
-0.035	0.07	0.369
-0.035	0.14	0.363
-0.035	0.21	0.348
-0.035	0.28	0.348
-0.035	0.35	0.35
-0.035	0.42	0.352
-0.035	0.49	0.354

X*	Y*	Z*
-0.035	0.559	0.352
-0.035	0.629	0.352
-0.035	0.699	0.355
-0.035	0.769	0.355
-0.035	0.839	0.355
-0.035	0.909	0.353
-0.07	0.07	0.368
-0.07	0.14	0.369
-0.07	0.21	0.353
-0.07	0.28	0.352
-0.07	0.35	0.351
-0.07	0.42	0.348
-0.07	0.49	0.351
-0.07	0.559	0.353
-0.07	0.629	0.354
-0.07	0.699	0.356
-0.07	0.769	0.356

X*	Y*	Z*
-0.07	0.839	0.355
-0.07	0.909	0.355
-0.105	0.07	0.37
-0.105	0.14	0.368
-0.105	0.21	0.357
-0.105	0.28	0.353
-0.105	0.35	0.35
-0.105	0.42	0.351
-0.105	0.49	0.349
-0.105	0.559	0.355
-0.105	0.629	0.353
-0.105	0.699	0.355
-0.105	0.769	0.355
-0.105	0.839	0.353
-0.105	0.909	0.353
-0.14	0.07	0.371
-0.14	0.14	0.371

Appendix 2.1 Water surface profile readings for the side weir flows in open channel (Q_R=0.792) Contd.

X*	Y*	Z*
-0.14	0.21	0.362
-0.14	0.28	0.353
-0.14	0.35	0.35
-0.14	0.42	0.353
-0.14	0.49	0.351
-0.14	0.559	0.354
-0.14	0.629	0.357
-0.14	0.699	0.358
-0.14	0.769	0.358
-0.14	0.839	0.357
-0.14	0.909	0.356
-0.21	0.07	0.374
-0.21	0.14	0.373
-0.21	0.21	0.367
-0.21	0.28	0.361
-0.21	0.35	0.357
-0.21	0.42	0.356

X*	Y*	Z*
-0.21	0.49	0.357
-0.21	0.559	0.356
-0.21	0.629	0.356
-0.21	0.699	0.357
-0.21	0.769	0.357
-0.21	0.839	0.356
-0.21	0.909	0.357
-0.315	0.07	0.374
-0.315	0.14	0.371
-0.315	0.21	0.37
-0.315	0.28	0.365
-0.315	0.35	0.36
-0.315	0.42	0.358
-0.315	0.49	0.359
-0.315	0.559	0.359
-0.315	0.629	0.367
-0.315	0.699	0.357

X*	Y*	Z*
-0.315	0.769	0.357
-0.315	0.839	0.356
-0.315	0.909	0.354
-0.42	0.07	0.371
-0.42	0.14	0.371
-0.42	0.21	0.369
-0.42	0.28	0.367
-0.42	0.35	0.362
-0.42	0.42	0.361
-0.42	0.49	0.36
-0.42	0.559	0.358
-0.42	0.629	0.357
-0.42	0.699	0.357
-0.42	0.769	0.357
-0.42	0.839	0.356
-0.42	0.909	0.355
-0.524	0.07	0.371

X*	Y*	Z*
-0.524	0.14	0.371
-0.524	0.21	0.366
-0.524	0.28	0.365
-0.524	0.35	0.364
-0.524	0.42	0.36
-0.524	0.49	0.359
-0.524	0.559	0.36
-0.524	0.629	0.358
-0.524	0.699	0.357
-0.524	0.769	0.356
-0.524	0.839	0.356
-0.524	0.909	0.355
-0.699	0.07	0.368
-0.699	0.14	0.37
-0.699	0.21	0.364
-0.699	0.28	0.364
-0.699	0.35	0.364

Appendix 2.1 Water surface profile readings for the side weir flows in open channel (Q_R=0.792) Contd.

X*	Y*	Z*
-0.699	0.42	0.36
-0.699	0.49	0.357
-0.699	0.559	0.356
-0.699	0.629	0.358
-0.699	0.699	0.356
-0.699	0.769	0.357
-0.699	0.839	0.356
-0.699	0.909	0.355
-1.923	0.07	0.367
-1.923	0.14	0.366
-1.923	0.21	0.367
-1.923	0.28	0.365
-1.923	0.35	0.363
-1.923	0.42	0.364
-1.923	0.49	0.364
-1.923	0.559	0.364
-1.923	0.629	0.364

X*	Y*	Z*
-1.923	0.699	0.362
-1.923	0.769	0.361
-1.923	0.839	0.361
-1.923	0.909	0.36
-1.923	0.979	0.36
-2.273	0.07	0.365
-2.273	0.14	0.365
-2.273	0.21	0.367
-2.273	0.28	0.364
-2.273	0.35	0.363
-2.273	0.42	0.364
-2.273	0.49	0.366
-2.273	0.559	0.367
-2.273	0.629	0.364
-2.273	0.699	0.365
-2.273	0.769	0.367
-2.273	0.839	0.367

X*	Y*	Z*
-2.273	0.909	0.362
-2.273	0.979	0.362
-2.622	0.07	0.371
-2.622	0.14	0.369
-2.622	0.21	0.367
-2.622	0.28	0.365
-2.622	0.35	0.367
-2.622	0.42	0.366
-2.622	0.49	0.366
-2.622	0.559	0.365
-2.622	0.629	0.362
-2.622	0.699	0.365
-2.622	0.769	0.364
-2.622	0.839	0.364
-2.622	0.909	0.364
-2.622	0.979	0.364
-2.972	0.07	0.37

X*	Y*	Z*
-2.972	0.14	0.369
-2.972	0.21	0.371
-2.972	0.28	0.369
-2.972	0.35	0.369
-2.972	0.42	0.367
-2.972	0.49	0.367
-2.972	0.559	0.367
-2.972	0.629	0.366
-2.972	0.699	0.365
-2.972	0.769	0.364
-2.972	0.839	0.363
-2.972	0.909	0.365
-2.972	0.979	0.365
-3.322	0.07	0.371
-3.322	0.14	0.371
-3.322	0.21	0.37
-3.322	0.28	0.369

Appendix 2.2: Water surface profile readings for side weir flows in open channel (Qr=0.604)

X*	Y*	Z*
0.07	1.101	0.336
0.14	1.101	0.338
0.21	1.101	0.338
0.28	1.101	0.342
0.35	1.101	0.032
0.42	1.101	0.348
0.49	1.101	0.348
0.559	1.101	0.346
0.629	1.101	0.348
0.699	1.101	0.353
0.769	1.101	0.354
0.839	1.101	0.355
0.909	1.101	0.355
0.979	1.101	0.353
0.07	1.031	0.334
0.14	1.031	0.337
0.21	1.031	0.337
0.28	1.031	0.341

X*	Y*	Z*
0.35	1.031	0.343
0.42	1.031	0.348
0.49	1.031	0.35
0.559	1.031	0.352
0.629	1.031	0.355
0.699	1.031	0.356
0.769	1.031	0.355
0.839	1.031	0.355
0.909	1.031	0.356
0.979	1.031	0.356
0.07	0.892	0.326
0.14	0.892	0.327
0.21	0.892	0.329
0.28	0.892	0.337
0.35	0.892	0.338
0.42	0.892	0.343
0.49	0.892	0.345
0.559	0.892	0.348

X*	Y*	Z*
0.629	0.892	0.35
0.699	0.892	0.354
0.769	0.892	0.355
0.839	0.892	0.355
0.909	0.892	0.356
0.979	0.892	0.356
0.07	0.752	0.323
0.14	0.752	0.314
0.21	0.752	0.319
0.28	0.752	0.327
0.35	0.752	0.331
0.42	0.752	0.34
0.49	0.752	0.345
0.559	0.752	0.344
0.629	0.752	0.348
0.699	0.752	0.351
0.769	0.752	0.36
0.839	0.752	0.358

X*	Y*	Z*
0.909	0.752	0.357
0.979	0.752	0.358
0.07	0.612	0.304
0.14	0.612	0.308
0.21	0.612	0.32
0.28	0.612	0.334
0.35	0.612	0.337
0.42	0.612	0.34
0.49	0.612	0.342
0.559	0.612	0.348
0.629	0.612	0.358
0.699	0.612	0.359
0.769	0.612	0.359
0.839	0.612	0.361
0.909	0.612	0.362
0.979	0.612	0.363
0.07	0.35	0.294
0.14	0.35	0.307

Appendix 2.2: Water surface profile readings for side weir flows in open channel (Qr=0.604) Contd.

X*	Y*	Z*
0.28	0.35	0.324
0.42	0.35	0.335
0.49	0.35	0.338
0.559	0.35	0.34
0.629	0.35	0.345
0.699	0.35	0.349
0.769	0.35	0.351
0.839	0.35	0.354
0.979	0.35	0.355
0.07	0.297	0.269
0.14	0.297	0.291
0.28	0.297	0.326
0.42	0.297	0.34
0.49	0.297	0.346
0.559	0.297	0.351
0.629	0.297	0.352
0.699	0.297	0.352

X*	Y*	Z*
0.839	0.297	0.359
0.979	0.297	0.359
0.07	0.14	0.303
0.14	0.14	0.31
0.28	0.14	0.335
0.42	0.14	0.344
0.49	0.14	0.349
0.559	0.14	0.354
0.629	0.14	0.355
0.699	0.14	0.356
0.769	0.14	0.357
0.839	0.14	0.357
0.979	0.14	0.361
0.07	-0.07	0.364
0.14	-0.07	0.362
0.28	-0.07	0.352
0.42	-0.07	0.357

X*	Y*	Z*
0.559	-0.07	0.356
0.629	-0.07	0.357
0.699	-0.07	0.359
0.769	-0.07	0.36
0.839	-0.07	0.361
0.979	-0.07	0.362

Appendix 2.3 : Water surface profile readings for side weir flows in open channel (Q_R=0.940)

X*	Y*	Z*
0.017	1.503	0.375
0.07	1.503	0.381
0.14	1.503	0.376
0.21	1.503	0.375
0.28	1.503	0.376
0.35	1.503	0.38
0.42	1.503	0.382
0.49	1.503	0.381
0.559	1.503	0.386
0.629	1.503	0.386
0.699	1.503	0.386
0.769	1.503	0.388
0.839	1.503	0.391
0.909	1.503	0.391
0.017	0.612	0.335
0.07	0.612	0.337
0.14	0.612	0.347

X*	Y*	Z*
0.28	0.612	0.371
0.35	0.612	0.372
0.42	0.612	0.378
0.49	0.612	0.384
0.559	0.612	0.386
0.629	0.612	0.388
0.699	0.612	0.389
0.769	0.612	0.393
0.839	0.612	0.392
0.909	0.612	0.392
0.017	0.297	0.287
0.07	0.297	0.315
0.14	0.297	0.336
0.21	0.297	0.35
0.28	0.297	0.361
0.35	0.297	0.366
0.42	0.297	0.375

X*	Y*	Z*
0.559	0.297	0.387
0.629	0.297	0.391
0.699	0.297	0.394
0.769	0.297	0.395
0.839	0.297	0.399
0.909	0.297	0.399
0.017	0.00	0.4
0.07	0.00	0.4
0.14	0.00	0.391
0.21	0.00	0.381
0.28	0.00	0.372
0.35	0.00	0.378
0.42	0.00	0.389
0.49	0.00	0.392
0.559	0.00	0.394
0.629	0.00	0.394
0.699	0.00	0.395

X*	Y*	Z*
0.839	0.00	0.398
0.909	0.00	0.398
0.017	-0.017	0.401
0.07	-0.017	0.4
0.14	-0.017	0.392
0.21	-0.017	0.382
0.28	-0.017	0.373
0.35	-0.017	0.379
0.42	-0.017	0.39
0.49	-0.017	0.393
0.559	-0.017	0.394
0.629	-0.017	0.395
0.699	-0.017	0.396
0.769	-0.017	0.398
0.839	-0.017	0.399

Appendix 2.4 Velocity data for the side weir flows in open channel, Run-I, (Q_R=0.792), Details are provided in Table 3.2.

X*	Y*	Z*	U (m/s)	V (m/s)
3.371	0.07	0.035	0.3047	0.0013
3.371	0.07	0.105	0.3304	0.0051
3.371	0.07	0.175	0.375	0.0025
3.371	0.07	0.245	0.3801	0.0069
3.371	0.07	0.315	0.4062	0.0032
3.371	0.157	0.035	0.3024	0.0061
3.371	0.157	0.105	0.3911	0.0026
3.371	0.157	0.175	0.4295	0.0051
3.371	0.157	0.245	0.4663	0.0021
3.371	0.157	0.315	0.4652	0.0061
3.371	0.245	0.035	0.3276	0.0008
3.371	0.245	0.105	0.3893	0.0022
3.371	0.245	0.175	0.4473	0.0025
3.371	0.245	0.245	0.4847	0.0034
3.371	0.245	0.315	0.477	0.0071
3.371	0.315	0.035	0.3455	0.0011
3.371	0.315	0.105	0.4106	0.0025

X*	Y*	Z*	U (m/s)	V (m/s)
3.371	0.315	0.175	0.4361	0.0062
3.371	0.315	0.245	0.4755	0.0046
3.371	0.315	0.315	0.4654	0.0105
3.371	0.42	0.035	0.3188	0.0046
3.371	0.42	0.105	0.4005	0.0005
3.371	0.42	0.175	0.4358	0.0034
3.371	0.42	0.245	0.4583	0.0055
3.371	0.42	0.315	0.4868	0.015
3.371	0.507	0.035	0.3529	-0.0041
3.371	0.507	0.105	0.3994	0.0029
3.371	0.507	0.175	0.4415	0.0072
3.371	0.507	0.245	0.492	0.0059
3.371	0.507	0.315	0.4863	0.0105
3.371	0.594	0.035	0.363	-0.0007
3.371	0.594	0.105	0.4265	0.0028
3.371	0.594	0.175	0.4646	0.0015
3.371	0.594	0.245	0.5129	0.0079

X*	Y*	Z*	U (m/s)	V (m/s)
3.371	0.594	0.315	0.4996	0.0144
3.371	0.682	0.035	0.353	0.0037
3.371	0.682	0.105	0.4043	0.0021
3.371	0.682	0.175	0.4414	0.0031
3.371	0.682	0.245	0.5063	0.0113
3.371	0.682	0.315	0.5086	0.0141
3.371	0.769	0.035	0.3206	0.0009
3.371	0.769	0.105	0.4122	0.0023
3.371	0.769	0.175	0.4631	0.0057
3.371	0.769	0.245	0.5102	0.0134
3.371	0.769	0.315	0.516	0.0144
3.371	0.857	0.035	0.362	0.0006
3.371	0.857	0.105	0.4553	0.0024
3.371	0.857	0.175	0.4969	0.0075
3.371	0.857	0.245	0.5409	0.0129
3.371	0.857	0.315	0.5184	0.015
3.371	0.944	0.035	0.3781	0.0124

X*	Y*	Z*	U (m/s)	V (m/s)
3.371	0.944	0.105	0.3968	0
3.371	0.944	0.175	0.4824	0.0078
3.371	0.944	0.245	0.5278	0.01
3.371	0.944	0.315	0.5151	0.0122
3.196	0.07	0.035	0.2904	-0.0017
3.196	0.07	0.105	0.2935	0.0072
3.196	0.07	0.175	0.3517	0.0015
3.196	0.07	0.245	0.332	0.0113
3.196	0.07	0.315	0.3863	0.0063
3.196	0.157	0.035	0.2815	0.0058
3.196	0.157	0.105	0.3866	0.0028
3.196	0.157	0.175	0.422	0.0073
3.196	0.157	0.245	0.4579	0.006
3.196	0.157	0.315	0.4508	0.0132
3.196	0.245	0.035	0.2901	0.0066
3.196	0.245	0.105	0.4076	-0.0009
3.371	0.944	0.105	0.3968	0

Appendix 2.4 Velocity data for the side weir flows in open channel (Q_R=0.792) Contd.

X*	Y*	Z*	U (m/s)	V (m/s)
3.196	0.245	0.175	0.4498	0.0054
3.196	0.245	0.245	0.4867	0.0089
3.196	0.245	0.315	0.4712	0.0144
3.196	0.315	0.035	0.3209	0.0046
3.196	0.315	0.105	0.4163	0.0062
3.196	0.315	0.175	0.4412	0.0067
3.196	0.315	0.245	0.4757	0.0068
3.196	0.315	0.315	0.4761	0.0122
3.196	0.42	0.035	0.3216	0.0055
3.196	0.42	0.105	0.4136	0.0048
3.196	0.42	0.175	0.4381	0.0032
3.196	0.42	0.245	0.4598	0.0083
3.196	0.42	0.315	0.4982	0.014
3.196	0.507	0.035	0.3108	0.0005
3.196	0.507	0.105	0.4127	0.0038
3.196	0.507	0.175	0.4371	0.0047
3.196	0.507	0.245	0.4848	0.0113

X*	Y*	Z*	U (m/s)	V (m/s)
3.196	0.507	0.315	0.5246	0.0187
3.196	0.594	0.035	0.3521	0.013
3.196	0.594	0.105	0.4378	0.0026
3.196	0.594	0.175	0.4689	0.0091
3.196	0.594	0.245	0.5577	0.0068
3.196	0.594	0.315	0.6843	0.0566
3.196	0.682	0.035	0.3479	0.0043
3.196	0.682	0.105	0.4145	0.0011
3.196	0.682	0.175	0.4423	0.0015
3.196	0.682	0.245	0.5028	0.0112
3.196	0.682	0.315	0.631	0.0259
3.196	0.769	0.035	0.309	0.0014
3.196	0.769	0.105	0.3958	0.0027
3.196	0.769	0.175	0.4548	0.0043
3.196	0.769	0.245	0.5013	0.0111
3.196	0.769	0.315	0.534	0.0151
3.196	0.857	0.035	0.3436	-0.0035

Appendix 2.4 Velocity data for the side weir flows in open channel (Q_R=0.792) Contd.

X*	Y*	Z*	U (m/s)	V (m/s)
3.196	0.857	0.105	0.444	0.0022
3.196	0.857	0.175	0.493	0.0069
3.196	0.857	0.245	0.5308	0.0147
3.196	0.857	0.315	0.5168	0.0106
3.196	0.944	0.035	0.3596	0.0063
3.196	0.944	0.105	0.4132	-0.0016
3.196	0.944	0.175	0.492	0.0077
3.196	0.944	0.245	0.5405	0.0109
3.196	0.944	0.315	0.5188	0.0091
3.021	0.07	0.035	0.2877	-0.0008
3.021	0.07	0.105	0.3269	0.001
3.021	0.07	0.175	0.371	0.0049
3.021	0.07	0.245	0.3676	0.0092
3.021	0.07	0.315	0.3934	0.0115
3.021	0.157	0.035	0.288	0.0037
3.021	0.157	0.105	0.3883	0.0007
3.021	0.157	0.175	0.4255	0.0048

X*	Y*	Z*	U (m/s)	V (m/s)
3.021	0.157	0.245	0.4591	0.0009
3.021	0.157	0.315	0.4549	0.0055
3.021	0.245	0.035	0.2962	0.0018
3.021	0.245	0.105	0.4018	0.0017
3.021	0.245	0.175	0.4512	0.0039
3.021	0.245	0.245	0.4851	0.0038
3.021	0.245	0.315	0.4632	0.0106
3.021	0.315	0.035	0.3319	0.001
3.021	0.315	0.105	0.4088	0.0037
3.021	0.315	0.175	0.4364	0.0039
3.021	0.315	0.245	0.4741	0.0037
3.021	0.315	0.315	0.4729	0.0147
3.021	0.42	0.035	0.3175	0.0017
3.021	0.42	0.105	0.3978	-0.0004
3.021	0.42	0.175	0.4276	0.0024
3.021	0.42	0.245	0.4521	0.0092
3.021	0.42	0.315	0.4769	0.0129

X*	Y*	Z*	U (m/s)	V (m/s)
3.021	0.507	0.035	0.3315	-0.0064
3.021	0.507	0.105	0.4087	0.0126
3.021	0.507	0.175	0.438	0.0071
3.021	0.507	0.245	0.4842	0.0092
3.021	0.507	0.315	0.4687	0.0293
3.021	0.594	0.035	0.3452	0.0038
3.021	0.594	0.105	0.4231	0.0017
3.021	0.594	0.175	0.4647	0.0036
3.021	0.594	0.245	0.5033	0.0072
3.021	0.594	0.315	0.5119	0.015
3.021	0.682	0.035	0.3317	0.0006
3.021	0.682	0.105	0.4049	-0.0001
3.021	0.682	0.175	0.4425	0.0027
3.021	0.682	0.245	0.4994	0.0093
3.021	0.682	0.315	0.5098	0.0123
3.021	0.769	0.035	0.3113	-0.0033
3.021	0.769	0.105	0.4153	0.0009

X*	Y*	Z*	U (m/s)	V (m/s)
3.021	0.769	0.175	0.4621	0.0026
3.021	0.769	0.245	0.4981	0.0075
3.021	0.769	0.315	0.5164	0.0157
3.021	0.857	0.035	0.3455	-0.0013
3.021	0.857	0.105	0.4486	0.0056
3.021	0.857	0.175	0.5053	0.0105
3.021	0.857	0.245	0.5379	0.0131
3.021	0.857	0.315	0.5137	0.0098
3.021	0.944	0.035	0.3379	0.0154
3.021	0.944	0.105	0.3847	-0.0003
3.021	0.944	0.175	0.472	0.006
3.021	0.944	0.245	0.5275	0.0072
3.021	0.944	0.315	0.4989	0.013
2.846	0.07	0.035	0.2813	-0.0006
2.846	0.07	0.105	0.3344	0.0017
2.846	0.07	0.175	0.3718	0.0003
2.846	0.07	0.245	0.3741	0.0036

X*	Y*	Z*	U (m/s)	V (m/s)
2.846	0.07	0.315	0.3925	0.0017
2.846	0.157	0.035	0.3091	0.0042
2.846	0.157	0.105	0.3787	0.002
2.846	0.157	0.175	0.4324	0.0045
2.846	0.157	0.245	0.4734	0.0012
2.846	0.157	0.315	0.4671	0.0058
2.846	0.245	0.035	0.2911	0.003
2.846	0.245	0.105	0.3975	0.0008
2.846	0.245	0.175	0.4465	0.0026
2.846	0.245	0.245	0.4895	0.0002
2.846	0.245	0.315	0.4771	0.0085
2.846	0.315	0.035	0.3259	-0.0015
2.846	0.315	0.105	0.4167	0.0028
2.846	0.315	0.175	0.4414	0.0046
2.846	0.315	0.245	0.4771	0.004
2.846	0.315	0.315	0.485	0.0031
2.846	0.42	0.035	0.315	0.0015

X*	Y*	Z*	U (m/s)	V (m/s)
2.846	0.42	0.105	0.3891	-0.0015
2.846	0.42	0.175	0.4268	0.1143
2.846	0.42	0.245	0.4708	0.0037
2.846	0.42	0.315	0.4952	0.0033
2.846	0.507	0.035	0.3358	-0.0033
2.846	0.507	0.105	0.407	-0.0014
2.846	0.507	0.175	0.4529	0.002
2.846	0.507	0.245	0.4919	0.0058
2.846	0.507	0.315	0.496	0.0159
2.846	0.594	0.035	0.3356	-0.0028
2.846	0.594	0.105	0.4279	-0.0002
2.846	0.594	0.175	0.4664	0.0006
2.846	0.594	0.245	0.5174	0.0063
2.846	0.594	0.315	0.4969	0.0136
2.846	0.682	0.035	0.3265	0.0003
2.846	0.682	0.105	0.4158	-0.0016
2.846	0.682	0.175	0.4393	0.0009

Appendix 2.4 Velocity data for the side weir flows in open channel (Q_R=0.792) Contd.

X*	Y*	Z*	U (m/s)	V (m/s)		X*	Y*	Z*	U (m/s)	V (m/s)
2.846	0.682	0.245	0.4999	0.0078		2.671	0.07	0.245	0.339	0.0124
2.846	0.682	0.315	0.5281	0.0189		2.671	0.07	0.315	0.3696	0.0075
2.846	0.769	0.035	0.3152	-0.0052		2.671	0.157	0.035	0.2869	0.0091
2.846	0.769	0.105	0.4105	-0.0006		2.671	0.157	0.105	0.3675	0.0051
2.846	0.769	0.175	0.4636	0.0027		2.671	0.157	0.175	0.4153	0.0097
2.846	0.769	0.245	0.5099	0.0116		2.671	0.157	0.245	0.4462	0.0096
2.846	0.769	0.315	0.5104	0.0131		2.671	0.157	0.315	0.4467	0.0116
2.846	0.857	0.035	0.3544	-0.0018		2.671	0.245	0.035	0.3155	0.0052
2.846	0.857	0.105	0.4566	0.0029		2.671	0.245	0.105	0.3867	0.0046
2.846	0.857	0.175	0.497	0.0033		2.671	0.245	0.175	0.4451	0.0085
2.846	0.857	0.245	0.5384	0.0089		2.671	0.245	0.245	0.4842	0.0112
2.846	0.857	0.315	0.5155	0.0121		2.671	0.245	0.315	0.4721	0.0167
2.846	0.944	0.035	0.3692	0.0092		2.671	0.315	0.035	0.3204	0.0056
2.846	0.944	0.105	0.3773	-0.0025		2.671	0.315	0.105	0.3993	0.0069
2.846	0.944	0.175	0.479	0.0062		2.671	0.315	0.175	0.4404	0.0103
2.846	0.944	0.245	0.5234	0.0074		2.671	0.315	0.245	0.4722	0.0131
2.846	0.944	0.315	0.5167	0.0125		2.671	0.315	0.315	0.4748	0.015
2.671	0.07	0.035	0.2843	0.0027		2.671	0.42	0.035	0.3291	0.0085
2.671	0.07	0.105	0.2886	0.0118		2.671	0.42	0.105	0.384	0.0043
2.671	0.07	0.175	0.3526	0.0057		2.671	0.42	0.175	0.4443	0.0086

Appendix 2.4 Velocity data for the side weir flows in open channel (Q_R=0.792)

X*	Y*	Z*	U (m/s)	V (m/s)		X*	Y*	Z*	U (m/s)	V (m/s)
2.671	0.42	0.245	0.4582	0.0109		2.671	0.769	0.245	0.4945	0.0137
2.671	0.42	0.315	0.4855	0.0179		2.671	0.769	0.315	0.5307	0.0215
2.671	0.507	0.035	0.3188	0.0023		2.671	0.857	0.035	0.3227	-0.0011
2.671	0.507	0.105	0.3935	0.0066		2.671	0.857	0.105	0.4368	0.0076
2.671	0.507	0.175	0.4456	0.0111		2.671	0.857	0.175	0.4857	0.0107
2.671	0.507	0.245	0.4768	0.0145		2.671	0.857	0.245	0.5293	0.0179
2.671	0.507	0.315	0.4918	0.0215		2.671	0.857	0.315	0.5224	0.0121
2.671	0.594	0.035	0.3286	0.0041		2.671	0.944	0.035	0.3969	0.0068
2.671	0.594	0.105	0.4331	0.0068		2.671	0.944	0.105	0.4259	0.0039
2.671	0.594	0.175	0.4641	0.0071		2.671	0.944	0.175	0.4842	0.0077
2.671	0.594	0.245	0.5145	0.0134		2.671	0.944	0.245	0.5443	0.0143
2.671	0.594	0.315	0.5086	0.0214		2.671	0.944	0.315	0.5233	0.0117
2.671	0.682	0.035	0.3306	0.0055		2.497	0.07	0.035	0.2713	0.0047
2.671	0.682	0.105	0.4091	0.0065		2.497	0.07	0.105	0.2881	0.0067
2.671	0.682	0.175	0.4483	0.0084		2.497	0.07	0.175	0.3257	0.0033
2.671	0.682	0.245	0.5079	0.0136		2.497	0.07	0.245	0.331	0.0049
2.671	0.682	0.315	0.5177	0.017		2.497	0.07	0.315	0.368	0.0068
2.671	0.769	0.035	0.3029	0.0029		2.497	0.157	0.035	0.2726	0.0041
2.671	0.769	0.105	0.4024	0.0034		2.497	0.157	0.105	0.355	0.0067
2.671	0.769	0.175	0.4469	0.0096		2.671	0.769	0.245	0.4945	0.0137

Appendix 2.4 Velocity data for the side weir flows in open channel (Q_R=0.792)

X*	Y*	Z*	U (m/s)	V (m/s)		X*	Y*	Z*	U (m/s)	V (m/s)
2.497	0.157	0.175	0.4028	0.0031		2.497	0.507	0.175	0.4355	0.0044
2.497	0.157	0.245	0.4464	0.0052		2.497	0.507	0.245	0.4672	0.007
2.497	0.157	0.315	0.4437	0.0047		2.497	0.507	0.315	0.491	0.013
2.497	0.245	0.035	0.2913	0.0053		2.497	0.594	0.035	0.3363	-0.0048
2.497	0.245	0.105	0.3892	-0.0001		2.497	0.594	0.105	0.4154	0.0018
2.497	0.245	0.175	0.4448	0.0007		2.497	0.594	0.175	0.4615	0.0011
2.497	0.245	0.245	0.4786	0.0051		2.497	0.594	0.245	0.505	0.0067
2.497	0.245	0.315	0.4687	0.0077		2.497	0.594	0.315	0.5011	0.0184
2.497	0.315	0.035	0.3201	0.0016		2.497	0.682	0.035	0.3345	0.0033
2.497	0.315	0.105	0.4047	0.0027		2.497	0.682	0.105	0.4137	-0.0014
2.497	0.315	0.175	0.4471	0.0035		2.497	0.682	0.175	0.4553	0.0002
2.497	0.315	0.245	0.481	0.0056		2.497	0.682	0.245	0.4981	0.0087
2.497	0.315	0.315	0.4783	0.0104		2.497	0.682	0.315	0.4977	0.0163
2.497	0.42	0.035	0.3111	0.0029		2.497	0.769	0.035	0.3003	-0.0054
2.497	0.42	0.105	0.3916	0.0015		2.497	0.769	0.105	0.3975	-0.0037
2.497	0.42	0.175	0.443	0.0028		2.497	0.769	0.175	0.4596	0.0041
2.497	0.42	0.245	0.4578	0.008		2.497	0.769	0.245	0.4944	0.0093
2.497	0.42	0.315	0.4811	0.0104		2.497	0.769	0.315	0.4958	0.0161
2.497	0.507	0.035	0.3023	-0.0007		2.497	0.857	0.035	0.3428	-0.0096
2.497	0.507	0.105	0.3925	0.0032		2.497	0.857	0.105	0.4412	-0.0003

X*	Y*	Z*	U (m/s)	V (m/s)		X*	Y*	Z*	U (m/s)	V (m/s)
2.497	0.857	0.175	0.4879	0.0048		2.392	0.245	0.105	0.3803	0.0007
2.497	0.857	0.245	0.5186	0.0106		2.392	0.245	0.175	0.4327	0.0044
2.497	0.857	0.315	0.5106	0.0108		2.392	0.245	0.245	0.4768	0.0075
2.497	0.944	0.035	0.3834	0.0051		2.392	0.245	0.315	0.4655	0.0072
2.497	0.944	0.105	0.4227	-0.0002		2.392	0.315	0.035	0.3062	0.0032
2.497	0.944	0.175	0.4775	0.0046		2.392	0.315	0.105	0.3938	0.0085
2.497	0.944	0.245	0.539	0.0113		2.392	0.315	0.175	0.4335	0.0058
2.497	0.944	0.315	0.5147	0.0102		2.392	0.315	0.245	0.4743	0.0059
2.392	0.07	0.035	0.2787	0.0025		2.392	0.315	0.315	0.4876	0.0101
2.392	0.07	0.105	0.2779	0.0042		2.392	0.42	0.035	0.3196	0.0062
2.392	0.07	0.175	0.3117	0.0031		2.392	0.42	0.105	0.3893	0.0049
2.392	0.07	0.245	0.3401	0.0055		2.392	0.42	0.175	0.4298	0.0045
2.392	0.07	0.315	0.3553	0.0081		2.392	0.42	0.245	0.4498	0.0073
2.392	0.157	0.035	0.3653	0.0014		2.392	0.42	0.315	0.4768	0.0109
2.392	0.157	0.105	0.2667	0.005		2.392	0.507	0.035	0.3024	-0.0021
2.392	0.157	0.175	0.3519	0.007		2.392	0.507	0.105	0.3836	0.0034
2.392	0.157	0.245	0.4097	0.0061		2.392	0.507	0.175	0.4322	0.0059
2.392	0.157	0.315	0.4381	0.0068		2.392	0.507	0.245	0.4586	0.0084
2.392	0.245	0.035	0.2823	0.0063		2.392	0.507	0.315	0.488	0.0123
2.497	0.857	0.175	0.4879	0.0048		2.392	0.594	0.035	0.3312	0.0003

Appendix 2.4 Velocity data for the side weir flows in open channel (Q_R=0.792) Contd.

X*	Y*	Z*	U (m/s)	V (m/s)		X*	Y*	Z*	U (m/s)	V (m/s)
2.392	0.594	0.105	0.4266	0.003		2.392	0.944	0.105	0.4336	0.0068
2.392	0.594	0.175	0.46	0.0059		2.392	0.944	0.175	0.4622	0.0046
2.392	0.594	0.245	0.5037	0.0098		2.392	0.944	0.245	0.5296	0.0132
2.392	0.594	0.315	0.4973	0.0113		2.392	0.944	0.315	0.5124	0.0189
2.392	0.682	0.035	0.3326	0.0026		2.287	0.07	0.035	0.2839	0.0035
2.392	0.682	0.105	0.3885	0.0042		2.287	0.07	0.105	0.2856	0.0109
2.392	0.682	0.175	0.431	0.0069		2.287	0.07	0.175	0.3411	0.006
2.392	0.682	0.245	0.4956	0.0127		2.287	0.07	0.245	0.3418	0.0089
2.392	0.682	0.315	0.5147	0.0165		2.287	0.07	0.315	0.3666	0.0064
2.392	0.769	0.035	0.2824	-0.0016		2.287	0.157	0.035	0.2867	0.0101
2.392	0.769	0.105	0.3844	0.0022		2.287	0.157	0.105	0.3752	0.004
2.392	0.769	0.175	0.4386	0.0072		2.287	0.157	0.175	0.4107	0.0078
2.392	0.769	0.245	0.485	0.0128		2.287	0.157	0.245	0.457	0.0092
2.392	0.769	0.315	0.5019	0.018		2.287	0.157	0.315	0.4615	0.0114
2.392	0.857	0.035	0.3298	-0.0069		2.287	0.245	0.035	0.2809	0.012
2.392	0.857	0.105	0.4259	0.0026		2.287	0.245	0.105	0.3922	0.0048
2.392	0.857	0.175	0.4847	0.0075		2.287	0.245	0.175	0.4466	0.0071
2.392	0.857	0.245	0.5152	0.0155		2.287	0.245	0.245	0.4888	0.0079
2.392	0.857	0.315	0.5087	0.0162		2.287	0.245	0.315	0.4884	0.0117
2.392	0.944	0.035	0.3615	0.0059		2.392	0.944	0.105	0.4336	0.0068

X*	Y*	Z*	U (m/s)	V (m/s)		X*	Y*	Z*	U (m/s)	V (m/s)
2.287	0.315	0.035	0.3182	0.005		2.287	0.682	0.035	0.3152	0.0057
2.287	0.315	0.105	0.3954	0.0068		2.287	0.682	0.105	0.4032	0.0048
2.287	0.315	0.175	0.4498	0.0088		2.287	0.682	0.175	0.459	0.0067
2.287	0.315	0.245	0.4744	0.0068		2.287	0.682	0.245	0.5068	0.01
2.287	0.315	0.315	0.4875	0.0116		2.287	0.682	0.315	0.5241	0.0139
2.287	0.42	0.035	0.3045	0.0044		2.287	0.769	0.035	0.3053	-0.0004
2.287	0.42	0.105	0.3918	0.0026		2.287	0.769	0.105	0.396	0.0032
2.287	0.42	0.175	0.4328	0.0086		2.287	0.769	0.175	0.4391	0.0085
2.287	0.42	0.245	0.458	0.0101		2.287	0.769	0.245	0.499	0.0122
2.287	0.42	0.315	0.4893	0.0138		2.287	0.769	0.315	0.5212	0.0157
2.287	0.507	0.035	0.303	-0.0013		2.287	0.857	0.035	0.3304	-0.0023
2.287	0.507	0.105	0.4015	0.0023		2.287	0.857	0.105	0.4481	0.0069
2.287	0.507	0.175	0.4468	0.0041		2.287	0.857	0.175	0.486	0.0083
2.287	0.507	0.245	0.4802	0.0118		2.287	0.857	0.245	0.5277	0.0158
2.287	0.507	0.315	0.5003	0.0153		2.287	0.857	0.315	0.5259	0.02
2.287	0.594	0.035	0.3299	0.0029		2.287	0.944	0.035	0.3844	0.0074
2.287	0.594	0.105	0.4292	0.0026		2.287	0.944	0.105	0.4222	0.0026
2.287	0.594	0.175	0.4703	0.0066		2.287	0.944	0.175	0.4595	0.0066
2.287	0.594	0.245	0.512	0.0097		2.287	0.944	0.245	0.5387	0.0177
2.287	0.594	0.315	0.5119	0.0153		2.287	0.944	0.315	0.5304	0.0285

Appendix 2.4 Velocity data for the side weir flows in open channel (Q_R=0.792) Contd.

X*	Y*	Z*	U (m/s)	V (m/s)		X*	Y*	Z*	U (m/s)	V (m/s)
2.182	0.07	0.035	0.2737	-0.0046		2.182	0.42	0.035	0.2993	0.0032
2.182	0.07	0.105	0.3013	0.001		2.182	0.42	0.105	0.4009	-0.0035
2.182	0.07	0.175	0.3468	0.0016		2.182	0.42	0.175	0.4502	0.0017
2.182	0.07	0.245	0.3582	0		2.182	0.42	0.245	0.4708	0.0058
2.182	0.07	0.315	0.376	0.0049		2.182	0.42	0.315	0.4936	0.0118
2.182	0.157	0.035	0.2667	0.0004		2.182	0.507	0.035	0.302	-0.0039
2.182	0.157	0.105	0.3872	-0.0046		2.182	0.507	0.105	0.3944	-0.0011
2.182	0.157	0.175	0.4268	-0.0015		2.182	0.507	0.175	0.4437	0.0012
2.182	0.157	0.245	0.4521	-0.0008		2.182	0.507	0.245	0.4789	0.0036
2.182	0.157	0.315	0.4653	0.0027		2.182	0.507	0.315	0.4989	0.0175
2.182	0.245	0.035	0.2845	-0.0016		2.182	0.594	0.035	0.3148	-0.0066
2.182	0.245	0.105	0.3798	-0.0037		2.182	0.594	0.105	0.4239	-0.0027
2.182	0.245	0.175	0.4566	-0.0013		2.182	0.594	0.175	0.4735	0.0011
2.182	0.245	0.245	0.4881	-0.0013		2.182	0.594	0.245	0.5122	0.0041
2.182	0.245	0.315	0.4856	0.0051		2.182	0.594	0.315	0.5161	0.0125
2.182	0.315	0.035	0.3061	-0.0016		2.182	0.682	0.035	0.314	-0.0018
2.182	0.315	0.105	0.399	0.0022		2.182	0.682	0.105	0.4045	-0.0012
2.182	0.315	0.175	0.4598	0.0009		2.182	0.682	0.175	0.4568	0.0003
2.182	0.315	0.245	0.4867	0.0038		2.182	0.682	0.245	0.5054	0.0043
2.182	0.315	0.315	0.5	0.0086		2.182	0.682	0.315	0.5282	0.0078

Appendix 2.4 Velocity data for the side weir flows in open channel (Q_R=0.792) Contd.

X*	Y*	Z*	U (m/s)	V (m/s)		X*	Y*	Z*	U (m/s)	V (m/s)
2.182	0.769	0.035	0.3	-0.0086		2.077	0.07	0.315	0.3642	0.0062
2.182	0.769	0.105	0.3935	-0.0018		2.077	0.157	0.035	0.2817	0.0003
2.182	0.769	0.175	0.4629	0.001		2.077	0.157	0.105	0.3886	0.0002
2.182	0.769	0.245	0.5048	0.0078		2.077	0.157	0.175	0.4278	-0.0021
2.182	0.769	0.315	0.528	0.0092		2.077	0.157	0.245	0.4584	0.0012
2.182	0.857	0.035	0.3368	-0.0011		2.077	0.157	0.315	0.462	0.0015
2.182	0.857	0.105	0.4492	0.0007		2.077	0.245	0.035	0.2929	0.0054
2.182	0.857	0.175	0.5107	0.0042		2.077	0.245	0.105	0.3908	-0.0046
2.182	0.857	0.245	0.5386	0.0089		2.077	0.245	0.175	0.4588	0.0004
2.182	0.857	0.315	0.5376	0.0105		2.077	0.245	0.245	0.4909	-0.0007
2.182	0.944	0.035	0.3749	0.0067		2.077	0.245	0.315	0.4778	0.0061
2.182	0.944	0.105	0.4111	-0.0014		2.077	0.315	0.035	0.2787	-0.0006
2.182	0.944	0.175	0.4608	0.0051		2.077	0.315	0.105	0.3991	-0.0013
2.182	0.944	0.245	0.5346	0.0112		2.077	0.315	0.175	0.458	-0.0005
2.182	0.944	0.315	0.5326	0.0428		2.077	0.315	0.245	0.4844	0.001
2.077	0.07	0.035	0.2916	-0.006		2.077	0.315	0.315	0.4811	0.0042
2.077	0.07	0.105	0.3101	0.0014		2.077	0.42	0.035	0.2969	-0.0044
2.077	0.07	0.175	0.3399	-0.0036		2.077	0.42	0.105	0.3948	-0.0045
2.077	0.07	0.245	0.3482	0.003		2.077	0.42	0.175	0.4463	-0.0013
2.182	0.769	0.035	0.3	-0.0086		2.077	0.42	0.245	0.4582	-0.0003

Appendix 2.4 Velocity data for the side weir flows in open channel (Q_R=0.792) Contd.

X*	Y*	Z*	U (m/s)	V (m/s)		X*	Y*	Z*	U (m/s)	V (m/s)
2.077	0.42	0.315	0.4929	0.0104		2.077	0.769	0.315	0.5242	0.0093
2.077	0.507	0.035	0.2939	-0.0063		2.077	0.857	0.035	0.3302	-0.0093
2.077	0.507	0.105	0.3836	-0.0035		2.077	0.857	0.105	0.444	-0.004
2.077	0.507	0.175	0.4523	0.0008		2.077	0.857	0.175	0.5073	0.0048
2.077	0.507	0.245	0.4781	0.0041		2.077	0.857	0.245	0.5308	0.0052
2.077	0.507	0.315	0.4941	0.0177		2.077	0.857	0.315	0.5341	0.0077
2.077	0.594	0.035	0.3287	-0.0109		2.077	0.944	0.035	0.3553	0.0038
2.077	0.594	0.105	0.4281	-0.005		2.077	0.944	0.105	0.4301	0.0014
2.077	0.594	0.175	0.4667	-0.0021		2.077	0.944	0.175	0.4604	0.0008
2.077	0.594	0.245	0.5079	0.0034		2.077	0.944	0.245	0.5306	0.0069
2.077	0.594	0.315	0.514	0.0118		2.077	0.944	0.315	0.5381	0.0083
2.077	0.682	0.035	0.3154	-0.0092		0.892	0.07	0.035	0.4959	0.0396
2.077	0.682	0.105	0.3957	-0.0073		0.892	0.07	0.105	0.5262	0.0336
2.077	0.682	0.175	0.4526	-0.0046		0.892	0.07	0.175	0.5515	0.0296
2.077	0.682	0.245	0.4985	0.0032		0.892	0.07	0.245	0.5231	0.0264
2.077	0.682	0.315	0.5236	0.0118		0.892	0.07	0.315	0.5314	0.0288
2.077	0.769	0.035	0.2912	-0.0092		0.892	0.14	0.035	0.4511	0.0806
2.077	0.769	0.105	0.39	-0.0047		0.892	0.14	0.105	0.519	0.0618
2.077	0.769	0.175	0.4658	-0.0005		0.892	0.14	0.175	0.5587	0.0527
2.077	0.769	0.245	0.4941	0.0044		2.077	0.769	0.315	0.5242	0.0093

Appendix 2.4 Velocity data for the side weir flows in open channel (Q_R=0.792) Contd.

X*	Y*	Z*	U (m/s)	V (m/s)		X*	Y*	Z*	U (m/s)	V (m/s)
0.892	0.14	0.245	0.5804	0.0472		0.892	0.42	0.245	0.514	0.0673
0.892	0.14	0.315	0.5777	0.047		0.892	0.42	0.315	0.5228	0.0634
0.874	0.21	0.035	0.4625	0.0807		0.892	0.49	0.035	0.3331	0.1165
0.892	0.21	0.105	0.5103	0.0753		0.892	0.49	0.105	0.4254	0.0889
0.892	0.21	0.175	0.5496	0.0649		0.892	0.49	0.175	0.4932	0.074
0.892	0.21	0.245	0.5732	0.0573		0.892	0.49	0.245	0.5028	0.0671
0.892	0.21	0.315	0.5708	0.0537		0.892	0.49	0.315	0.5076	0.0637
0.892	0.28	0.035	0.4098	0.108		0.892	0.559	0.035	0.31	0.1054
0.892	0.28	0.105	0.4921	0.0818		0.892	0.559	0.105	0.4138	0.0812
0.892	0.28	0.175	0.5271	0.0723		0.892	0.559	0.175	0.4838	0.0709
0.892	0.28	0.245	0.5415	0.0631		0.892	0.559	0.245	0.5	0.0604
0.892	0.28	0.315	0.5514	0.0618		0.892	0.559	0.315	0.5184	0.0582
0.892	0.35	0.035	0.3701	0.1216		0.892	0.629	0.035	0.2748	0.0874
0.892	0.35	0.105	0.4355	0.091		0.892	0.629	0.105	0.3831	0.0758
0.892	0.35	0.175	0.4972	0.076		0.892	0.629	0.175	0.4526	0.0644
0.892	0.35	0.245	0.5223	0.0676		0.892	0.629	0.245	0.4972	0.0584
0.892	0.35	0.315	0.5298	0.065		0.892	0.629	0.315	0.5064	0.0524
0.892	0.42	0.035	0.3583	0.1209		0.892	0.699	0.035	0.2805	0.0972
0.892	0.42	0.105	0.4375	0.0927		0.892	0.699	0.105	0.3749	0.0688
0.892	0.42	0.175	0.4911	0.0745		0.892	0.699	0.175	0.4407	0.0581

Appendix 2.4 Velocity data for the side weir flows in open channel (Q_R=0.792) Contd.

X*	Y*	Z*	U (m/s)	V (m/s)		X*	Y*	Z*	U (m/s)	V (m/s)
0.892	0.699	0.245	0.4905	0.0512		0.892	0.979	0.245	0.3589	0.0014
0.892	0.699	0.315	0.503	0.0459		0.892	0.979	0.315	0.3496	0.0076
0.892	0.769	0.035	0.337	0.0913		0.822	0.07	0.035	0.5121	0.0781
0.892	0.769	0.105	0.4011	0.0665		0.822	0.07	0.105	0.5632	0.0626
0.892	0.769	0.175	0.457	0.0516		0.822	0.07	0.175	0.5938	0.0507
0.892	0.769	0.245	0.4981	0.0428		0.822	0.07	0.245	0.5815	0.0527
0.892	0.769	0.315	0.4993	0.0463		0.822	0.07	0.315	0.5774	0.0479
0.892	0.839	0.035	0.3263	0.0675		0.822	0.14	0.035	0.4686	0.1124
0.892	0.839	0.105	0.4153	0.0533		0.822	0.14	0.105	0.5443	0.0905
0.892	0.839	0.175	0.4552	0.0503		0.822	0.14	0.175	0.5849	0.0761
0.892	0.839	0.245	0.4866	0.0391		0.822	0.14	0.245	0.5998	0.0683
0.892	0.839	0.315	0.4968	0.0355		0.822	0.14	0.315	0.5964	0.0638
0.892	0.909	0.035	0.2919	0.0357		0.822	0.21	0.035	0.4209	0.1407
0.892	0.909	0.105	0.3565	0.0317		0.822	0.21	0.105	0.5146	0.1059
0.892	0.909	0.175	0.3451	0.0346		0.822	0.21	0.175	0.5622	0.0865
0.892	0.909	0.245	0.4413	0.0211		0.822	0.21	0.245	0.5774	0.0774
0.892	0.909	0.315	0.4298	0.0245		0.822	0.21	0.315	0.5792	0.071
0.892	0.979	0.035	0.1537	0.0195		0.822	0.28	0.035	0.3915	0.1441
0.892	0.979	0.105	0.2343	0.0139		0.822	0.28	0.105	0.5058	0.1114
0.892	0.979	0.175	0.2327	0.0162		0.892	0.979	0.245	0.3589	0.0014

Appendix 2.4 Velocity data for the side weir flows in open channel (Q_R=0.792) Contd.

X*	Y*	Z*	U (m/s)	V (m/s)		X*	Y*	Z*	U (m/s)	V (m/s)
0.822	0.28	0.175	0.5516	0.0935		0.822	0.559	0.175	0.4856	0.0859
0.822	0.28	0.245	0.5644	0.0836		0.822	0.559	0.245	0.5251	0.0738
0.822	0.28	0.315	0.5711	0.076		0.822	0.559	0.315	0.5315	0.0692
0.822	0.35	0.035	0.3847	0.1439		0.822	0.629	0.035	0.297	0.1066
0.822	0.35	0.105	0.4621	0.1047		0.822	0.629	0.105	0.3919	0.0811
0.822	0.35	0.175	0.5202	0.0931		0.822	0.629	0.175	0.4691	0.0725
0.822	0.35	0.245	0.5382	0.0822		0.822	0.629	0.245	0.5032	0.0669
0.822	0.35	0.315	0.5505	0.0792		0.822	0.629	0.315	0.5241	0.0615
0.822	0.42	0.035	0.3816	0.1487		0.822	0.699	0.035	0.3188	0.1205
0.822	0.42	0.105	0.4596	0.1091		0.822	0.699	0.105	0.4002	0.0797
0.822	0.42	0.175	0.5113	0.0913		0.822	0.699	0.175	0.4544	0.0688
0.822	0.42	0.245	0.5389	0.0798		0.822	0.699	0.245	0.494	0.0583
0.822	0.42	0.315	0.5485	0.0763		0.822	0.699	0.315	0.5115	0.0572
0.822	0.49	0.035	0.3494	0.1341		0.822	0.769	0.035	0.3477	0.102
0.822	0.49	0.105	0.4628	0.1047		0.822	0.769	0.105	0.426	0.0775
0.822	0.49	0.175	0.5037	0.0922		0.822	0.769	0.175	0.4819	0.0643
0.822	0.49	0.245	0.5201	0.0805		0.822	0.769	0.245	0.5113	0.0514
0.822	0.49	0.315	0.5333	0.0746		0.822	0.769	0.315	0.5192	0.0539
0.822	0.559	0.035	0.3962	0.0813		0.822	0.839	0.035	0.3371	0.08
0.822	0.559	0.105	0.4371	0.0934		0.822	0.839	0.105	0.4296	0.0598

Appendix 2.4 Velocity data for the side weir flows in open channel (Q_R=0.792) Contd.

X*	Y*	Z*	U (m/s)	V (m/s)		X*	Y*	Z*	U (m/s)	V (m/s)
0.822	0.839	0.175	0.444	0.0603		0.752	0.14	0.105	0.5984	0.1205
0.822	0.839	0.245	0.5076	0.0487		0.752	0.14	0.175	0.6305	0.1
0.822	0.839	0.315	0.5116	0.0415		0.752	0.14	0.245	0.6225	0.0836
0.822	0.909	0.035	0.2901	0.041		0.752	0.14	0.315	0.5698	0.0782
0.822	0.909	0.105	0.3556	0.0363		0.752	0.21	0.035	0.501	0.1493
0.822	0.909	0.175	0.33	0.0424		0.752	0.21	0.105	0.5648	0.1292
0.822	0.909	0.245	0.4283	0.0288		0.752	0.21	0.175	0.5779	0.111
0.822	0.909	0.315	0.4685	0.0271		0.752	0.21	0.245	0.5877	0.0967
0.822	0.979	0.035	0.2054	0.0119		0.752	0.21	0.315	0.585	0.0856
0.822	0.979	0.105	0.2092	0.0105		0.752	0.28	0.035	0.4623	0.1538
0.822	0.979	0.175	0.2439	0.0103		0.752	0.28	0.105	0.5202	0.1276
0.822	0.979	0.245	0.342	0.0062		0.752	0.28	0.175	0.543	0.1108
0.822	0.979	0.315	0.3273	0.0216		0.752	0.28	0.245	0.5624	0.0946
0.752	0.07	0.035	0.6039	0.1034		0.752	0.28	0.315	0.5468	0.0921
0.752	0.07	0.105	0.6431	0.0847		0.752	0.35	0.035	0.4073	0.1469
0.752	0.07	0.175	0.6476	0.0719		0.752	0.35	0.105	0.4768	0.131
0.752	0.07	0.245	0.6176	0.0577		0.752	0.35	0.175	0.5182	0.1056
0.752	0.07	0.315	0.5862	0.0583		0.752	0.35	0.245	0.5365	0.0962
0.752	0.14	0.035	0.5467	0.1406		0.752	0.35	0.315	0.5382	0.0914
0.822	0.839	0.175	0.444	0.0603		0.752	0.42	0.035	0.4008	0.1452

Appendix 2.4 Velocity data for the side weir flows in open channel (Q_R=0.792) Contd.

X*	Y*	Z*	U (m/s)	V (m/s)		X*	Y*	Z*	U (m/s)	V (m/s)
0.752	0.42	0.105	0.4733	0.1232		0.752	0.699	0.105	0.4131	0.0881
0.752	0.42	0.175	0.5085	0.1052		0.752	0.699	0.175	0.4625	0.0724
0.752	0.42	0.245	0.5179	0.0931		0.752	0.699	0.245	0.487	0.0689
0.752	0.42	0.315	0.5337	0.0951		0.752	0.699	0.315	0.4847	0.0675
0.752	0.49	0.035	0.3723	0.1363		0.752	0.769	0.035	0.3731	0.1004
0.752	0.49	0.105	0.4418	0.1143		0.752	0.769	0.105	0.4264	0.0825
0.752	0.49	0.175	0.5026	0.1029		0.752	0.769	0.175	0.4815	0.0751
0.752	0.49	0.245	0.5183	0.0896		0.752	0.769	0.245	0.4809	0.0649
0.752	0.49	0.315	0.5184	0.0848		0.752	0.769	0.315	0.4795	0.0607
0.752	0.559	0.035	0.3409	0.1188		0.752	0.839	0.035	0.3597	0.0784
0.752	0.559	0.105	0.4289	0.1027		0.752	0.839	0.105	0.4021	0.0708
0.752	0.559	0.175	0.488	0.0939		0.752	0.839	0.175	0.4415	0.0653
0.752	0.559	0.245	0.5071	0.0837		0.752	0.839	0.245	0.483	0.0549
0.752	0.559	0.315	0.5035	0.0804		0.752	0.839	0.315	0.4803	0.0495
0.752	0.629	0.035	0.3088	0.1044		0.752	0.909	0.035	0.2907	0.0356
0.752	0.629	0.105	0.3955	0.089		0.752	0.909	0.105	0.2915	0.0473
0.752	0.629	0.175	0.462	0.0804		0.752	0.909	0.175	0.3238	0.041
0.752	0.629	0.245	0.4915	0.0742		0.752	0.909	0.245	0.4261	0.0328
0.752	0.629	0.315	0.4946	0.0759		0.752	0.909	0.315	0.4364	0.0313
0.752	0.699	0.035	0.3529	0.1129		0.752	0.979	0.035	0.1373	0.1069

Appendix 2.4 Velocity data for the side weir flows in open channel (Q_R=0.792) Contd.

X*	Y*	Z*	U (m/s)	V (m/s)		X*	Y*	Z*	U (m/s)	V (m/s)
0.752	0.979	0.105	0.1886	0.0119		0.682	0.28	0.035	0.4629	0.1931
0.752	0.979	0.175	0.2003	0.0181		0.682	0.28	0.105	0.5371	0.1615
0.752	0.979	0.245	0.3192	0.0115		0.682	0.28	0.175	0.5706	0.1382
0.752	0.979	0.315	0.3148	0.0155		0.682	0.28	0.245	0.5784	0.1211
0.682	0.07	0.035	0.7013	0.1958		0.682	0.28	0.315	0.5741	0.1126
0.682	0.07	0.105	0.7287	0.1614		0.682	0.35	0.035	0.4405	0.1832
0.682	0.07	0.175	0.7165	0.1253		0.682	0.35	0.105	0.4837	0.1492
0.682	0.07	0.245	0.678	0.0958		0.682	0.35	0.175	0.5396	0.1313
0.682	0.07	0.315	0.6479	0.0802		0.682	0.35	0.245	0.5624	0.1151
0.682	0.14	0.035	0.5967	0.2129		0.682	0.35	0.315	0.5617	0.1139
0.682	0.14	0.105	0.6468	0.1778		0.682	0.42	0.035	0.4187	0.1783
0.682	0.14	0.175	0.6679	0.145		0.682	0.42	0.105	0.5033	0.1476
0.682	0.14	0.245	0.6633	0.1214		0.682	0.42	0.175	0.53	0.1288
0.682	0.14	0.315	0.6338	0.1078		0.682	0.42	0.245	0.5536	0.1162
0.682	0.21	0.035	0.5284	0.2047		0.682	0.42	0.315	0.5529	0.11
0.682	0.21	0.105	0.5896	0.1712		0.682	0.49	0.035	0.405	0.1576
0.682	0.21	0.175	0.6168	0.1474		0.682	0.49	0.105	0.4831	0.135
0.682	0.21	0.245	0.618	0.1241		0.682	0.49	0.175	0.5188	0.1251
0.682	0.21	0.315	0.6125	0.1139		0.682	0.49	0.245	0.5411	0.1091
0.752	0.979	0.105	0.1886	0.0119		0.682	0.49	0.315	0.5366	0.1046

Appendix 2.4 Velocity data for the side weir flows in open channel (Q_R=0.792) Contd.

X*	Y*	Z*	U (m/s)	V (m/s)		X*	Y*	Z*	U (m/s)	V (m/s)
0.682	0.559	0.035	0.3495	0.1348		0.682	0.839	0.035	0.3441	0.0779
0.682	0.559	0.105	0.4384	0.1177		0.682	0.839	0.105	0.3474	0.0809
0.682	0.559	0.175	0.4996	0.1074		0.682	0.839	0.175	0.4192	0.0713
0.682	0.559	0.245	0.5253	0.0981		0.682	0.839	0.245	0.4644	0.0633
0.682	0.559	0.315	0.5189	0.0989		0.682	0.839	0.315	0.4709	0.0556
0.682	0.629	0.035	0.3125	0.1272		0.682	0.909	0.035	0.2816	0.0435
0.682	0.629	0.105	0.3861	0.1045		0.682	0.909	0.105	0.2592	0.0451
0.682	0.629	0.175	0.4521	0.0894		0.682	0.909	0.175	0.2679	0.045
0.682	0.629	0.245	0.4816	0.0859		0.682	0.909	0.245	0.3782	0.0336
0.682	0.629	0.315	0.4898	0.0906		0.682	0.909	0.315	0.4202	0.0364
0.682	0.699	0.035	0.3453	0.1293		0.682	0.979	0.035	0.1266	0.0079
0.682	0.699	0.105	0.4033	0.1022		0.682	0.979	0.105	0.126	0.0164
0.682	0.699	0.175	0.4581	0.0901		0.682	0.979	0.175	0.1808	0.0163
0.682	0.699	0.245	0.4711	0.0822		0.682	0.979	0.245	0.2952	0.0164
0.682	0.699	0.315	0.4737	0.0813		0.682	0.979	0.315	0.2739	0.0205
0.682	0.769	0.035	0.3658	0.1159		0.612	0.07	0.035	0.7123	0.3189
0.682	0.769	0.105	0.4232	0.0976		0.612	0.07	0.105	0.7514	0.2587
0.682	0.769	0.175	0.4732	0.0866		0.612	0.07	0.175	0.7472	0.2038
0.682	0.769	0.245	0.4734	0.0746		0.612	0.07	0.245	0.7045	0.146
0.682	0.769	0.315	0.4749	0.0711		0.682	0.839	0.035	0.3441	0.0779

Appendix 2.4 Velocity data for the side weir flows in open channel (Q_R=0.792) Contd.

X*	Y*	Z*	U (m/s)	V (m/s)		X*	Y*	Z*	U (m/s)	V (m/s)
0.612	0.07	0.315	0.6749	0.1173		0.612	0.35	0.315	0.5424	0.131
0.612	0.14	0.035	0.5603	0.2955		0.612	0.42	0.035	0.3468	0.2059
0.612	0.14	0.105	0.6384	0.2379		0.612	0.42	0.105	0.4576	0.1687
0.612	0.14	0.175	0.6745	0.1954		0.612	0.42	0.175	0.4947	0.1504
0.612	0.14	0.245	0.6637	0.1546		0.612	0.42	0.245	0.5238	0.1326
0.612	0.14	0.315	0.6498	0.1405		0.612	0.42	0.315	0.5235	0.1291
0.612	0.21	0.035	0.4728	0.2629		0.612	0.49	0.035	0.3108	0.1788
0.612	0.21	0.105	0.5651	0.2173		0.612	0.49	0.105	0.4221	0.152
0.612	0.21	0.175	0.6055	0.1819		0.612	0.49	0.175	0.4743	0.1393
0.612	0.21	0.245	0.611	0.1533		0.612	0.49	0.245	0.4961	0.1221
0.612	0.21	0.315	0.6069	0.1431		0.612	0.49	0.315	0.5125	0.1179
0.612	0.28	0.035	0.405	0.2423		0.612	0.559	0.035	0.2898	0.1636
0.612	0.28	0.105	0.4936	0.1907		0.612	0.559	0.105	0.3804	0.13
0.612	0.28	0.175	0.5372	0.1684		0.612	0.559	0.175	0.4547	0.1205
0.612	0.28	0.245	0.5579	0.1473		0.612	0.559	0.245	0.4993	0.1111
0.612	0.28	0.315	0.5567	0.1368		0.612	0.559	0.315	0.5007	0.1118
0.612	0.35	0.035	0.3923	0.231		0.612	0.629	0.035	0.3014	0.1708
0.612	0.35	0.105	0.4694	0.1781		0.612	0.629	0.105	0.3705	0.1139
0.612	0.35	0.175	0.4983	0.1529		0.612	0.629	0.175	0.4343	0.105
0.612	0.35	0.245	0.5282	0.1373		0.612	0.629	0.245	0.4852	0.101

Appendix 2.4 Velocity data for the side weir flows in open channel (Q_R=0.792) Contd.

X*	Y*	Z*	U (m/s)	V (m/s)		X*	Y*	Z*	U (m/s)	V (m/s)
0.612	0.629	0.315	0.4882	0.1032		0.612	0.909	0.315	0.3973	0.0386
0.612	0.699	0.035	0.3253	0.1492		0.612	0.979	0.035	0.0426	0.0153
0.612	0.699	0.105	0.3803	0.1196		0.612	0.979	0.105	0.0805	0.0106
0.612	0.699	0.175	0.4252	0.0982		0.612	0.979	0.175	0.0761	0.0096
0.612	0.699	0.245	0.477	0.0919		0.612	0.979	0.245	0.2655	0.0175
0.612	0.699	0.315	0.4686	0.092		0.612	0.979	0.315	0.3041	0.0231
0.612	0.769	0.035	0.3254	0.1296		0.577	0.07	0.035	0.705	0.4132
0.612	0.769	0.105	0.3995	0.1123		0.577	0.07	0.105	0.7562	0.3327
0.612	0.769	0.175	0.4501	0.1033		0.577	0.07	0.175	0.7562	0.2579
0.612	0.769	0.245	0.4708	0.0872		0.577	0.07	0.245	0.7244	0.1833
0.612	0.769	0.315	0.4704	0.0832		0.577	0.07	0.28	0.6932	0.1419
0.612	0.839	0.035	0.3084	0.0932		0.577	0.14	0.035	0.5592	0.3428
0.612	0.839	0.105	0.3322	0.0914		0.577	0.14	0.105	0.6459	0.2785
0.612	0.839	0.175	0.3609	0.0849		0.577	0.14	0.175	0.6693	0.2306
0.612	0.839	0.245	0.4515	0.0695		0.577	0.14	0.245	0.6784	0.182
0.612	0.839	0.315	0.4367	0.0535		0.577	0.14	0.28	0.6633	0.1597
0.612	0.909	0.035	0.1967	0.042		0.577	0.21	0.035	0.4634	0.2962
0.612	0.909	0.105	0.2165	0.0463		0.577	0.21	0.105	0.5619	0.2432
0.612	0.909	0.175	0.2469	0.0501		0.577	0.21	0.175	0.6147	0.2036
0.612	0.909	0.245	0.3665	0.0418		0.612	0.909	0.315	0.3973	0.0386

Appendix 2.4 Velocity data for the side weir flows in open channel (Q_R=0.792) Contd.

X*	Y*	Z*	U (m/s)	V (m/s)		X*	Y*	Z*	U (m/s)	V (m/s)
0.577	0.21	0.245	0.6211	0.174		0.577	0.49	0.245	0.5269	0.1326
0.577	0.21	0.28	0.618	0.1617		0.577	0.49	0.28	0.5294	0.1291
0.577	0.28	0.035	0.4406	0.2748		0.577	0.559	0.035	0.5172	0.1183
0.577	0.28	0.105	0.5019	0.2134		0.577	0.559	0.105	0.3068	0.1768
0.577	0.28	0.175	0.5517	0.1838		0.577	0.559	0.175	0.4665	0.1245
0.577	0.28	0.245	0.5778	0.1607		0.577	0.559	0.245	0.5096	0.118
0.577	0.28	0.28	0.5825	0.152		0.577	0.559	0.28	0.5212	0.1187
0.577	0.35	0.035	0.3962	0.2526		0.577	0.629	0.035	0.3081	0.169
0.577	0.35	0.105	0.492	0.2006		0.577	0.629	0.105	0.3931	0.1327
0.577	0.35	0.175	0.527	0.1689		0.577	0.629	0.175	0.4465	0.1152
0.577	0.35	0.245	0.5521	0.149		0.577	0.629	0.245	0.495	0.1054
0.577	0.35	0.28	0.5579	0.1426		0.577	0.629	0.28	0.515	0.100
0.577	0.42	0.035	0.3544	0.2197		0.577	0.699	0.035	0.346	0.1738
0.577	0.42	0.105	0.4743	0.1825		0.577	0.699	0.105	0.4068	0.1298
0.577	0.42	0.175	0.5196	0.1586		0.577	0.699	0.175	0.4606	0.1097
0.577	0.42	0.245	0.54	0.1425		0.577	0.699	0.245	0.4902	0.0985
0.577	0.42	0.28	0.5456	0.1391		0.577	0.699	0.28	0.5009	0.0953
0.577	0.49	0.035	0.3132	0.19		0.577	0.769	0.035	0.3296	0.1295
0.577	0.49	0.105	0.4378	0.1662		0.577	0.769	0.105	0.4056	0.1249
0.577	0.49	0.175	0.4937	0.147		0.577	0.769	0.175	0.4745	0.1056

Appendix 2.4 Velocity data for the side weir flows in open channel (Q_R=0.792) Contd.

X*	Y*	Z*	U (m/s)	V (m/s)		X*	Y*	Z*	U (m/s)	V (m/s)
0.577	0.769	0.245	0.4951	0.0966		0.542	0.07	0.175	0.7385	0.3082
0.577	0.769	0.28	0.4887	0.0862		0.542	0.07	0.245	0.7151	0.2188
0.577	0.839	0.035	0.2863	0.0867		0.542	0.07	0.28	0.6847	0.1672
0.577	0.839	0.105	0.3529	0.0894		0.542	0.14	0.035	0.5261	0.3955
0.577	0.839	0.175	0.3764	0.0826		0.542	0.14	0.105	0.6237	0.3235
0.577	0.839	0.245	0.4558	0.0723		0.542	0.14	0.175	0.6657	0.2618
0.577	0.839	0.28	0.4857	0.0683		0.542	0.14	0.245	0.6607	0.2083
0.577	0.909	0.035	0.2089	0.0368		0.542	0.14	0.28	0.6455	0.1848
0.577	0.909	0.105	0.2122	0.0463		0.542	0.21	0.035	0.4341	0.3269
0.577	0.909	0.175	0.2152	0.049		0.542	0.21	0.105	0.5394	0.2662
0.577	0.909	0.245	0.3514	0.0361		0.542	0.21	0.175	0.5903	0.2282
0.577	0.909	0.28	0.4005	0.0398		0.542	0.21	0.245	0.6027	0.1939
0.577	0.979	0.035	0.0224	0.0127		0.542	0.21	0.28	0.606	0.1809
0.577	0.979	0.105	0.0673	0.0103		0.542	0.28	0.035	0.3973	0.2974
0.577	0.979	0.175	0.0898	0.0118		0.542	0.28	0.105	0.4768	0.2279
0.577	0.979	0.245	0.2616	0.0136		0.542	0.28	0.175	0.534	0.1996
0.577	0.979	0.28	0.2956	0.021		0.542	0.28	0.245	0.5528	0.1778
0.542	0.07	0.035	0.663	0.4925		0.542	0.28	0.28	0.5622	0.1682
0.542	0.07	0.105	0.7314	0.3993		0.542	0.35	0.035	0.3554	0.2618
0.577	0.769	0.245	0.4951	0.0966		0.542	0.35	0.105	0.4616	0.2142

Appendix 2.4 Velocity data for the side weir flows in open channel (Q_R=0.792) Contd.

X*	Y*	Z*	U (m/s)	V (m/s)		X*	Y*	Z*	U (m/s)	V (m/s)
0.542	0.35	0.175	0.4884	0.1841		0.542	0.629	0.175	0.4261	0.1207
0.542	0.35	0.245	0.528	0.1647		0.542	0.629	0.245	0.4713	0.1114
0.542	0.35	0.28	0.54	0.1552		0.542	0.629	0.28	0.485	0.1113
0.542	0.42	0.035	0.3004	0.2246		0.542	0.699	0.035	0.2912	0.1794
0.542	0.42	0.105	0.427	0.1901		0.542	0.699	0.105	0.3865	0.1444
0.542	0.42	0.175	0.4917	0.1709		0.542	0.699	0.175	0.4251	0.1203
0.542	0.42	0.245	0.5179	0.152		0.542	0.699	0.245	0.4694	0.1109
0.542	0.42	0.28	0.5249	0.149		0.542	0.699	0.28	0.4738	0.1096
0.542	0.49	0.035	0.2791	0.2025		0.542	0.769	0.035	0.3142	0.134
0.542	0.49	0.105	0.3958	0.1679		0.542	0.769	0.105	0.3729	0.1343
0.542	0.49	0.175	0.4649	0.1542		0.542	0.769	0.175	0.4236	0.1183
0.542	0.49	0.245	0.5031	0.1419		0.542	0.769	0.245	0.462	0.0982
0.542	0.49	0.28	0.5138	0.1368		0.542	0.769	0.28	0.47	0.0927
0.542	0.559	0.035	0.2724	0.1899		0.542	0.839	0.035	0.2816	0.0901
0.542	0.559	0.105	0.3547	0.1481		0.542	0.839	0.105	0.315	0.0852
0.542	0.559	0.175	0.4382	0.1356		0.542	0.839	0.175	0.317	0.0842
0.542	0.559	0.245	0.4795	0.1293		0.542	0.839	0.245	0.4222	0.0763
0.542	0.559	0.28	0.5004	0.1227		0.542	0.839	0.28	0.4553	0.0675
0.542	0.629	0.035	0.3025	0.1835		0.542	0.909	0.035	0.133	0.0386
0.542	0.629	0.105	0.3651	0.1331		0.542	0.909	0.105	0.1773	0.0369

Appendix 2.4 Velocity data for the side weir flows in open channel (Q_R=0.792) Contd.

X*	Y*	Z*	U (m/s)	V (m/s)		X*	Y*	Z*	U (m/s)	V (m/s)
0.507	0.07	0.035	0.5977	0.5689		0.507	0.35	0.035	0.3153	0.2799
0.507	0.07	0.105	0.7013	0.4515		0.507	0.35	0.105	0.465	0.2291
0.507	0.07	0.175	0.7307	0.3504		0.507	0.35	0.175	0.5053	0.2063
0.507	0.07	0.245	0.716	0.2526		0.507	0.35	0.245	0.5275	0.1806
0.507	0.07	0.28	0.6857	0.1977		0.507	0.35	0.28	0.5356	0.1712
0.507	0.14	0.035	0.486	0.4407		0.507	0.42	0.035	0.2991	0.2458
0.507	0.14	0.105	0.5952	0.3586		0.507	0.42	0.105	0.4294	0.2112
0.507	0.14	0.175	0.6519	0.2962		0.507	0.42	0.175	0.4914	0.1869
0.507	0.14	0.245	0.6549	0.2401		0.507	0.42	0.245	0.5128	0.169
0.507	0.14	0.28	0.6515	0.2117		0.507	0.42	0.28	0.5141	0.1611
0.507	0.21	0.035	0.4139	0.371		0.507	0.49	0.035	0.2611	0.2172
0.507	0.21	0.105	0.5245	0.2923		0.507	0.49	0.105	0.3829	0.1785
0.507	0.21	0.175	0.5805	0.2522		0.507	0.49	0.175	0.4526	0.1634
0.507	0.21	0.245	0.6007	0.2194		0.507	0.49	0.245	0.4903	0.1483
0.507	0.21	0.28	0.608	0.2025		0.507	0.49	0.28	0.511	0.1476
0.507	0.28	0.035	0.36	0.3226		0.507	0.559	0.035	0.2757	0.216
0.507	0.28	0.105	0.4684	0.2555		0.507	0.559	0.105	0.349	0.1562
0.507	0.28	0.175	0.5207	0.2179		0.507	0.559	0.175	0.4271	0.1424
0.507	0.28	0.245	0.5508	0.1975		0.507	0.559	0.245	0.48	0.1337
0.507	0.28	0.28	0.5554	0.1871		0.507	0.559	0.28	0.4927	0.1338

Appendix 2.4 Velocity data for the side weir flows in open channel (Q_R=0.792) Contd.

X*	Y*	Z*	U (m/s)	V (m/s)		X*	Y*	Z*	U (m/s)	V (m/s)
0.507	0.629	0.035	0.2811	0.2011		0.472	0.07	0.035	0.4997	0.5862
0.507	0.629	0.105	0.3875	0.1588		0.472	0.07	0.105	0.6237	0.4962
0.507	0.629	0.175	0.4321	0.1374		0.472	0.07	0.175	0.6975	0.3868
0.507	0.629	0.245	0.4725	0.1213		0.472	0.07	0.245	0.6971	0.2774
0.507	0.629	0.28	0.4784	0.1218		0.472	0.07	0.28	0.7184	0.235
0.507	0.699	0.035	0.2819	0.1728		0.472	0.14	0.035	0.4349	0.4879
0.507	0.699	0.105	0.4024	0.1565		0.472	0.14	0.105	0.5697	0.394
0.507	0.699	0.175	0.4475	0.1421		0.472	0.14	0.175	0.6325	0.3254
0.507	0.699	0.245	0.4733	0.1171		0.472	0.14	0.245	0.6501	0.2667
0.507	0.699	0.28	0.4715	0.1144		0.472	0.14	0.28	0.6496	0.2403
0.507	0.769	0.035	0.2813	0.1432		0.472	0.21	0.035	0.3789	0.3929
0.507	0.769	0.105	0.3663	0.134		0.472	0.21	0.105	0.5014	0.3214
0.507	0.769	0.175	0.4223	0.119		0.472	0.21	0.175	0.5515	0.273
0.507	0.769	0.245	0.4549	0.1056		0.472	0.21	0.245	0.5936	0.2396
0.507	0.769	0.28	0.4708	0.0959		0.472	0.21	0.28	0.5905	0.2241
0.507	0.839	0.035	0.2104	0.11		0.472	0.28	0.035	0.3344	0.3453
0.507	0.839	0.105	0.2865	0.0695		0.472	0.28	0.105	0.4552	0.2809
0.507	0.839	0.175	0.2774	0.0864		0.472	0.28	0.175	0.4992	0.2451
0.507	0.839	0.245	0.4126	0.0737		0.472	0.28	0.245	0.5482	0.2118
0.507	0.839	0.28	0.4516	0.076		0.472	0.28	0.28	0.5512	0.2045

Appendix 2.4 Velocity data for the side weir flows in open channel (Q_R=0.792) Contd.

X*	Y*	Z*	U (m/s)	V (m/s)		X*	Y*	Z*	U (m/s)	V (m/s)
0.472	0.35	0.035	0.2993	0.2977		0.472	0.629	0.035	0.29	0.1964
0.472	0.35	0.105	0.448	0.2525		0.472	0.629	0.105	0.3662	0.1576
0.472	0.35	0.175	0.4995	0.2176		0.472	0.629	0.175	0.4215	0.141
0.472	0.35	0.245	0.5253	0.1952		0.472	0.629	0.245	0.466	0.1326
0.472	0.35	0.28	0.5294	0.1882		0.472	0.629	0.28	0.474	0.1323
0.472	0.42	0.035	0.2588	0.2509		0.472	0.699	0.035	0.2711	0.1839
0.472	0.42	0.105	0.4025	0.2143		0.472	0.699	0.105	0.3938	0.1671
0.472	0.42	0.175	0.4883	0.2007		0.472	0.699	0.175	0.4262	0.1499
0.472	0.42	0.245	0.5077	0.1765		0.472	0.699	0.245	0.4531	0.1229
0.472	0.42	0.28	0.5169	0.1699		0.472	0.699	0.28	0.4725	0.1222
0.472	0.49	0.035	0.2482	0.2473		0.472	0.769	0.035	0.2704	0.1426
0.472	0.49	0.105	0.3639	0.1833		0.472	0.769	0.105	0.3506	0.1395
0.472	0.49	0.175	0.4511	0.168		0.472	0.769	0.175	0.3666	0.133
0.472	0.49	0.245	0.4961	0.1611		0.472	0.769	0.245	0.4522	0.1144
0.472	0.49	0.28	0.503	0.1538		0.472	0.769	0.28	0.4554	0.1034
0.472	0.559	0.035	0.2682	0.2211		0.472	0.839	0.035	0.2197	0.0826
0.472	0.559	0.105	0.3611	0.1764		0.472	0.839	0.105	0.2579	0.0853
0.472	0.559	0.175	0.4276	0.1475		0.472	0.839	0.175	0.2368	0.0855
0.472	0.559	0.245	0.4747	0.1442		0.472	0.839	0.245	0.3964	0.0828
0.472	0.559	0.28	0.4943	0.1398		0.472	0.839	0.28	0.4227	0.0775

Appendix 2.4 Velocity data for the side weir flows in open channel (Q_R=0.792) Contd.

X*	Y*	Z*	U (m/s)	V (m/s)		X*	Y*	Z*	U (m/s)	V (m/s)
0.437	0.07	0.035	0.5442	0.5921		0.437	0.35	0.105	0.461	0.2567
0.437	0.07	0.105	0.6301	0.4804		0.437	0.35	0.175	0.5023	0.2303
0.437	0.07	0.175	0.6671	0.3947		0.437	0.35	0.245	0.5231	0.2164
0.437	0.07	0.245	0.6697	0.3043		0.437	0.35	0.28	0.5102	0.2057
0.437	0.14	0.035	0.4555	0.468		0.437	0.42	0.035	0.3169	0.245
0.437	0.14	0.105	0.5644	0.4011		0.437	0.42	0.105	0.419	0.2175
0.437	0.14	0.175	0.6105	0.3408		0.437	0.42	0.175	0.4901	0.2026
0.437	0.14	0.245	0.6318	0.2874		0.437	0.42	0.245	0.5123	0.1847
0.437	0.14	0.28	0.5141	0.2137		0.437	0.42	0.28	0.5104	0.1776
0.437	0.21	0.035	0.4113	0.3924		0.437	0.49	0.035	0.3122	0.2303
0.437	0.21	0.105	0.5077	0.3324		0.437	0.49	0.105	0.4012	0.1891
0.437	0.21	0.175	0.5544	0.293		0.437	0.49	0.175	0.4563	0.18
0.437	0.21	0.245	0.5792	0.2636		0.437	0.49	0.245	0.4949	0.1698
0.437	0.21	0.28	0.5806	0.2487		0.437	0.49	0.28	0.4923	0.1675
0.437	0.28	0.035	0.3943	0.3719		0.437	0.559	0.035	0.3316	0.2078
0.437	0.28	0.105	0.5039	0.3162		0.437	0.559	0.105	0.3687	0.1755
0.437	0.28	0.175	0.5198	0.2569		0.437	0.559	0.175	0.4482	0.1552
0.437	0.28	0.245	0.543	0.2335		0.437	0.559	0.245	0.4843	0.1574
0.437	0.28	0.28	0.5353	0.2301		0.437	0.559	0.28	0.4881	0.1525
0.437	0.35	0.035	0.3584	0.2931		0.437	0.629	0.035	0.3472	0.2011

Appendix 2.4 Velocity data for the side weir flows in open channel (Q_R=0.792) Contd.

X*	Y*	Z*	U (m/s)	V (m/s)		X*	Y*	Z*	U (m/s)	V (m/s)
0.437	0.629	0.105	0.392	0.1697		0.437	0.629	0.105	0.392	0.1697
0.437	0.629	0.175	0.4389	0.151		0.437	0.629	0.175	0.4389	0.151
0.437	0.629	0.245	0.4722	0.1396		0.437	0.629	0.245	0.4722	0.1396
0.437	0.629	0.28	0.4373	0.1446		0.437	0.629	0.28	0.4373	0.1446
0.437	0.699	0.035	0.343	0.1724		0.437	0.699	0.035	0.343	0.1724
0.437	0.699	0.105	0.3961	0.1538		0.437	0.699	0.105	0.3961	0.1538
0.437	0.699	0.175	0.4469	0.1498		0.437	0.699	0.175	0.4469	0.1498
0.437	0.699	0.245	0.455	0.1295		0.437	0.699	0.245	0.455	0.1295
0.437	0.699	0.28	0.4309	0.1356		0.437	0.699	0.28	0.4309	0.1356
0.437	0.769	0.035	0.3148	0.1288		0.437	0.769	0.035	0.3148	0.1288
0.437	0.769	0.105	0.3198	0.1343		0.437	0.769	0.105	0.3198	0.1343
0.437	0.769	0.175	0.3988	0.1208		0.437	0.769	0.175	0.3988	0.1208
0.437	0.769	0.245	0.4569	0.1092		0.437	0.769	0.245	0.4569	0.1092
0.437	0.769	0.28	0.4417	0.1131		0.437	0.769	0.28	0.4417	0.1131
0.437	0.839	0.035	0.2194	0.0693		0.437	0.839	0.035	0.2194	0.0693
0.437	0.839	0.105	0.1337	0.0738		0.437	0.839	0.105	0.1337	0.0738
0.437	0.839	0.175	0.3029	0.0746		0.437	0.839	0.175	0.3029	0.0746
0.437	0.839	0.245	0.4252	0.0773		0.437	0.839	0.245	0.4252	0.0773
0.437	0.839	0.28	0.2476	0.0956		0.437	0.839	0.28	0.2476	0.0956
0.437	0.909	0.035	0.013	0.0316		0.437	0.909	0.035	0.013	0.0316

Appendix 2.4 Velocity data for the side weir flows in open channel (Q_R=0.792) Contd.

X*	Y*	Z*	U (m/s)	V (m/s)		X*	Y*	Z*	U (m/s)	V (m/s)
0.402	0.07	0.035	0.3337	0.1843		0.402	0.35	0.035	0.1877	0.3403
0.402	0.07	0.105	0.5517	0.582		0.402	0.35	0.105	0.3903	0.2728
0.402	0.07	0.175	0.6509	0.4749		0.402	0.35	0.175	0.4783	0.2575
0.402	0.07	0.245	0.6809	0.3909		0.402	0.35	0.245	0.5069	0.2318
0.402	0.07	0.28	0.6859	0.3509		0.402	0.35	0.28	0.5225	0.2172
0.402	0.14	0.035	0.2368	0.5574		0.402	0.42	0.035	0.217	0.3082
0.402	0.14	0.105	0.4756	0.4641		0.402	0.42	0.105	0.3603	0.2323
0.402	0.14	0.175	0.5726	0.3983		0.402	0.42	0.175	0.4523	0.2175
0.402	0.14	0.245	0.6157	0.34		0.402	0.42	0.245	0.4948	0.2035
0.402	0.14	0.28	0.6357	0.3201		0.402	0.42	0.28	0.504	0.2011
0.402	0.21	0.035	0.2494	0.4519		0.402	0.49	0.035	0.2269	0.2725
0.402	0.21	0.105	0.4465	0.3913		0.402	0.49	0.105	0.3483	0.2143
0.402	0.21	0.175	0.5158	0.3344		0.402	0.49	0.175	0.4182	0.1901
0.402	0.21	0.245	0.5713	0.2938		0.402	0.49	0.245	0.4821	0.1733
0.402	0.21	0.28	0.5744	0.2824		0.402	0.49	0.28	0.4842	0.1789
0.402	0.28	0.035	0.2164	0.4077		0.402	0.559	0.035	0.1821	0.2504
0.402	0.28	0.105	0.4302	0.3349		0.402	0.559	0.105	0.3543	0.19
0.402	0.28	0.175	0.4892	0.2915		0.402	0.559	0.175	0.4035	0.1692
0.402	0.28	0.245	0.5258	0.2588		0.402	0.559	0.245	0.4603	0.1632
0.402	0.28	0.28	0.5381	0.2526		0.402	0.559	0.28	0.4677	0.1578

X*	Y*	Z*	U (m/s)	V (m/s)		X*	Y*	Z*	U (m/s)	V (m/s)
0.402	0.629	0.035	0.2644	0.2221		0.402	0.909	0.035	0.0239	0.0316
0.402	0.629	0.105	0.3609	0.1925		0.402	0.909	0.105	-0.004	-0.0023
0.402	0.629	0.175	0.4177	0.175		0.402	0.909	0.175	0.0798	0.0311
0.402	0.629	0.245	0.4531	0.1504		0.402	0.909	0.245	0.246	0.0317
0.402	0.629	0.28	0.4444	0.1513		0.402	0.909	0.28	0.3147	0.0218
0.402	0.699	0.035	0.1752	0.1767		0.402	0.979	0.035	-0.0113	0.0033
0.402	0.699	0.105	0.364	0.1766		0.402	0.979	0.105	-0.0462	0.0032
0.402	0.699	0.175	0.4151	0.162		0.402	0.979	0.175	0.0113	0.006
0.402	0.699	0.245	0.4568	0.1427		0.402	0.979	0.245	0.1606	0.0064
0.402	0.699	0.28	0.456	0.1406		0.402	0.979	0.28	0.1869	0.0047
0.402	0.769	0.035	0.1713	0.1173		0.367	0.07	0.035	0.2549	0.2147
0.402	0.769	0.105	0.2393	0.129		0.367	0.07	0.105	0.5154	0.5984
0.402	0.769	0.175	0.3624	0.1223		0.367	0.07	0.175	0.6156	0.5031
0.402	0.769	0.245	0.4545	0.1153		0.367	0.07	0.245	0.6605	0.4244
0.402	0.769	0.28	0.4865	0.1121		0.367	0.07	0.28	0.6675	0.3914
0.402	0.839	0.035	0.1084	0.0827		0.367	0.14	0.035	0.1573	0.5546
0.402	0.839	0.105	0.1427	0.0602		0.367	0.14	0.105	0.4657	0.4818
0.402	0.839	0.175	0.1843	0.0649		0.367	0.14	0.175	0.557	0.4171
0.402	0.839	0.245	0.3384	0.073		0.367	0.14	0.245	0.6046	0.3669
0.402	0.839	0.28	0.4196	0.0785		0.402	0.909	0.035	0.0239	0.0316

Appendix 2.4 Velocity data for the side weir flows in open channel (Q_R=0.792) Contd.

X*	Y*	Z*	U (m/s)	V (m/s)		X*	Y*	Z*	U (m/s)	V (m/s)
0.367	0.14	0.28	0.6169	0.3454		0.367	0.42	0.28	0.5155	0.2088
0.367	0.21	0.035	0.2047	0.4754		0.367	0.49	0.035	0.2214	0.2833
0.367	0.21	0.105	0.4467	0.4078		0.367	0.49	0.105	0.3525	0.2293
0.367	0.21	0.175	0.5122	0.3567		0.367	0.49	0.175	0.4328	0.2069
0.367	0.21	0.245	0.5614	0.3139		0.367	0.49	0.245	0.4903	0.1884
0.367	0.21	0.28	0.5598	0.3009		0.367	0.49	0.28	0.4972	0.1932
0.367	0.28	0.035	0.2278	0.4079		0.367	0.559	0.035	0.146	0.2521
0.367	0.28	0.105	0.4161	0.3476		0.367	0.559	0.105	0.3628	0.2233
0.367	0.28	0.175	0.4913	0.2964		0.367	0.559	0.175	0.4267	0.196
0.367	0.28	0.245	0.5276	0.2741		0.367	0.559	0.245	0.4611	0.1807
0.367	0.28	0.28	0.548	0.2634		0.367	0.559	0.28	0.4882	0.1684
0.367	0.35	0.035	0.2222	0.3424		0.367	0.629	0.035	0.2866	0.2363
0.367	0.35	0.105	0.378	0.284		0.367	0.629	0.105	0.4208	0.201
0.367	0.35	0.175	0.4617	0.2654		0.367	0.629	0.175	0.4388	0.1908
0.367	0.35	0.245	0.5231	0.2478		0.367	0.629	0.245	0.4732	0.1687
0.367	0.35	0.28	0.5373	0.2297		0.367	0.629	0.28	0.4695	0.1578
0.367	0.42	0.035	0.216	0.3376		0.367	0.699	0.035	0.268	0.1823
0.367	0.42	0.105	0.356	0.2483		0.367	0.699	0.105	0.3495	0.1732
0.367	0.42	0.175	0.4372	0.2287		0.367	0.699	0.175	0.4143	0.1572
0.367	0.42	0.245	0.5095	0.2165		0.367	0.699	0.245	0.4695	0.1545

Appendix 2.4 Velocity data for the side weir flows in open channel (Q_R=0.792) Contd.

X*	Y*	Z*	U (m/s)	V (m/s)		X*	Y*	Z*	U (m/s)	V (m/s)
0.367	0.699	0.28	0.4687	0.1391		0.367	0.979	0.28		0.0213
0.367	0.769	0.035	0.2209	0.085		0.332	0.07	0.035	0.1367	0.1628
0.367	0.769	0.105	0.2434	0.1073		0.332	0.07	0.105	0.4557	0.6008
0.367	0.769	0.175	0.2979	0.1123		0.332	0.07	0.175	0.5671	0.5259
0.367	0.769	0.245	0.4327	0.1167		0.332	0.07	0.245	0.6077	0.4531
0.367	0.769	0.28	0.4578	0.1154		0.332	0.07	0.28	0.6199	0.4277
0.367	0.839	0.035	0.1126	0.0436		0.332	0.14	0.035	0.1603	0.5712
0.367	0.839	0.105	0.0565	0.0416		0.332	0.14	0.105	0.4307	0.5043
0.367	0.839	0.175	0.1475	0.0568		0.332	0.14	0.175	0.5123	0.4388
0.367	0.839	0.245	0.3505	0.0717		0.332	0.14	0.245	0.5639	0.3906
0.367	0.839	0.28	0.4023	0.0706		0.332	0.14	0.28	0.5881	0.3703
0.367	0.909	0.035	0.0395	0.0175		0.332	0.21	0.035	0.1699	0.4733
0.367	0.909	0.105	-0.046	0.0089		0.332	0.21	0.105	0.4257	0.4192
0.367	0.909	0.175	0.0364	0.0089		0.332	0.21	0.175	0.4866	0.3731
0.367	0.909	0.245	0.2421	0.024		0.332	0.21	0.245	0.5225	0.3357
0.367	0.909	0.28	0.2836	0.0255		0.332	0.21	0.28	0.5472	0.3194
0.367	0.979	0.035	-0.0515	0.0011		0.332	0.28	0.035	0.1621	0.4362
0.367	0.979	0.105	-0.0602	0.0013		0.332	0.28	0.105	0.3801	0.344
0.367	0.979	0.175	0.002	-0.0008		0.332	0.28	0.175	0.4751	0.3231
0.367	0.979	0.245	0.1193	0.0015		0.367	0.979	0.28		0.0213

X*	Y*	Z*	U (m/s)	V (m/s)		X*	Y*	Z*	U (m/s)	V (m/s)
0.332	0.28	0.245	0.5204	0.2905		0.297	0.07	0.035	0.1067	0.2785
0.332	0.28	0.28	0.5154	0.282		0.297	0.07	0.105	0.4135	0.5973
0.332	0.35	0.035	0.1309	0.3655		0.297	0.07	0.175	0.4994	0.5302
0.332	0.35	0.105	0.3601	0.2897		0.297	0.07	0.245	0.5442	0.4671
0.332	0.35	0.175	0.4537	0.2724		0.297	0.07	0.28	0.5525	0.4442
0.332	0.35	0.245	0.5033	0.257		0.297	0.14	0.035	0.1619	0.5572
0.332	0.35	0.28	0.5231	0.2529		0.297	0.14	0.105	0.3848	0.5095
0.332	0.42	0.035	0.2579	0.3119		0.297	0.14	0.175	0.4652	0.4457
0.332	0.42	0.105	0.048	0.3362		0.297	0.14	0.245	0.5144	0.4018
0.332	0.42	0.175	0.3264	0.2914		0.297	0.14	0.28	0.5199	0.3856
0.332	0.42	0.245	0.4111	0.2382		0.297	0.21	0.035	0.158	0.4779
0.332	0.42	0.28	0.4467	0.2261		0.297	0.21	0.105	0.3621	0.4211
0.332	0.49	0.035	0.0295	0.0019		0.297	0.21	0.175	0.4539	0.3843
0.332	0.49	0.105	0.1448	0.3134		0.297	0.21	0.245	0.4911	0.3475
0.332	0.49	0.175	0.3232	0.2548		0.297	0.21	0.28	0.5025	0.3317
0.332	0.49	0.245	0.3945	0.2219		0.297	0.28	0.035	0.1125	0.3877
0.332	0.49	0.28	0.436	0.2175		0.297	0.28	0.105	0.3317	0.3529
0.332	0.559	0.035	0	0		0.297	0.28	0.175	0.4514	0.3177
0.332	0.559	0.105	0.1323	0.2893		0.297	0.28	0.245	0.4786	0.3086
0.332	0.559	0.175	0.3532	0.2421		0.297	0.28	0.28	0.4918	0.2948

X*	Y*	Z*	U (m/s)	V (m/s)		X*	Y*	Z*	U (m/s)	V (m/s)
0.297	0.35	0.035	0.1964	0.3633		0.297	0.629	0.035	0.2419	0.2021
0.297	0.35	0.105	0.3239	0.3088		0.297	0.629	0.105	0.3079	0.2058
0.297	0.35	0.175	0.4014	0.2824		0.297	0.629	0.175	0.3721	0.1952
0.297	0.35	0.245	0.4712	0.2646		0.297	0.629	0.245	0.4271	0.1782
0.297	0.35	0.28	0.4764	0.2591		0.297	0.629	0.28	0.4407	0.1541
0.297	0.42	0.035	0.215	0.3151		0.297	0.699	0.035	0.2019	0.1469
0.297	0.42	0.105	0.3081	0.2725		0.297	0.699	0.105	0.2405	0.1348
0.297	0.42	0.175	0.3999	0.2485		0.297	0.699	0.175	0.296	0.1489
0.297	0.42	0.245	0.4576	0.2278		0.297	0.699	0.245	0.4195	0.1442
0.297	0.42	0.28	0.4582	0.2293		0.297	0.699	0.28	0.4193	0.1426
0.297	0.49	0.035	0.2412	0.2882		0.297	0.769	0.035	0.1802	0.0726
0.297	0.49	0.105	0.332	0.2525		0.297	0.769	0.105	0.1302	0.0689
0.297	0.49	0.175	0.3837	0.2195		0.297	0.769	0.175	0.200	0.0852
0.297	0.49	0.245	0.4322	0.2021		0.297	0.769	0.245	0.3801	0.1024
0.297	0.49	0.28	0.4433	0.2028		0.297	0.769	0.28	0.4043	0.1058
0.297	0.559	0.035	0.2263	0.239		0.297	0.839	0.035	-0.0012	0.0171
0.297	0.559	0.105	0.3375	0.2359		0.297	0.839	0.105	-0.0217	0.0295
0.297	0.559	0.175	0.371	0.2085		0.297	0.839	0.175	0.0825	0.029
0.297	0.559	0.245	0.4209	0.1948		0.297	0.839	0.245	0.273	0.0586
0.297	0.559	0.28	0.4263	0.181		0.297	0.839	0.28	0.3656	0.0604

Appendix 2.4 Velocity data for the side weir flows in open channel (Q_R=0.792) Contd.

X*	Y*	Z*	U (m/s)	V (m/s)		X*	Y*	Z*	U (m/s)	V (m/s)
0.297	0.909	0.035	-0.0648	-0.0073		0.262	0.14	0.28	0.5347	0.3966
0.297	0.909	0.105	-0.0466	-0.0039		0.262	0.21	0.035	0.1551	0.4661
0.297	0.909	0.175	0.0338	0.0161		0.262	0.21	0.105	0.3624	0.4256
0.297	0.909	0.245	0.2222	0.012		0.262	0.21	0.175	0.4697	0.3899
0.297	0.909	0.28	0.2845	0.0173		0.262	0.21	0.245	0.5102	0.3603
0.297	0.979	0.035	-0.0796	0.004		0.262	0.21	0.28	0.4996	0.3437
0.297	0.979	0.105	-0.0523	0.0023		0.262	0.28	0.035	0.1546	0.3893
0.297	0.979	0.175	0.0453	-0.0031		0.262	0.28	0.105	0.3588	0.3518
0.297	0.979	0.245	0.1042	0.2248		0.262	0.28	0.175	0.4503	0.3339
0.297	0.979	0.28	0.1256	0.2097		0.262	0.28	0.245	0.5045	0.313
0.262	0.07	0.035	0.0885	0.3027		0.262	0.28	0.28	0.5118	0.3076
0.262	0.07	0.105	0.4213	0.5927		0.262	0.35	0.035	0.2337	0.3484
0.262	0.07	0.175	0.4704	0.5433		0.262	0.35	0.105	0.3387	0.3025
0.262	0.07	0.245	0.5483	0.475		0.262	0.35	0.175	0.4328	0.2831
0.262	0.07	0.28	0.5466	0.4597		0.262	0.35	0.245	0.4867	0.2668
0.262	0.14	0.035	0.1621	0.5622		0.262	0.35	0.28	0.4919	0.2687
0.262	0.14	0.105	0.3929	0.5132		0.262	0.42	0.035	0.2274	0.322
0.262	0.14	0.175	0.4627	0.46		0.262	0.42	0.105	0.3645	0.2842
0.262	0.14	0.245	0.5125	0.4147		0.262	0.42	0.175	0.417	0.2481
0.297	0.909	0.035	-0.0648	-0.0073		0.262	0.42	0.245	0.4841	0.2259

Appendix 2.4 Velocity data for the side weir flows in open channel (Q_R=0.792) Contd.

X*	Y*	Z*	U (m/s)	V (m/s)
0.262	0.42	0.28	0.5027	0.2212
0.262	0.49	0.035	0.3106	0.3007
0.262	0.49	0.105	0.3713	0.261
0.262	0.49	0.175	0.4127	0.2259
0.262	0.49	0.245	0.4645	0.2147
0.262	0.49	0.28	0.4828	0.2059
0.262	0.559	0.035	0.2611	0.2303
0.262	0.559	0.105	0.3685	0.2419
0.262	0.559	0.175	0.4233	0.2235
0.262	0.559	0.245	0.4569	0.1965
0.262	0.559	0.28	0.476	0.1846
0.262	0.629	0.035	0.2772	0.1719
0.262	0.629	0.105	0.2871	0.1795
0.262	0.629	0.175	0.4236	0.1826
0.262	0.629	0.245	0.4725	0.1783
0.262	0.629	0.28	0.4739	0.1739
0.262	0.699	0.035	0.1965	0.1049
0.262	0.699	0.105	0.2119	0.1278
0.262	0.699	0.175	0.3107	0.1224
0.262	0.699	0.245	0.4345	0.1494
0.262	0.699	0.28	0.4659	0.1333
0.262	0.769	0.035	0.1815	0.0637
0.262	0.769	0.105	0.0838	0.0528
0.262	0.769	0.175	0.2368	0.08
0.262	0.769	0.245	0.3984	0.0996
0.262	0.769	0.28	0.4524	0.0972
0.262	0.839	0.035	0.0622	0.017
0.262	0.839	0.105	0.0068	0.0063
0.262	0.839	0.175	0.1461	0.0345
0.262	0.839	0.245	0.2886	0.0421
0.262	0.839	0.28	0.3474	0.055

Appendix 2.5 Velocity data for the side weir flows in open channel (Q_R=0.940) - RUN II, Details are provided in Table 3.2.

X*	Y*	Z*	U (m/s)	V (m/s)		X*	Y*	Z*	U (m/s)	V (m/s)
0.8741	0.0699	0.035	0.353	0.0284		0.8741	0.9091	0.035	0.2834	0.0293
0.8741	0.0699	0.1049	0.3941	0.0296		0.8741	0.9091	0.1049	0.3121	0.0406
0.8741	0.0699	0.1748	0.4254	0.0308		0.8741	0.9091	0.1748	0.3903	0.0308
0.8741	0.0699	0.2448	0.4257	0.0277		0.8741	0.9091	0.2448	0.4473	0.0273
0.8741	0.0699	0.3147	0.436	0.0242		0.8741	0.9091	0.3147	0.4752	0.0282
0.8741	0.2797	0.035	0.3362	0.0664		0.6119	0.0699	0.035	0.6486	0.5293
0.8741	0.2797	0.1049	0.3982	0.0599		0.6119	0.0699	0.1049	0.7106	0.4399
0.8741	0.2797	0.1748	0.4319	0.0548		0.6119	0.0699	0.1748	0.7236	0.3496
0.8741	0.2797	0.2448	0.4595	0.0503		0.6119	0.0699	0.2448	0.7062	0.2624
0.8741	0.2797	0.3147	0.5019	0.0485		0.6119	0.0699	0.3147	0.6344	0.1767
0.8741	0.4895	0.035	0.3167	0.0764		0.6119	0.2797	0.035	0.3281	0.311
0.8741	0.4895	0.1049	0.4116	0.0706		0.6119	0.2797	0.1049	0.4206	0.27
0.8741	0.4895	0.1748	0.4369	0.0668		0.6119	0.2797	0.1748	0.4736	0.2324
0.8741	0.4895	0.2448	0.4646	0.0537		0.6119	0.2797	0.2448	0.5046	0.1984
0.8741	0.4895	0.3147	0.4907	0.0458		0.6119	0.2797	0.3147	0.5402	0.1702
0.8741	0.6993	0.035	0.2631	0.0612		0.6119	0.4895	0.035	0.209	0.2303
0.8741	0.6993	0.1049	0.3337	0.0586		0.6119	0.4895	0.1049	0.3255	0.1755
0.8741	0.6993	0.1748	0.3896	0.0498		0.6119	0.4895	0.1748	0.3875	0.1691
0.8741	0.6993	0.2448	0.4509	0.044		0.6119	0.4895	0.2448	0.4518	0.1489
0.8741	0.6993	0.3147	0.4998	0.0431		0.6119	0.4895	0.3147	0.5037	0.1414

Appendix 2.6 Velocity data for the side weir flows in open channel (Q_R=0.604) - RUN II Contd.

X*	Y*	Z*	U (m/s)	V (m/s)
0.6119	0.6993	0.035	0.1605	0.1567
0.6119	0.6993	0.1049	0.3167	0.1496
0.6119	0.6993	0.1748	0.3924	0.1185
0.6119	0.6993	0.2448	0.4451	0.1103
0.6119	0.6993	0.3147	0.4742	0.1018
0.6119	0.9091	0.035	0.0047	0.0647
0.6119	0.9091	0.1049	0.1449	0.014
0.6119	0.9091	0.1748	0.2323	0.0452
0.6119	0.9091	0.2448	0.3411	0.055
0.6119	0.9091	0.3147	0.3834	0.0597
0.2972	0.0699	0.035	0.2614	0.4015
0.2972	0.0699	0.1049	0.1589	0.4499
0.2972	0.0699	0.1748	0.4588	0.592
0.2972	0.0699	0.2448	0.5236	0.5216
0.2972	0.0699	0.3147	0.6081	0.4561
0.2972	0.2797	0.035	0.078	0.411
0.2972	0.2797	0.1049	0.129	0.405
0.2972	0.2797	0.1748	0.3299	0.3741
0.2972	0.2797	0.2448	0.4833	0.3291
0.2972	0.2797	0.3147	0.5361	0.2958

X*	Y*	Z*	U (m/s)	V (m/s)
0.2972	0.4895	0.035	-0.1029	0.3118
0.2972	0.4895	0.1049	0.1488	0.2882
0.2972	0.4895	0.1748	0.3226	0.2686
0.2972	0.4895	0.2448	0.4275	0.2184
0.2972	0.4895	0.3147	0.4879	0.2055
0.2972	0.6993	0.035	-0.2027	0.1911
0.2972	0.6993	0.1049	0.108	0.2417
0.2972	0.6993	0.1748	0.368	0.1622
0.2972	0.6993	0.2448	0.4384	0.1168
0.2972	0.6993	0.3147	0.4722	0.1475

Appendix 2.6 Velocity data for the side weir flows in open channel (Q_R=0.604) - RUN III, Details are provided in Table 3.2.

X*	Y*	Z*	U (m/s)	V (m/s)		X*	Y*	Z*	U (m/s)	V (m/s)
0.8741	0.0699	0.035	0.4367	-0.0242		0.8741	0.9091	0.035	0.4764	-0.031
0.8741	0.0699	0.1049	0.4882	-0.028		0.8741	0.9091	0.1049	0.5338	-0.0301
0.8741	0.0699	0.1748	0.5055	-0.0222		0.8741	0.9091	0.1748	0.5971	-0.0248
0.8741	0.0699	0.2448	0.5569	-0.0311		0.8741	0.9091	0.2448	0.6058	-0.0146
0.8741	0.0699	0.2797	0.4869	-0.0349		0.8741	0.9091	0.2797	0.5626	-0.0176
0.8741	0.2797	0.035	0.447	-0.0552		0.6119	0.0699	0.035	0.7393	0.2714
0.8741	0.2797	0.1049	0.5336	-0.051		0.6119	0.0699	0.1049	0.7813	0.2203
0.8741	0.2797	0.1748	0.6116	-0.0474		0.6119	0.0699	0.1748	0.7755	0.1608
0.8741	0.2797	0.2448	0.6301	-0.0419		0.6119	0.0699	0.2448	0.7354	0.1036
0.8741	0.2797	0.2797	0.6213	-0.0394		0.6119	0.0699	0.2797	0.737	0.1049
0.8741	0.4895	0.035	0.4594	-0.0651		0.6119	0.2797	0.035	0.446	0.2014
0.8741	0.4895	0.1049	0.5287	-0.055		0.6119	0.2797	0.1049	0.5618	0.1707
0.8741	0.4895	0.1748	0.5604	-0.0432		0.6119	0.2797	0.1748	0.6464	0.1493
0.8741	0.4895	0.2448	0.5864	-0.0371		0.6119	0.2797	0.2448	0.6774	0.1241
0.8741	0.4895	0.2797	0.5963	-0.0341		0.6119	0.2797	0.2797	0.6441	0.1151
0.8741	0.6993	0.035	0.3484	-0.0406		0.6119	0.4895	0.035	0.3656	0.1626
0.8741	0.6993	0.1049	0.4845	-0.0399		0.6119	0.4895	0.1049	0.5129	0.1406
0.8741	0.6993	0.1748	0.5629	-0.0351		0.6119	0.4895	0.1748	0.5807	0.1224
0.8741	0.6993	0.2448	0.5943	-0.0335		0.6119	0.4895	0.2448	0.603	0.1036
0.8741	0.6993	0.2797	0.5802	-0.0347		0.6119	0.4895	0.2797	0.5935	0.09

Appendix 2.6 Velocity data for the side weir flows in open channel (Q_R=0.604) - RUN III Contd.

X*	Y*	Z*	U (m/s)	V (m/s)
0.6119	0.6993	0.035	0.3466	0.1321
0.6119	0.6993	0.1049	0.4273	0.0959
0.6119	0.6993	0.1748	0.5339	0.0846
0.6119	0.6993	0.2448	0.5749	0.0814
0.6119	0.6993	0.2797	0.5683	0.0858
0.6119	0.9091	0.035	0.3098	0.0684
0.6119	0.9091	0.1049	0.406	0.0681
0.6119	0.9091	0.1748	0.5056	0.0663
0.6119	0.9091	0.2448	0.5441	0.0597
0.6119	0.9091	0.2797	0.5298	0.0668
0.2972	0.0699	0.035	-0.0186	0.2828
0.2972	0.0699	0.1049	0.2382	0.2121
0.2972	0.0699	0.1748	0.5263	0.5984
0.2972	0.0699	0.2448	0.5492	0.5422
0.2972	0.2797	0.035	0.1409	0.4063
0.2972	0.2797	0.1049	0.3762	0.4096
0.2972	0.2797	0.1748	0.4607	0.3884
0.2972	0.2797	0.2448	0.5359	0.3752
0.2972	0.4895	0.035	0.1861	0.2956
0.2972	0.4895	0.1049	0.357	0.2796
0.2972	0.4895	0.1748	0.4788	0.2797
0.2972	0.4895	0.2448	0.5519	0.2908
0.2972	0.4895	0.2797	0.5303	0.2851
0.2972	0.6993	0.035	0.2546	0.246
0.2972	0.6993	0.1049	0.4215	0.2555
0.2972	0.6993	0.1748	0.4776	0.2508
0.2972	0.6993	0.2448	0.5397	0.2406
0.2972	0.6993	0.2797	0.5073	0.2345
0.2972	0.9091	0.035	-0.0026	-0.0014
0.2972	0.9091	0.1049	0.0786	0.0357
0.2972	0.9091	0.1748	0.3666	0.1207
0.2972	0.9091	0.2448	0.4319	0.1542
0.2972	0.9091	0.2797	0.4115	0.155